

Identifying Ap stars in TESS Cycle 1 observations and determining their rotation periods

by

Matthew James Scargill

A thesis submitted in partial fulfilment for the requirements for the degree of
MSc (by Research) at the University of Central Lancashire

December 2021

STUDENT DECLARATION FORM

Type of Award **Master of Science (By Research)**

School **School of Natural Sciences**

*Sections marked * delete as appropriate*

1. Concurrent registration for two or more academic awards

*I declare that while registered as a candidate for the research degree, I have not been a registered candidate or enrolled student for another award of the University or other academic or professional institution

2. Material submitted for another award

*I declare that no material contained in the thesis has been used in any other submission for an academic award and is solely my own work

3. Collaboration

Where a candidate's research programme is part of a collaborative project, the thesis must indicate in addition clearly the candidate's individual contribution and the extent of the collaboration. Please state below:

N/A

4. Use of a Proof-reader

*No proof-reading service was used in the compilation of this thesis.

Signature of Candidate



Print name: **Matthew James Scargill**

Abstract

Data from the Transiting Exoplanet Survey Satellite (TESS) was used to identify chemically peculiar A-type (Ap) stars within the southern ecliptic hemisphere. A routine was developed to automatically download and process data from all 13 sectors of TESS Cycle 1 observations. This routine differentiates Ap stars from other rotationally variable stars through analysis of the object's Lomb Scargle Periodogram, and apply phase dispersion minimisation (PDM) to determine the dominant frequency of variability present with a degree of confidence. When combined with manual inspection of light curves, this process gave a non-exhaustive list of 610 candidate Ap stars within TESS Cycle 1, from which 90 had literature values.

Contents

| | | |
|----------|---|-----------|
| 1 | Introduction | 1 |
| 1.1 | Ap Stars | 1 |
| 1.2 | Importance of Period Determination with Ap Stars | 3 |
| 1.3 | Other Luminosity Variability Sources | 4 |
| 1.4 | TESS Data | 6 |
| 2 | Testing Period Searching Methods | 9 |
| 2.1 | Fourier | 10 |
| 2.2 | Box Least Squares Periodogram | 11 |
| 2.3 | Lomb-Scargle Periodogram | 11 |
| 2.4 | Phase Dispersion Minimisation | 13 |
| 2.5 | Comparison of Methods | 15 |
| 3 | Development of Routine | 16 |
| 3.1 | Data Acquisition | 17 |
| 3.2 | Data Handling | 18 |
| 3.3 | Identifying Ap Stars; Handling False Positives | 18 |
| 3.4 | Determining Rotation Periods of Stars | 19 |
| 3.5 | Errors | 20 |
| 4 | Testing of Routine | 21 |
| 4.1 | Initial Testing to Develop Routines | 21 |
| 4.2 | Testing on Cunha Dataset | 22 |
| 4.3 | Testing False Positives | 23 |
| 4.4 | Refinement of Routine from Testing | 25 |
| 5 | Results of Routine Run-through | 26 |
| 5.1 | Comparisons between Sectors | 26 |
| 5.2 | Long Period Stars in the Data | 29 |
| 5.2.1 | Long Period Stars ($14 < P_{\text{rot}} < 28$ days) | 30 |
| 5.2.2 | Very Long Period Stars ($28 \text{ days} < P_{\text{rot}}$) | 35 |
| 5.3 | Low Temperature Stars in the Data | 36 |
| 5.4 | Analysing Stars Observed in Multiple Sectors | 38 |
| 5.5 | Manual Investigation of Data | 39 |
| 6 | Discussion | 40 |
| 6.1 | Results | 40 |
| 6.1.1 | Representing the Results on a HR Diagram | 42 |
| 6.1.2 | Discussion of Individual Objects | 44 |
| 6.2 | Routine and Methods | 49 |
| 6.2.1 | Identification and Acquisition of Data | 49 |
| 6.2.2 | Lomb Scargle and False Positive Identification | 50 |

| | | |
|----------|--|-----------|
| 6.2.3 | Phase Dispersion Minimisation | 51 |
| 6.2.4 | Analysis of Data and Reduction of Ap Candidate List | 52 |
| 6.3 | Preliminary Testing | 53 |
| 6.3.1 | Testing of Period Searching Methods | 53 |
| 6.3.2 | Preliminary Testing of the Routine | 54 |
| 6.3.3 | Accuracy of PDM | 54 |
| 6.3.4 | False Positive Identification | 55 |
| 6.4 | Future Work | 55 |
| 6.4.1 | Sectors from Cycle 2 Onwards | 55 |
| 6.4.2 | Further Analysis of Objects Observed in Multiple Sectors | 56 |
| 6.4.3 | Utilising TESS Full Frame Images | 56 |
| 6.4.4 | Follow-up Observations | 57 |
| 6.4.5 | Changes and Adjustments to the Routine | 58 |
| 7 | Conclusion | 59 |
| | References | 59 |
| | Appendices | 64 |
| A | Final List of Candidate Ap Stars | 64 |
| B | Routine Code | 77 |

List of Figures

| | | |
|----|---|----|
| 1 | Light curve of an Ap star, demonstrating clear repetition on the order of ~ 5 days. This light curve is of TIC281668790, which likely has two surface spots. | 1 |
| 2 | Lomb Scargle periodogram of the light curve from TIC281668790. The two major peaks are clearly identifiable. The first peak is representative of half the rotation period of the object, and the second period is the full rotation period. | 2 |
| 3 | The light curve of TIC281668790, folded over its rotation period of 3.948(3) days. This demonstrates how the rotation period can be determined from the star's luminosity variability. | 4 |
| 4 | Top-left, the light curve of TIC66434034, a δ Sct star. Top-right, TIC219234987, a γ Dor star. Bottom-left, the light curve of the same δ Sct star, folded over a period of 0.17 days, demonstrates the high-frequency variation within this type of star. | 5 |
| 5 | Phase folded light curves of, from top-left clockwise: a detached (TIC436158814), semi-detached (TIC55092869), and contact eclipsing binary (TIC66646031), demonstrating their variation from one another. | 6 |
| 6 | The observed regions for a single sector in TESS, depicting the area of the sky each CCD covers. Image courtesy of Ricker et al. (2014). | 7 |
| 7 | Box Least Squares processed for TIC281668790, with incrementally larger autopower values. Calculation times are also presented. | 12 |
| 8 | Box Least Squares periodograms compared with Lomb-Scargle periodograms for three separate stars. | 13 |
| 9 | Lomb Scargle processed for TIC281668790. Similarly to Figure 7, this is presented with incrementally finer grid spacing and calculation time included. | 14 |
| 10 | The process of the routine. | 16 |
| 11 | The results from the routine plotted against the results from Cunha 2019. The continuous red line represents a 1:1 ratio; the dotted red line represents a 2:1 ratio. | 23 |
| 12 | Period determined for the routine plotted against the effective temperature of the object, for all light curves where the routine provided a rotation period. | 27 |
| 13 | The light curve of TIC358511856 demonstrated in (top to bottom) sectors 4, 6 and 8. This demonstrates the larger missing gaps of data in sectors 4 and 8 that reduced their quality of data. | 28 |
| 14 | Phase Dispersion Minimisation for TIC35905913. The shaded regions are the regions the routine investigated with PDM. | 31 |
| 15 | Top-left: light curve of TIC183802904. Top-right: folded with the routine's value of 21.2(2) days. Bottom: folded with a value of 19.49(17) days determined by a wider PDM search. | 32 |

| | | |
|----|---|----|
| 16 | Phase Dispersion Minimisation for TIC183802904. The shaded regions are the regions the routine investigated with PDM. | 33 |
| 17 | Phase Dispersion Minimisation for TIC170060823. The shaded regions are the regions the routine investigated with PDM. | 33 |
| 18 | Top left: the unfolded light curve for TIC41026067. Top right: the folded light curve for the same object. Bottom: the PDM graph, with the regions the routine investigated highlighted. This object is not an Ap star and does not show any repetition in its light curve. | 34 |
| 19 | The unfolded light curves of TIC279741942 and TIC382067804, which the routine identified as having periods beyond 14 days in specific sectors. Upon inspection, these are eclipsing binary stars. | 35 |
| 20 | The unfolded light curve of TIC349647797 demonstrates the discontinuity in sector 10 and 11 data. | 36 |
| 21 | TIC21504987 light curve, folded over the identified rotation period of 2.26(1) days, demonstrates varying amplitude typical of a lower-temperature star. | 37 |
| 22 | Folded light curve of TIC7780491 over a period of 1.87834(5) days. . . . | 41 |
| 23 | The plot of rotational period against effective temperature, for only the final set of 610 Ap candidate stars. | 42 |
| 24 | The Kiel diagram for the data. Clockwise from top-left: for all stars within the initial data set, for all stars where the routine returned a value, and for only the stars in the final data set. | 43 |
| 25 | Left; sector 4 light curve for TIC44889961. Right, same object in sector 5. | 45 |
| 26 | Left, the unfolded light curve of TIC258837989 as observed in sector 11. Right, the same light curve folded over a period of 0.888 days. | 45 |
| 27 | Light curve for TIC323999777. | 46 |
| 28 | Left; folded light curve for TIC78566138 using the routine's period value of 7.5(1) days. Right; same object folded over the value of 7.89(3) days from a wider PDM search. | 47 |
| 29 | Light curve for TIC393162912. | 48 |
| 30 | Folded light curves for TIC469246567, with a period of 2.050(3) days, and TIC141127435, with a period of 3.241(4) days. | 48 |
| 31 | Sectors 1-13 data for TIC358459933 plotted on the same axis. This demonstrates how data could potentially be stitched together from multiple sectors to provide a longer time base, though also demonstrates the issue with discontinuities that comes up when trying this. | 57 |

List of Tables

| | | |
|---|---|----|
| 1 | The table of objects that were used for development and initial testing of the routine. Period values are from (Cunha et al., 2019). ^[1] This is the approximate period of the main frequency group within γ Dor (Antoci et al., 2019). | 10 |
| 2 | This table is an expansion of Table 1. As with Table 1, literature values for the period are from (Cunha et al., 2019). ^[1] This is the approximate period of the main frequency group within γ Dor (Antoci et al., 2019). | 21 |
| 3 | Performance of the routine when testing false positive objects. | 24 |
| 4 | The results from the routine broken down by sector, presented in absolute values and in terms of percentages. | 29 |
| 5 | The period lengths from the routine broken down by sector. The long period stars are inclusive of the very long period stars. | 29 |
| 6 | The low temperature results from the routine broken down by sector. Low T_{eff} is inclusive of very low T_{eff} | 37 |

1 Introduction

1.1 Ap Stars

A-type stars are stars that have an effective temperature within the range of 7500-10000K. Ap stars are a subset of A-type stars that are characterised by magnetic peculiarities and overabundances of elements such as Si, Cr, Sr or Eu. They have strong magnetic fields, on the order of kilo-Gauss, which stabilise the star's atmosphere and allow atomic diffusion to occur (Kochukhov, 2011). Atomic diffusion separates the elements through the combined effects of radiative levitation and gravitational settling. This results in unevenly distributed elements at the surface of the star, causing long-lived surface spots to form (Kurtz, 1990; Cunha et al., 2019). These chemical spots cause variations in the luminosity of the star which characterises the light curve of Ap stars, as demonstrated in Figure 1.

When a periodogram is generated for an Ap star, such as in Figure 2, multiple evenly spaced peaks are present. These represent harmonics within the original light curve of the fundamental frequency. This fundamental frequency represents the rotation period in an Ap star. Harmonics occur when multiple sine waves are needed to properly fit a sinusoidal model to the light curve; they show up on the periodogram as factors of the fundamental frequency. They are easily identifiable by the repetition of peaks and dips. They serve as a good way to determine if the light curve is stable, as would be expected in Ap stars. If a star has two near-identical spots, half a rotation could be misidentified as the fundamental frequency.

Ap stars are slow rotators and tend to have significantly longer rotation periods than typical A-type stars (Shultz et al., 2018), averaging 3-4 times slower rotation than typical A-type stars (Stepien, 1998). This is theorised to be the result of a magnetic braking

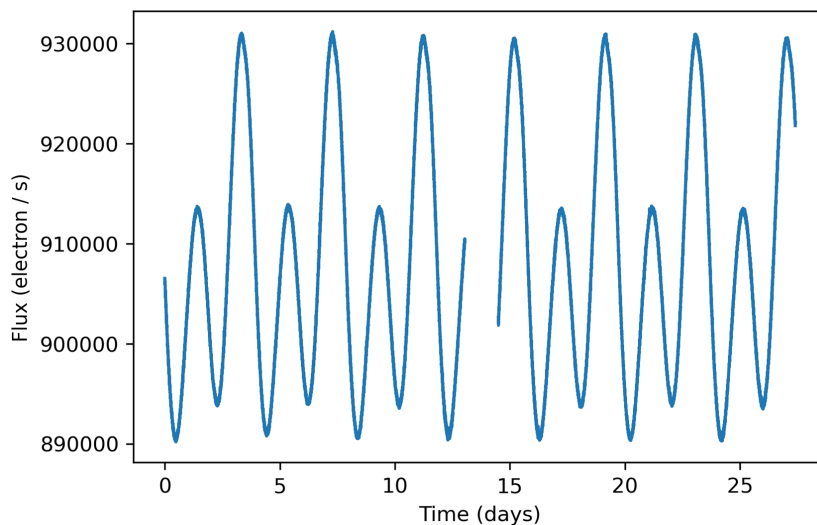


Figure 1: Light curve of an Ap star, demonstrating clear repetition on the order of ~ 5 days. This light curve is of TIC281668790, which likely has two surface spots.

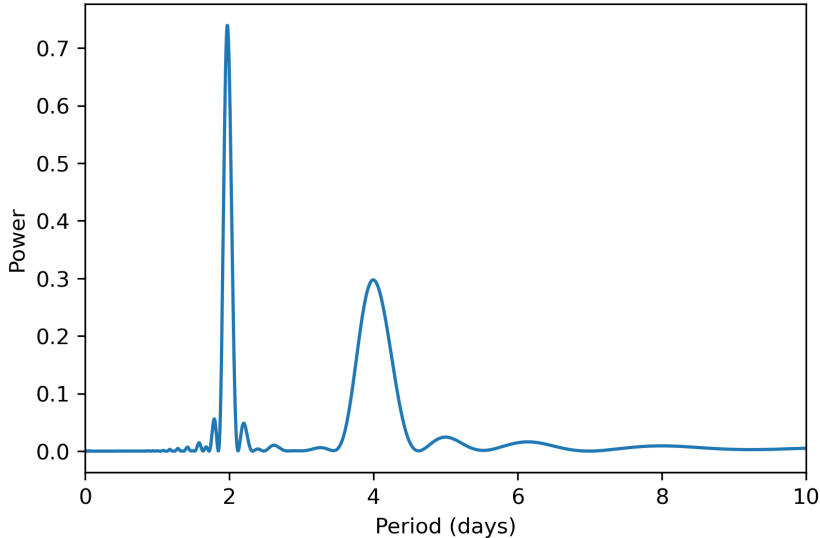


Figure 2: Lomb Scargle periodogram of the light curve from TIC281668790. The two major peaks are clearly identifiable. The first peak is representative of half the rotation period of the object, and the second period is the full rotation period.

mechanism at play within these stars extracting their spin angular momentum (Liu & Chen, 2014), which likely occurs during the pre-main sequence phase of stellar evolution (Stepien, 1998). Ap stars can have rotation periods as low as half a day (Mathys, 2004). The upper limit on rotation periods is not well constrained, with some estimates suggesting centuries (Mathys, Kurtz, & Holdsworth, 2020).

As the star rotates, the aforementioned chemical surface spots come into view and cause low frequency luminosity variability that is visible in the star’s light curve. On Ap stars, these spots have lifetimes that are significantly longer than the typical rotational period of their stars (Mathys et al., 2020), thus the presence of these spots, alongside the resultant luminosity variability, can be used to calculate the rotational period of a given Ap star.

There are a few factors that make Ap stars ideal candidates for investigating magnetic chemically peculiar stars. Typical main sequence A-type stars do not usually exhibit star spots. Smaller, lower mass stars, such as F-type and G-type stars, may develop short-lived star spots from disturbances in their magnetic fields, that could cause them to be mistaken for Ap stars (Sikora et al., 2019). Larger, higher mass stars may develop star spots from chemical peculiarities, though rapid rotation in the stars creates a turbulent convection which means the chemical surface spots don’t remain stable over the period of multiple rotations (Cantiello & Braithwaite, 2011) and can complicate the period-determination process.

Ap stars are comparatively uncommon, with Renson and Manfroid (2009) identifying only 3652 known (or probable) Ap stars. Many of these do not have known rotation periods. The number of known Ap stars will have risen since Renson and Manfroid’s paper, however they are still vastly outnumbered by chemically ordinary stars. Sikora

et al. (2019) suggests magnetic chemically peculiar stars account for a tenth of main sequence A-type stars with masses around 3 solar mass; Kochukhov and Bagnulo (2006) suggested 5-10% of upper main sequence stars are chemically peculiar.

Ap stars typically have large-scale organised magnetic fields (Hubrig, North, Schöller, & Mathys, 2006). 300 G is seen as the effective minimum magnetic flux for Ap stars (Aurière et al., 2007). Ap stars have been discovered that contain very large surface magnetic fields, in excess of 11 kG (Babel & North, 1997). By comparison only a small fraction of magnetic chemically normal A stars have magnetic fields in excess of 3kG (Bagnulo, Landstreet, Lo Curto, Szeifert, & Wade, 2003). The strongest magnetic fields are found in faster rotating Ap stars (Hubrig, North, & Mathys, 2000).

There are further subcategories of Ap stars, which are discussed in Cunha et al. (2019). Rapidly oscillating Ap (roAp) stars are a type of Ap star that demonstrates high frequency pulsation alongside the rotation of the star. Meanwhile, the term non-oscillating Ap (noAp) stars is used to refer to stars that demonstrate properties similar to roAp stars though do not show any sign of pulsations. α^2 Canum Venaticorum variables ($\alpha^2 CVn$) are Ap stars or Bp stars that have observable modulation in their light curves.

On the HR diagram, normal A-type stars cover the whole width of the main sequence; however magnetic stars - including Ap stars - are concentrated towards the centre of the main-sequence band and have usually completed at least 30% of their main-sequence lifetime (Hubrig et al., 2006). Younger Ap stars may exist, less far along the main sequence, and Folsom et al. (2012) reports an Ap star candidate that has been detected on the pre-main sequence, however this is not a widely reported occurrence.

1.2 Importance of Period Determination with Ap Stars

We can learn more about Ap stars from observing them. Their rotational periods can be determined through the luminosity variability in the star as the light curves will phase fold over the rotation period, as demonstrated in Figure 3.

Furthermore, Ap stars present the best examples of stellar magnetic fields beyond our own sun, representing a large portion of known magnetic stars. Historically, Ap stars have been the only stars besides the sun in which we have been capable of directly detecting a magnetic field (Hubrig et al., 2006). Their magnetic fields can be observed to further understand a range of mechanisms in stars, such as atomic diffusion (Hümmerich, Paunzen, & Bernhard, 2020), the effects of period differentiation that lead to a wide variation in stellar rotation periods (Mathys et al., 2019), and the effect of magnetic fields on the formation of chemical surface spots (Rusomarov, Kochukhov, & Piskunov, 2014). These can all be studied in further detail with more known Ap stars, and how these aspects affect the star's rotation period can be investigated.

The mechanisms behind the chemical peculiarities and strong magnetic fields in Ap stars aren't understood entirely. The chemical peculiarities are most commonly explained through atomic diffusion (Rusomarov et al., 2014), wherein the opposed effects of radiative levitation and gravitational settling within the star cause some elements to sink and

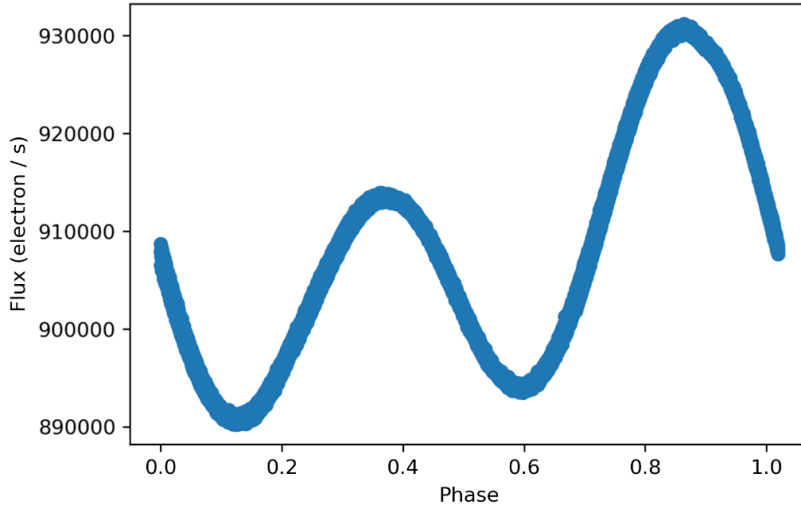


Figure 3: The light curve of TIC281668790, folded over its rotation period of 3.948(3) days. This demonstrates how the rotation period can be determined from the star’s luminosity variability.

others to be driven outwards. These make Ap stars useful for investigating the effects of radiative levitation and gravitational settling.

The magnetic fields are thought to be fossil remnants of flux swept up during the star formation process, or alternately produced in the pre-main sequence stage of the star’s life (Braithwaite & Spruit, 2004). Again, their origin isn’t understood well.

Further, Ap stars’ braking mechanisms are also not fully understood, and the range in rotation periods in Ap stars will be constrained by the braking mechanism, so studying their rotation periods also helps facilitate a greater understanding of their braking mechanisms.

1.3 Other Luminosity Variability Sources

Light curves can also demonstrate variability due to many factors other than spots that are of interest here. This complicates the identification of Ap stars through light curves and making determining their rotational frequencies also more difficult. Understanding these possible sources of variability helps control for them.

Delta Scuti (δ Sct) and Gamma Doradus (γ Dor) stars are two classes of pulsator stars. The higher-frequency variations observed within these stars are caused by perturbations in the radius of the star. For γ Dor stars, this is high-radial-order gravity (g) modes with low frequencies (*periods* $\gtrsim 0.25d$), whereas δ Sct stars are due to low-radial-order pressure (p) modes which operate on a high frequency (*periods* $\lesssim 0.25d$) (Antoci et al., 2019). δ Sct stars can be excluded by their high frequencies, whereas γ Dor stars have to be excluded based on the presence of non-harmonic repeating variations in their light curves. Light curves for examples of each of these are presented in Figure 4. High amplitude δ Sct stars (HADS) have large amplitudes and non-sinusoidal light curves (Antoci et al., 2019).

Slowly Pulsating B-type (SPB) stars are multi-periodic pulsating stars that pulsate

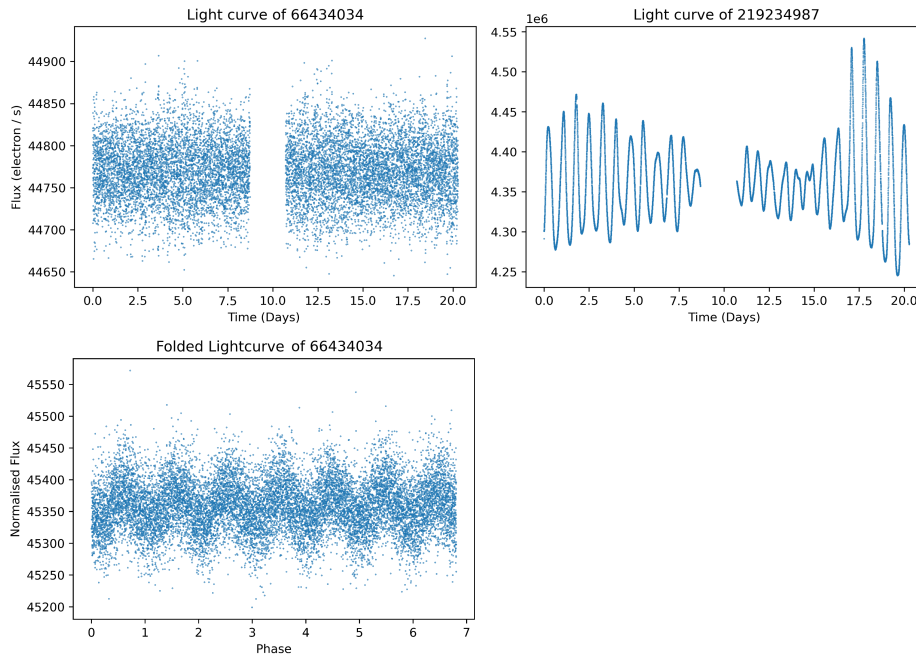


Figure 4: Top-left, the light curve of TIC66434034, a δ Sct star. Top-right, TIC219234987, a γ Dor star. Bottom-left, the light curve of the same δ Sct star, folded over a period of 0.17 days, demonstrates the high-frequency variation within this type of star.

due to the same g modes present in γ Dor stars. They show photometric variability with periods ranging from 0.3 days to 5 days (Fedurco, Paunzen, Hümmerich, Bernhard, & Parimucha, 2020). They are able to be discarded as period analysis demonstrates multiple non-harmonic periods.

Pulsation variability is also observed from cepheid variables, which undergo radial and non-radial pulsation. They otherwise are not well constrained by magnetic fields nor rotation rate (Neilson & Ignace, 2015). Beta-cepheids pulsate radially, between two amplitudes over a period on the order of hours. Mira variables are long-period variables that may demonstrate pulsation lengths in the region of years (Groenewegen, 2017).

A large number of stars located in eclipsing binary systems are likely to be a common source of object variability. Stars in a binary system eclipse one another, blocking out their light, resulting in a light curve with two (typically asymmetric) dips. Eclipsing binary stars can be classified as detached, semi-detached, and contact binaries; these depend on the distance between the two stars relative to their size, and the state of shared atmospheres and envelopes.

The light curves of contact binaries are strongly distorted due to the stars' close proximity; their maxima are rounded, and they typically have a period of less than 1 day (Deb & Singh, 2011). Semi detached and detached eclipsing binaries show progressively flatter light curves between eclipses (Graczyk, 2003). The comparison between detached, semi-detached and contact binaries is demonstrated in Figure 5, using objects from Mortensen, Eisner, IJspeert, Kochoska, and Prsa (2021).

Consideration also needs to be paid to F-type and G-type variable stars. These are

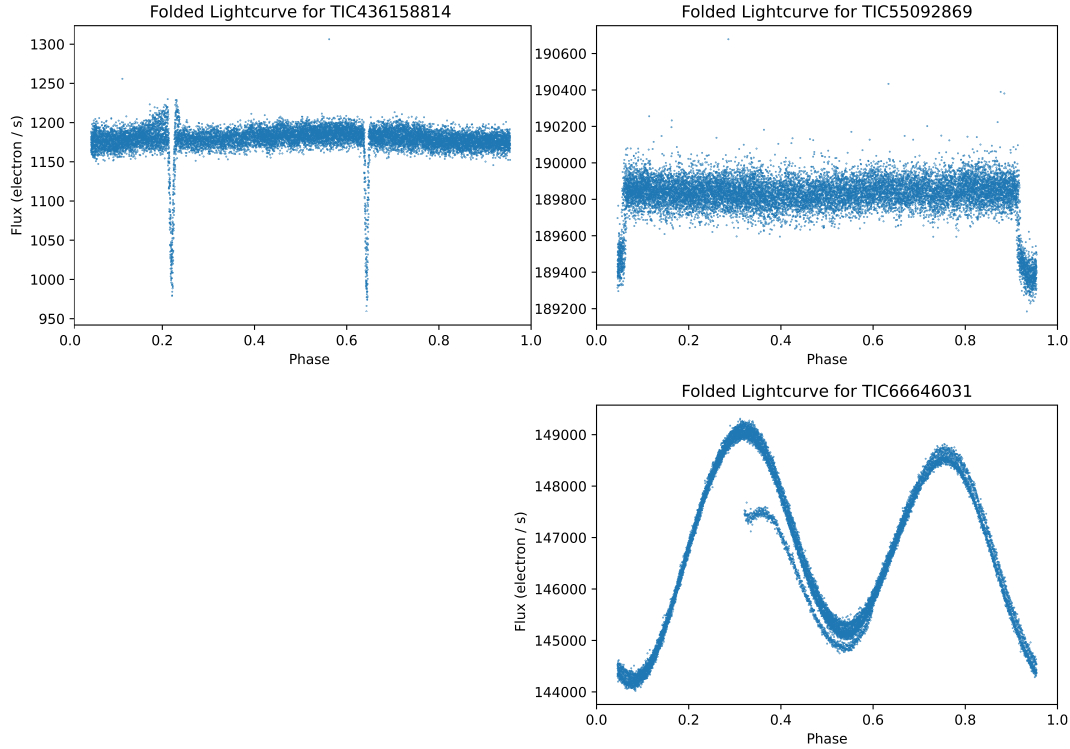


Figure 5: Phase folded light curves of, from top-left clockwise: a detached (TIC436158814), semi-detached (TIC55092869), and contact eclipsing binary (TIC66646031), demonstrating their variation from one another.

lower-temperature stars than Ap stars, that can develop short-lived surface spots from perturbations in their magnetic fields. They do not show the chemical and magnetic peculiarities of Ap stars, though the variations in their light curves also are the result of surface spots.

Most pulsating stars, outside the ones previously mentioned, have lower amplitude variation, at a higher frequency than rotational modulation. This allows them to be limited by ignoring high-frequency variability sources with periods below 8 hours.

Ap stars were identified during the project using the luminosity variability in their light curves. Since an Ap star is classified by these chemical abundances, and not by the low-frequency variability, it is possible for an Ap star to demonstrate no luminosity variability if: the rotation period is too long; the rotation axis is oriented towards the observer; the magnetic axis and rotation axis are near-aligned; or chemical spots have not formed away from the magnetic poles. The reliability of the results from the routine is investigated later.

1.4 TESS Data

The data for the project was sourced from the Transiting Exoplanet Survey Satellite (TESS). TESS was launched by NASA in April 2018 and began observing in July 2018. The goal of the primary mission was to discover new exoplanets, with high-resolution

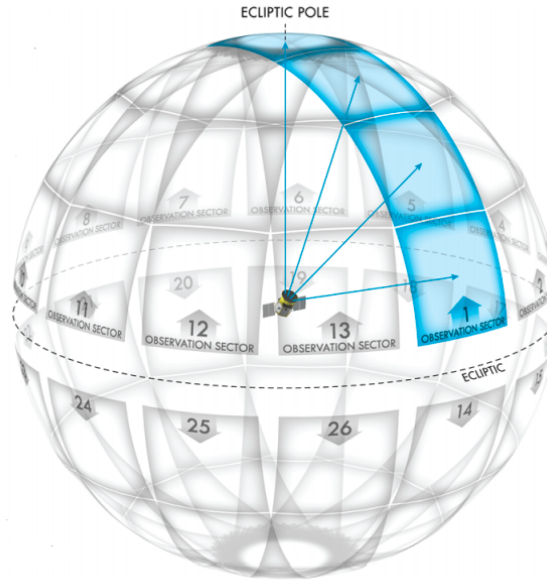


Figure 6: The observed regions for a single sector in TESS, depicting the area of the sky each CCD covers. Image courtesy of Ricker et al. (2014).

results, sensitive to short-term luminosity variability prioritised. The specifications of TESS are outlined in detail in Ricker et al. (2014). The satellite is positioned in a highly-elliptical 13.7 day orbit and is fitted with four wide-field optical CCD cameras that cover a sector of sky of $24\text{deg} \times 96\text{deg}$. These observe the brightness of pre-selected main-sequence dwarf stars within a sector that are likely to have exoplanets, at a two-minute cadence over the course of 27 days (two complete orbits). There is some overlap in these sectors of sky, primarily near the ecliptic poles, so certain stars are observed within multiple sectors of sky. This overlap is demonstrated in Figure 6.

Following the completion of the primary mission goal in July 2020 with the observations in Cycles 1 and 2, TESS moved on to its extended mission. With this, TESS began re-observing the southern ecliptic hemisphere, observing similar fields as in the main mission goal. Variations in the TESS orbit over time mean these do not line up exactly. Objects that were in gaps between sectors in the primary mission are being observed in the extended mission, furthermore a number of objects observed in the first cycles are being re-observed. The 2-minute cadence observations for the extended mission are identical, though 1000 pre-selected targets are also being observed with a 20-second cadence, and the full frame images are being observed with a shorter 10-minute cadence.

Data releases for TESS are freely available on the Mikulski Archive for Space Telescope (MAST) site. These data releases consist both of raw data for the stars and calibrated light curve data with the aforementioned 2 minute cadence. Full frame images of the entire sky region are also released, with a cadence of 30 minutes. These full frame images could allow data collection for any stars not preselected for 2 minute cadence observations, instead utilising their stellar field data, although they were not utilised within this project.

The calibrated data is data that has been processed by the Science Processing Opera-

tions Center’s (SPOC) TESS data processing pipeline, discussed in (Jenkins et al., 2016). Spikes in luminosity could appear on the data from coronal mass ejections, however the pipeline is intended to reduce the effect on these. This pipeline prescribes null values to luminosity readings in the data wherever poor quality data is removed. These need to be handled, though overall improve the quality of the final light curve.

There are numerous limits that are imposed from the constraints of the TESS data. It is only possible to identify any object with a period of rotation shorter than half the observation period. For an object present in a single TESS sector, this will be ~ 14 days. The 2-minute cadence also technically constrains a minimum observable period on the order of minutes, though that is significantly below the minimum known rotational periods of any Ap stars.

The objects observed with TESS are typically within the magnitude ranges of $5 \lesssim T_{\text{essMag}} \lesssim 16$ where T_{essMag} represents the bandpass of 600 to 1000 nm (Ricker et al., 2014; Fausnaugh et al., 2018). It is possible to observe stars brighter than this range, however the vast majority of observed objects lay within the range.

Results from TESS have already been used widely for scientific research, as the data collected is ideal for astroseismology, gyrochronology, identifying exoplanets, and the study of eclipsing binary stars, among other topics.

Cunha et al. (2019) analyses 83 specific Ap stars using data from the first two TESS sectors to evaluate the quality of the TESS data, and further uses the short-cadence TESS data to evaluate previously known roAp stars against the data.

Sikora et al. (2019) evaluates the first 4 sectors of TESS, evaluating 1962 A-type stars within the set to determine any that exhibit variable light curves in line with rotational modulation; Monte Carlo simulations of synthetic light curves, alongside Lomb Scargle periodograms, were used to inform their search for the expected shape of Ap star periodograms, which was used as a search criteria to eventually identify 134 high-probability candidate rotational variables.

Mathys et al. (2020) covers data from the entirety of TESS Cycle 1, however searches instead for known Ap stars that show no variability in their light curve and postulates that these must be long-period. Their search investigates only 1014 known Ap or Ap-candidate stars, and determines 54 of these to be long-period Ap stars.

These all demonstrate the use of TESS data for identifying or classifying Ap stars and their parameters. Two of these use prior identified Ap stars. There is a focus on the earlier TESS sectors. Further, these papers all work with significantly smaller sets of data than this project, and demonstrate less automated investigations into Ap stars. All these papers were used to inform the procedures taken for this project.

The aim of this project was to develop a routine to identify magnetic chemically peculiar A-type (Ap stars) stars within the southern hemisphere using data from TESS Cycle 1 observations. This routine was intended to be capable of identifying Ap stars alongside their rotational periods, as well as being capable of discarding false positives in the form of other types of variable objects. The routine was written in Python, and was intended to perform this automatically.

2 Testing Period Searching Methods

Period analysis of objects allows for the investigation of repeating signals in an object's light curve. For any light curve analysed as part of this project, this needs to be performed to aid in identifying the type of variability present in the object. This helps for the false positive identification that is required for the routine, to eliminate objects that are not Ap stars. These need to eventually be performed automatically as part of the routine developed for the project, so simplifying the process is important. Following on, the period analysis can be used to identify the most likely period of rotation of the object.

There are numerous methods that can be employed to determine the frequencies present in light curves. Fourier analysis fits sinusoidal waves to the data. Box least squares periodograms fit boxes to the data, and search for the repetition in the boxes. Lomb Scargle performs a least-squares fitting of a sine wave. Phase dispersion minimisation investigates non-sinusoidal variation by folding the data then evaluating the spread of the data points. All four of these methods were investigated to determine their effectiveness and whether they are viable for the purposes of the routine.

There are also a number of more complex period-searching algorithms that have been developed: Shin and Byun (2004) developed an algorithm that performs a coarse search followed by a finer search to process large volumes of data with relative high speed. Feroz, Hobson, and Bridges (2009) meanwhile presents a more complex Bayesian analysis tool that is claimed to be highly efficient. However, for the simplification of the routine, these complex algorithms were disregarded and not investigated.

Some of these aforementioned methods require data without gaps. Further, they can produce very different qualities of results and may vary largely in terms of calculation time. Fourier series, box least squares periodograms, Lomb-Scargle periodograms, and phase dispersion minimisation were all tested to evaluate how effectively they can perform period analysis with TESS data, with all these factors being discussed below.

Since the routine was intended to be written in the Python coding language, this testing of period analysis was performed with Python implementations of the methods. The specific implementations are indicated where relevant. The routine will also be running on a large number of light curves - in the region of ~ 80000 from 13 sectors of TESS - so the processing time of these methods is of great importance.

A small set of data was collected to aid with this period testing, alongside the initial development of the routine. This data is identified in Cunha et al. (2019) and Antoci et al. (2019), and is discussed in further detail in Section 4.1 of the thesis. Table 1 summarises these objects, providing known periods from literature alongside the amplitudes of the variability. Amplitudes are taken as the difference between the maximum and minimum flux values. Larger amplitudes show less noise.

| TICID | Known Period | Amplitude ($e^{-1}s^{-1}$) | Type |
|-----------|---------------------------------|------------------------------|----------------|
| 350146296 | 4.2006(1) days | 373 | roAp |
| 237336864 | 2.661 21(29) days | 1057 | roAp |
| 211404370 | 6.442(12) days | 457 | roAp |
| 281668790 | 3.9517(1) days | 41019 | noAp |
| 307642246 | 1.8607(2) days | 4530 | $\alpha^2 CVn$ |
| 219234987 | ~ 0.77 days ^[1] | 276582 | γ Dor |

Table 1: The table of objects that were used for development and initial testing of the routine. Period values are from (Cunha et al., 2019). ^[1] This is the approximate period of the main frequency group within γ Dor (Antoci et al., 2019).

2.1 Fourier

The Fourier transform is a method of producing a power spectrum of frequencies for a given data set, facilitating frequency analysis of a star. There are numerous algorithms to apply a Fourier transform to a light curve, however these ultimately attempt to fit sinusoidal functions to the given data set. This can be performed as detailed in Cooley and Tukey (1965), which is the definition utilised by numpy’s inbuilt fast Fourier transform (fft) tool.

The Fourier transform is a well-tested and reliable technique, and it has been applied to TESS data previously: Cunha et al. (2019) uses Fourier transforms to detect low-frequency rotational modulation in light curves; meanwhile Bognár et al. (2020) uses Fourier transforms with TESS data identify significant frequencies below the false alarm probability in multiple objects which may be utilised as inputs for future analysis of the pulsators observed. Deb and Singh (2009) suggest it as a potential pre-processor for more complex light-curve analysis. Thus, theoretically Fourier transforms could be used as a coarse and non computationally-intensive method to analyse the parameters of a light curve, identify if there are any significant frequencies to filter out non-variable stars, and identify if the significant frequencies present are harmonic and of the frequencies expected from rotation modulation.

While Fourier analysis was a quick method, and theoretically showed a lot of promise for the project, it proved temperamental in testing. The numpy implementation of the fft was used for testing. Dependent on how the data was handled before and after fft was applied, the method would identify a frequency corresponding to a period an order of magnitude below the literature value (e.g., an 8 minute period for an object with a known 11 day period), or would spike at a value of 0.

The reason behind the Fourier transform not working was not determined. Further, the fft implementation of the Fourier transform could not handle non-uniform time gaps between data points, such as are present in the TESS data. A different implementation of Fourier, such as the discrete Fourier transform, may have been able to accomplish the task. After the testing, and considering the advantages and disadvantages of the Fourier method, it was not considered productive to persevere further with this method.

2.2 Box Least Squares Periodogram

Box least squares (BLS) periodograms (Kovács, Zucker, & Mazeh, 2002) fit boxes to the data by searching for variation between two discrete levels in the light curves. Repetition in the fitted boxes is then used to generate a power spectrum. This requires data without gaps, however it produces high-quality results with relatively little computing time.

The astropy implementation of BLS was used for testing. This method also calculated a grid of periods to test using the autopower function; a lower autopower results in more periods being tested and a finer output graph, at the cost of an increased computation time.

The autopower can be set to any numeric value. This allows the method to investigate frequencies on an incrementally finer level, at the expense of increasing the calculation time for the method. This can be finely tuned, as is demonstrated in Figure 7. This correlation between sampling frequency and calculation speed is direct and is discussed in Kovács et al. (2002). Typically an autopower of 100-250 was optimal for providing a fine search. As can be seen on the figure, a finer frequency grid allows BLS to investigate higher frequencies. Halving the autopower doubles the maximum investigated frequency. An autopower of 250 allowed the probing of frequencies within the TESS data of up to 1.5day^{-1} ; an autopower of 100 or lower means BLS can begin to probe pulsation signatures.

The period grid calculated from the autopower can be adjusted for BLS, and minimum and maximum investigated periods can be set, which allows this to investigate a large number of periods very quickly. With more manual oversight on the analysis of the light curves, this ability to fine-tune the results could be greatly beneficial, however this is not practical for the purposes of an automated routine. BLS would be a highly useful and powerful technique if the project had a stronger focus on individual objects. Furthermore, the resulting power spectrum produces fine results, and peaks representing frequencies are narrow and well defined, as can be seen in Figure 7. This would allow the determination and location of multiple well-defined variability frequencies with a single run-through of the process.

BLS was sensitive to harmonics, and the speed of computation was highly dependent on the sensitivity of the period grid, and it had an inability to deal with null values and gaps in data (even with the largely evenly spaced TESS data).

2.3 Lomb-Scargle Periodogram

The Lomb-Scargle periodogram (Lomb, 1976; Scargle, 1982) performs a least squares fitting of a sine wave to the data set. It is based on the methods of the classical periodogram, which are themselves defined by the application of the Fourier power spectrum (VanderPlas, 2018).

Lomb-Scargle is an effective tool for separating noise from frequency components (Vio, Andreani, & Biggs, 2010), and results in a power spectrum similar to those presented from BLS. A comparison between the two resultant methods is presented in Figure 8.

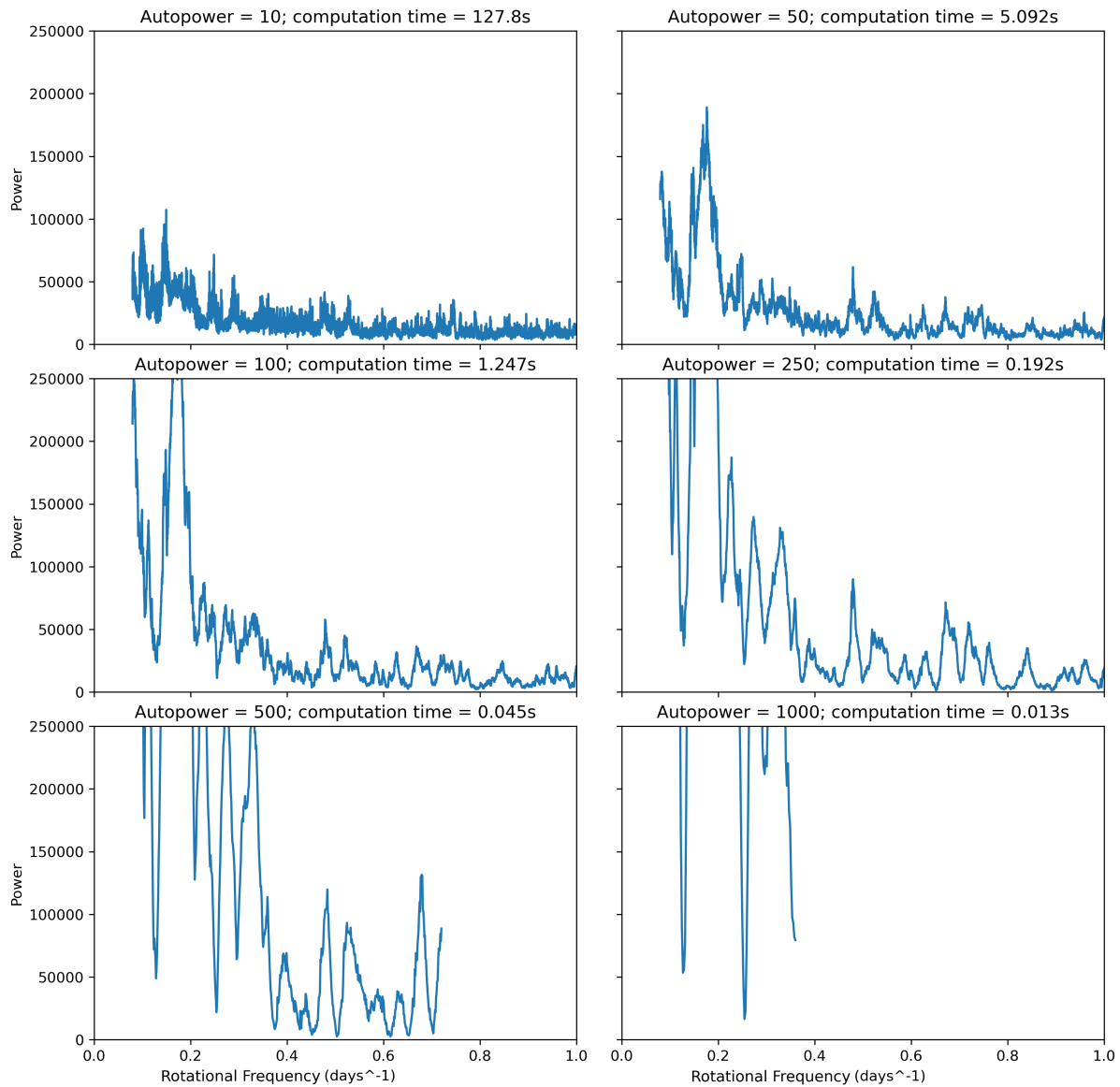


Figure 7: Box Least Squares processed for TIC281668790, with incrementally larger autopower values. Calculation times are also presented.

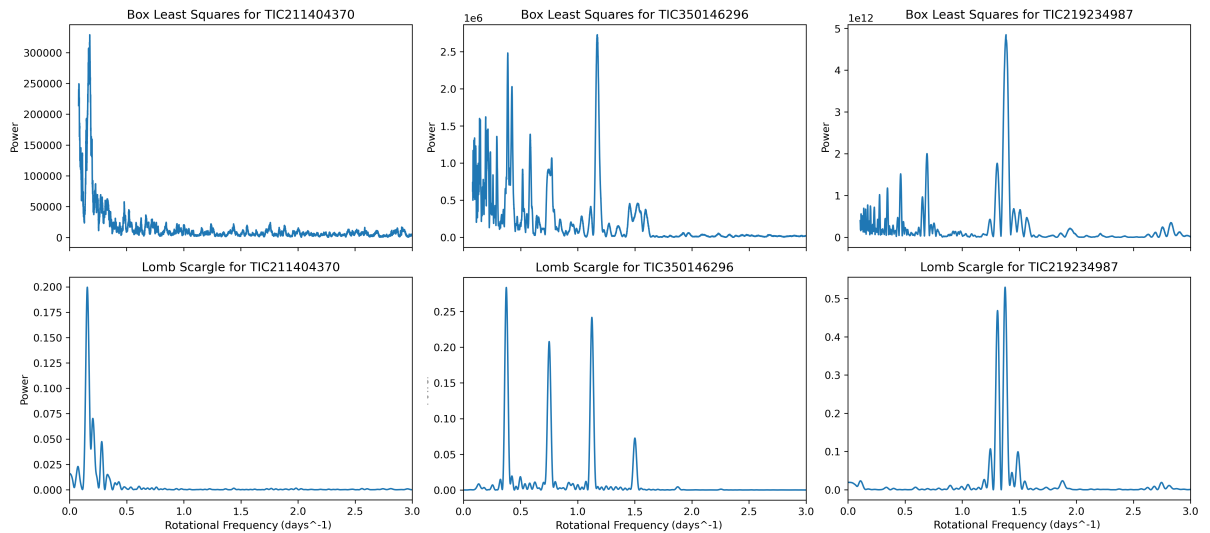


Figure 8: Box Least Squares periodograms compared with Lomb-Scargle periodograms for three separate stars.

Lomb-Scargle is capable of handling unevenly-spaced data. Lomb-Scargle also has a lower sensitivity than Box Least Squares to very low-frequency signals, and provides clearer, more well-defined peaks which are more suited for the automation of the routine. Since the identification of Ap stars, discussed later, is accomplished using a number of basic assumptions, the clearer peaks of Lomb-Scargle are well-suited to keeping the routine basic and efficient.

The astropy implementation of Lomb Scargle was used for testing. The autopower function of Lomb-Scargle appeared to give less control than that of BLS, though the frequency grid provided a similar range of control as BLS. The Lomb-Scargle frequency grid is based on the samples per peak value, where it is assumed each peak represents a width of $\sim 1/T$, where T is the time base of the observations. Commonly, a value of 5-10 samples per peak is used. The trade-off between grid spacing and computational time that was present in BLS was similarly true with Lomb-Scargle, however the computational time is far less affected by smaller grid spacing in Lomb-Scargle than with BLS. This is demonstrated in Figure 9.

The Lomb-Scargle periodogram has been used before for identification of Ap stars within TESS data, in Sikora et al. (2019). It is one of the best-known and most common methods for calculating periodic content in a signal and - though it's specialised for more unevenly spaced data - it is a proven and effective method.

2.4 Phase Dispersion Minimisation

Phase Dispersion Minimisation (PDM) is a phase-folding method of period determination, and involves folding the data over a set number of test periods and evaluating the smoothness of the folded data sets. This is performed using the method detailed by Stellingwerf (1978). A range of pre-determined periods is investigated: the data are folded

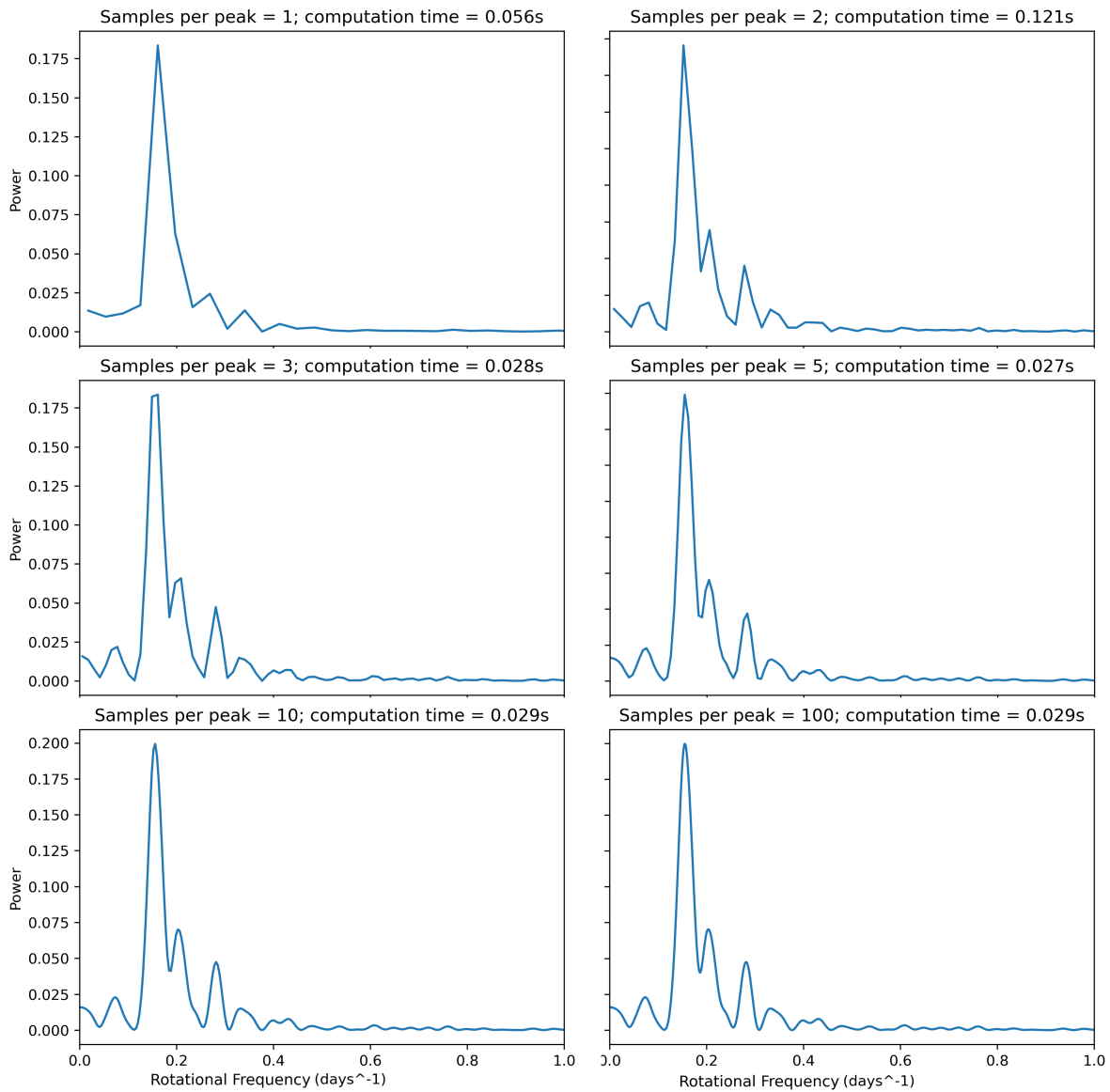


Figure 9: Lomb Scargle processed for TIC281668790. Similarly to Figure 7, this is presented with incrementally finer grid spacing and calculation time included.

on these periods sequentially, then binned in bins of an equal, pre-determined width. For each non-empty bin, the variance of its data points is calculated. This equation is given in Stellingwerf (1978) and is defined by equation 1:

$$\sigma^2 = \frac{\sum(x_i - \bar{x})^2}{N-1}$$

These variances are compared against the variance of the data overall, and the process is repeated with each period. Once complete, the periods can be plotted against their individual variances. Where this graph reaches a minima indicates a frequency of variability.

Generally, PDM is a technique positioned for investigating non-sinusoidal variation and can be effective when sparse data is present. It does not require even time intervals.

The candidate periods tested during this method are equally spaced between two pre-determined limits. More test periods increases the accuracy, at the cost of increasing the processing time. However with few spaced out test periods, representing a coarse search, this process risks missing important minima. Similarly, the number of bins can affect the calculation time. Both factors could easily compound and escalate, resulting in a significantly increase in calculation time.

The PDM method implemented was a custom implementation. This gave the method a high level of adjustability.

From testing, PDM proved to be a time-inefficient method that outputted accurate rotation periods. The search parameters of the method could be adjusted to a wide degree. This rendered it an inefficient method for a coarse period search, however very useful for finer searches over a restricted range of periods.

2.5 Comparison of Methods

Lomb-Scargle and BLS are very different methods with comparatively similar results. Both methods would be suitable for performing a coarse search, which is used to identify and classify the type of variability demonstrated by an object. Either could have been utilised for the routine and achieved the desired effect. Lomb-Scargle was ultimately chosen for its increased reliability and faster processing time, to be implemented into the routine as a coarse searching method.

In terms of a fine search method, to focus on a determined peak and its harmonics, PDM produced the best results. PDM was chosen to be used in conjunction with Lomb-Scargle, first being run on the harmonics of the detected rotational period from Lomb-Scargle, then being run again finer still on the most prominent harmonic to determine a highly accurate value for the period of any detected Ap stars.

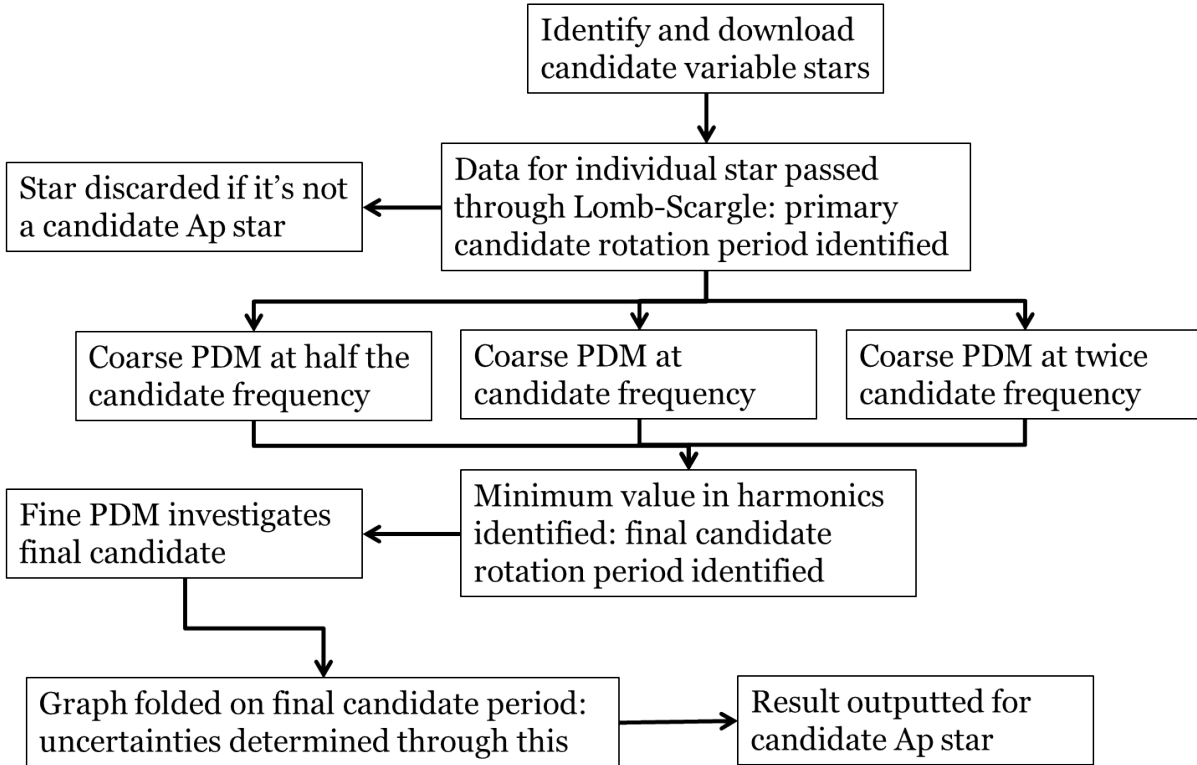


Figure 10: The process of the routine.

3 Development of Routine

The routine for this project was developed to detect Ap stars efficiently. Due to the large volume of data in the project, reducing processing time as much as possible was a central aspect of the routine's development. The routine works in multiple stages. Initially, all candidate stars are identified and if their effective temperature is within the pre-determined parameters, they are downloaded from the MAST servers. The individual star light curves are passed through the Lomb-Scargle routine; wherein primary rotation periods are identified or, if the star shows variability not consistent with Ap stars, the given light curve for the star is discarded.

The primary rotation periods, where identified, are carried forward. The light curves are then passed through three coarse PDM tests, investigating the primary rotation period, alongside half that period and twice that period to cover the most likely cases where LS identified harmonics. The minimum value from these three tests is then carried forward and put through PDM again with a finer test period grid to identify a final candidate period.

The light curve is then folded on this final candidate period, with the variance in the points along the folded line helping to determine the uncertainties in the calculated period. With this complete, the candidate Ap star is identified with a given rotation period and uncertainty.

A flow chart of this process is demonstrated in Figure 10. The individual steps of the routine are covered in more detail below.

3.1 Data Acquisition

The acquisition of bulk amounts of data from the MAST database was handled through Astroquery, as part of a second supplementary Python script. The Astroquery package for Python, detailed in Ginsburg et al. (2019), is an efficient tool that is capable of querying NASA’s MAST database following given specifications. This has been used in the project to quickly and simply handle, download and investigate the required data.

This identification and acquisition of data forms the first part of the routine. The routine queries the MAST database for TESS data on a sector by sector basis, searching for observations with timeseries data available. The acquired data products are the TESS Science Processing Operations Center (SPOC) 2-minute cadence light curves (Caldwell et al., 2020). For each data product that satisfies these criteria, the TIC ID of the observed object is recorded by the routine.

This provides a list of 20000 unique IDs per sector. Once the query is complete, Astroquery is used again to search up the IDs in this list within the TESS Input Catalogue, and from it find the star’s effective temperature. Each star is then categorised by its recorded temperature in one of three categories: stars with temperature within the specified range; outside the specified range; and no recorded effective temperature. These temperature parameters are specified within the code, and can be easily modified. For the purposes of the project, the parameters were set at a minimum of 6000K and a maximum of 20000K. The minimum was chosen as advised in Cunha et al. (2019), to match the effective temperature range of A-type stars and the approximate lower range of Ap star temperatures. This wider range ensures we have sampled the coolest of Ap stars and incorporated the intrinsic errors into the range, including uncertainty that results from the cooler spots of Ap stars. More stringent temperature cut-offs could be applied to the data for analysis easily.

The main advantage of handling the acquisition through code is the automation of the process. The process is also faster than manually acquiring the data, however is still limited by the connection to the MAST servers. When timed, the routine is capable of identifying and categorising all stars within a single sector in approximately 90 minutes.

Within an individual sector, these temperature criteria reduce the number of objects to investigate down to 4000-8000 stars, dependent on the sector. The vast majority of stars lay outside the temperature parameters. Fewer than a thousand stars per sector have no given effective temperature.

The list of objects outputted by the identification process can then be used by Astroquery again to download the relevant light curves. Any time series data products where the given TICID and observation ID (sector number) match those provided by the identification routine are downloaded. This process is more time-consuming than the identification process and is, again, limited by the connection to the MAST servers. Downloading the relevant data for a single TESS sector takes approximately a day. All data required for the routine is downloaded before the rest of the routine is run.

3.2 Data Handling

By acquiring the pre-processed light curves from NASA’s Data Processing Pipeline, as detailed in Jenkins et al. (2016), the data used has already been handled to account for instrumental issues. The processing also includes photometric analysis to fit and remove background flux resulting from the stellar background light from zodiacal light and the diffuse stellar background. It further identifies and corrects for instrumental signatures or step discontinuities within the CCDs present on the TESS satellite.

A negative consequence of this pre-processing is that some systematic errors that are adjusted could be the result of low-frequency signals that aren’t present in a single sector’s data. This could likely mean Ap stars with rotation periods on the order of months could be unidentifiable even if a full year’s worth of data is available for it. Nevertheless, the pre-processing is beneficial for the routine and project. This means data acquired for the project does not need to undergo significant additional processing.

Once a light curve is read into the routine, the TICID, time data, flux data, and sector number are read in by the script. A number of flux values are removed from the processed data as part of the pipeline, and are represented as nan-values in the flux data. These are data points where the median absolute deviation of the flux exceeds 1×10^{-3} , or which otherwise have data quality flags and issues with them (Fausnaugh et al., 2018). These nan-values in the flux data are removed by the routine, and for each removed flux value, the associated time data point is also removed. This preserves the time axis. Furthermore, for ease of reading the axis, the minimum time is also subtracted from all time data points, so the time axis starts on $t = 0$.

The variance in flux for the data set, σ^2 , is also calculated at this point for the use of PDM. This is not intensive to compute, and results in a negligible increase in calculation time.

3.3 Identifying Ap Stars; Handling False Positives

The data is then passed through a coarse Lomb-Scargle periodogram. This coarse search is calculated with 30 samples per peak, which approximates to 291600 periodogram evaluations (VanderPlas, 2018). The Lomb Scargle search is performed over the range of periods possible to be observed with the data. It could be argued that it is inefficient to investigate periods up to the length of the data set, and a dynamic upper period for the investigated frequencies would be more optimal. Similarly, the 30 samples per peak is vastly oversampled. However, the calculation time for this Lomb-Scargle process, even with these inefficiencies, is vastly quicker than the time taken for PDM to process, and these inefficiencies provide the highest quality periodogram for the false positive detection to work from.

The resulting power spectrum from this is then used to identify potential false positive objects, as well as to identify the primary candidate rotation period for the star. Peaks in the power spectrum are identified by running through the power spectrum and calculating the false alarm probability of each point. The false alarm probability is the chance of any

significant peak being the result of noise in the data or a legitimate signal, and is discussed further in VanderPlas (2018). Any points where this false alarm probability is below 0.001 (representative of 3 standard deviations from random) represents a statistically significant frequency, and the point is stored in a separate array. Once the entire set of data points is run through, the stored frequencies are then investigated. Typically a single peak is represented in multiple data points, so the routine removes data points if there are any neighbouring points with a lower false alarm probability. This, in effect, reduces the Lomb-Scargle data down to an array of its significant peaks by frequency and statistical significance.

To identify any false positives, the code performs three checks: no significant peaks, non-harmonic peaks, and frequency too high. Light curves with no significant peaks, such as from non-variable stars, demonstrate very low amplitude peaks in their Lomb-Scargle periodograms, generally noisy data, and were easily identified as the false alarm probability of all the points is significantly above the cut-off and the false alarm probability removes all frequencies.

Light curves that show too high a frequency are less likely to be rotationally variable Ap stars. Ap stars can have rotation periods as low as 12 hours, thus stars with a primary candidate period shorter than 12 hours are removed. Later in the process, this lower limit is raised to ~ 19 hours as it is preferable to exclude candidate Ap stars to reduce the number of false positive objects.

Harmonics are investigated by taking the period of the first significant peak and investigating if subsequent peaks have periods that are a multiple of the first one. If the frequencies of all significant peaks are divisible to a tolerance of $\pm 5\%$, the peaks are deemed to be harmonic. Else, the light curve is discarded for having non-harmonic peaks. If a light curve only has a single significant peak, which may occur if the star's rotation period is slow enough to be observed only once or twice in the data, this check is skipped.

Any light curves that satisfy these three conditions are determined to be candidate Ap stars, and their frequencies are investigated further. PDM is then applied to the approximate frequencies correlating to the first, second and fourth peak.

3.4 Determining Rotation Periods of Stars

The rotation periods of the candidate Ap stars is identified through PDM. PDM is utilised for a coarse investigation of the identified candidate periods as well as harmonics of the candidate period. It is then further utilised for a fine investigation to determine the most likely candidate period with a greater degree of accuracy. This uses the same implementation of PDM as in the testing.

The coarse investigation examines the primary rotation candidate from the Lomb Scargle procedure, as well as the frequencies half and twice that value. In a harmonic periodogram, this would represent the first, second and fourth peaks. This decreases the chance of the final light curve being a factor or multiple of the true value. For each of

the three investigated frequencies, 20 test periods are calculated, ranging from 90% of the period to 110% of the period. Once this is performed for all three test values, the lowest calculated phase dispersion from the three tests is taken as the most likely rotation period.

The second, fine investigation performs the same PDM routine around just this most likely value. Again, 20 test periods are calculated, with the range investigated reducing to between 95% and 105% of the test period.

3.5 Errors

Uncertainty within the final determined result is calculated from the variance within the folded light curve. This is accomplished using the following equation, which is adapted from Montgomery and Odonoghue (1999):

$$\sigma(f) = \sqrt{\frac{6}{N} \frac{1}{T} \frac{\sigma(m)}{a}}$$

Within this equation, N represents the number of data points overall, T represents the time baseline of the observations, $\sigma(m)$ represents the scatter of data points at any point along the line, and a represents the amplitude in the graph. $\sigma(m)$ is calculated as the difference between minimum and maximum data points at the minima and maxima of the graph, averaged: it is a representation of the scatter of points at an approximately flat point on the plot. The amplitude is measured from minima to maxima.

The factor of π from the equation presented in Montgomery & O'Donoghue is removed, as that is to handle the sinusoidal signal the initial derivation was handling. The final period error is also inflated by a factor of 10, as advised in the original paper. With this inflation factor, the uncertainties agree within uncertainty from values presented in literature in the vast majority of cases.

4 Testing of Routine

Once development of the routine concluded, testing needed to be performed with a limited selection of objects to develop a degree of confidence in the routine. There are two major points with which the routine needed to be tested: whether the routine could correctly identify Ap stars and discard non-Ap stars; and whether the routine was returning the correct rotational periods within uncertainty for identified Ap stars. This testing could then be utilised to further make improvements to the routine, and to identify points at which it was failing. The routine was tested multiple times with different data at different points along its development.

4.1 Initial Testing to Develop Routines

During development of the routine, any testing carried out was performed using a limited set of light curves. These light curves include a number of stars that are well-discussed in literature. These light curves were intended to represent any potential light curve the routine could face, and to ensure the routine was performing as expected.

Six stars, each discussed in Cunha et al. (2019) and covered earlier in Table 1, were included in this testing. Table 2 demonstrates the stars again alongside the rotation periods calculated by the final iteration of the routine.

TIC237336864 has several observable pulsation multiplets which creates a challenging pulsation spectra, however this does not affect the detection of any low-frequency rotation signals within the star and the routine correctly identified the rotation period. TIC350146296 was tested with sector 1 and sector 4 observation data. Both times it provided a period in agreement with the literature value. TIC281668790 is a noAp star that has a distinct double-wave feature; the routine identified a value that, whilst not within uncertainty of the literature value, was approximately the same as literature. TIC307642246 was in agreement with the value from the literature.

TIC211404370 was disregarded by the routine for demonstrating non-harmonic peaks. This object has no clear harmonics present in its periodogram. Combining this with the light curve's low amplitude and the effects of instrumental noise, it is reasonable the

| TICID | Known Period | Routine Period | Amplitude ($e^{-1}s^{-1}$) | Type |
|-----------|---------------------------------|----------------|------------------------------|----------------|
| 350146296 | 2.661 21(29) days | 2.66(2) days | 373 | roAp |
| 237336864 | 4.2006(1) days | 4.20(2) days | 1057 | roAp |
| 211404370 | 6.442(12) days | N/A | 457 | roAp |
| 281668790 | 3.9517(1) days | 3.948(3) days | 41019 | noAp |
| 307642246 | 1.8607(2) days | 1.8607(2) days | 4530 | $\alpha^2 CVn$ |
| 219234987 | ~ 0.77 days ^[1] | N/A | 276582 | γ Dor |

Table 2: This table is an expansion of Table 1. As with Table 1, literature values for the period are from (Cunha et al., 2019). ^[1] This is the approximate period of the main frequency group within γ Dor (Antoci et al., 2019).

routine discarded this. The last star, TIC219234987, is better known as γ Dor (Antoci et al., 2019). The routine identified its power spectrum to have non-harmonic peaks, and correctly disregarded it.

4.2 Testing on Cunha Dataset

Since the development of the routine was performed using only a few known variable stars, its adaptability to other light curves was untested. To validate the routine, it was then tested on the set of variable stars identified within Cunha et al. (2019). This is a set of 83 stars, primarily Ap stars and roAp stars, with a few δ Sct, γ Dor and otherwise unidentified rotators present. A couple of these stars were already discussed and tested earlier. Most of these stars were given periods with uncertainties in the paper and, where available, prior literary periods were quoted.

Light curves for the stars listed in the literature were downloaded from as many of the available sectors as possible, using the process described earlier. Any stars with no period given in literature were discounted. A number of these objects were present in multiple sectors, and 360 light curve files were downloaded. These light curves were processed and analysed using the routine blindly and without any human input.

Of the 377 total light curves, 223 produced the correct result. The number of light curves that produce a given answer are used for this comparison since a single object may have multiple light curves that could produce results that disagree with one another. These light curves represented 53 correctly identified stars within the group of 85 - wherein they returned a value that either agreed within uncertainty with the literature value. This corresponds to a 62% agreement with the Cunha results.

Of the 154 “incorrect” results, 38 of these came from the routine identifying a harmonic of the rotation period and quoting a period twice the expected value. The other 116 incorrect results arose from light curves being incorrectly identified as not-Ap stars due to their peaks in the Lomb-Scargle periodogram not agreeing within the limits set, and being disregarded as a result. No light curves that were meant to be disregarded were incorrectly not-disregarded, however this data set had a strong focus on Ap stars and the routine wasn’t tested greatly on its ability to disregard false positives.

Nevertheless, this test demonstrated the accuracy of the period determination method utilised in the routine. The combination of Lomb-Scargle and PDM investigating harmonics resulted in a value near or within experimental uncertainty of the literature value 85% of the time, and confidently provided either the correct value or the closest harmonic in all cases where light curves were not disregarded. The accuracy of these values with respect to the literature values provided in Cunha et al. (2019) is demonstrated in Figure 11.

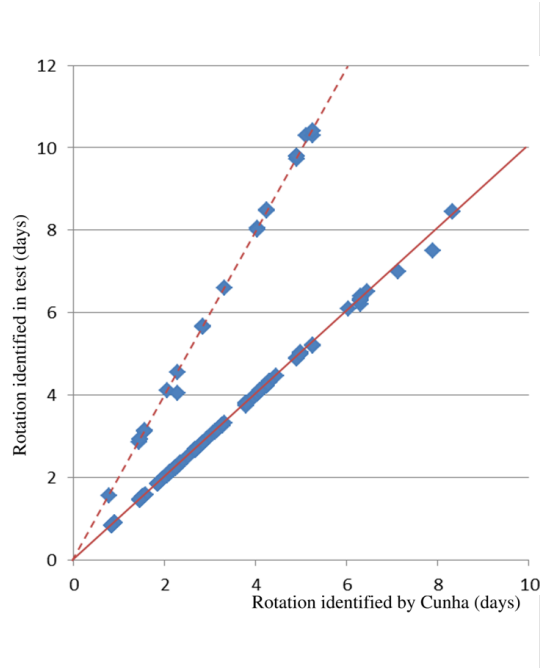


Figure 11: The results from the routine plotted against the results from Cunha 2019. The continuous red line represents a 1:1 ratio; the dotted red line represents a 2:1 ratio.

4.3 Testing False Positives

A small data set of potential false positive objects was then collated, collected and tested against the routine. This data set included binary stars, δ Sct, γ Dor, SPB, F-type and G-type variable stars, and non-variable stars. Each set of these false positive objects were passed through the routine. The intention of this test was to establish if the routine was capable of identifying and discounting different potential non-Ap objects consistently and beyond a random chance. The results of this test are demonstrated in Table 3.

Due to the small scale of the data set, data was selected manually with the intention of representing a random sample, and the light curve files were collected using the same astroquery script developed for the full routine. None of the light curves used in this set of tests were tested prior on the routine, and the routine acted blindly and without human oversight for this.

The routine was tested first against a semi-random selection of eclipsing binary stars outlined in Kirk et al. (2016) from the Kepler database. Only stars with a period under 15 days were investigated, as this is the range of periods TESS data is able to probe confidently. 10 objects, and 27 total light curves, were processed through the routine. 26 light curves were correctly disregarded by the routine, with a single light curve being incorrectly processed by the routine.

δ Sct and γ Dor stars, though covered somewhat in the previous tests, were tested more thoroughly to ensure the routine would not handle them incorrectly. This used a random selection of 19 δ Sct and γ Dor stars identified in Antoci et al. (2019). All of these were correctly identified and discarded by the routine for either having non-harmonic peaks or a primary peak at too high a frequency ($> 3 \text{ days}^{-1}$).

A small selection of SPB stars, beta-Cepheids and Maia stars identified in Balona and Ozuyar (2020) were also tested with the routine, with 20 light curves from 12 objects being processed. 19 light curves were correctly disregarded, with only TIC4207261 - a star demonstrating both SPB and beta-Cepheid variability - being incorrectly processed.

To investigate the handling of non-variable stars, 40 light curves from 11 stars were chosen using the list of stars. These stars were identified by Kepler, Giovannini, Kanaan, Wood, and Claver (1995). All 40 light curves were correctly disregarded. Whilst it was expected that the routine would disregard all these due to a lack of significant peaks in the Lomb-Scargle power spectrum, only 17 were disregarded for that. The other light curves were disregarded instead as they had peaks that were not harmonic of one another.

Variable lower-temperature stars, such as F-type and G-type stars, which would have unstable surface spots, were also tested. Rather than selecting stars manually for this test, stars were identified with astroquery. This works the same as in the routine, though the search parameters are looking only for stars of $T_{\text{eff}} < 7500\text{K}$ within TESS sector 1. This process was interrupted after 132 lower-temperature stars were identified, as this was considered a large enough sample size. Then, downloading from the entire TESS catalogue, 826 light curves were acquired. As with all the previous tests, these were processed with the routine.

Of the 826 light curves fed into the routine, 132 were incorrectly processed. 225 were disregarded for having no significant peaks in the Lomb-Scargle power spectrum. 445 were disregarded for having non-harmonic peaks. 24 were disregarded for having too high a frequency. This corresponds to approximately 84% of lower-temperature stars being correctly disregarded by the routine.

As the light curves in this final test were only pre-selected for their temperature, it is possible not all of them showed forms of variability - for example if they did not have visible surface spots during the observation period. The 225 disregarded for no significant peaks indicates this is true for 27% of the data selected. Discounting those, the routine correctly disregarded only 84% of variable lower-temperature stars. The routine does not seem as effective at handling lower-temperature variable stars as it is with previous tested variable objects. This is not of a great concern, as the routine already checks and rejects stars by temperature. Typically, these lower-temperature stars would be identified when looking up their temperature with astroquery, and would not be included. However, in the case of a star with unknown temperature, or an incorrectly measured temperature in

| Object Type | Sample | Correctly Rejected | Accuracy |
|----------------------------|--------|--------------------|----------|
| Binary Stars | 27 | 26 | 96% |
| δ Sct/ γ Dor | 19 | 19 | 100% |
| SPB | 20 | 19 | 95% |
| F-/G-type Variables | 826 | 694 | 84% |
| Non-variable Stars | 40 | 40 | 100% |

Table 3: Performance of the routine when testing false positive objects.

the catalogue, this result indicates a $\sim 84\%$ chance they will be caught by the routine.

The routine handled between 84% and 100% of potential false positive objects with this set of testing, averaging 94% correct over all sets of data discussed. Overall, the quantity of light curves included in this testing is limited, however the random sampling for each set of objects is intended to cover the most general and most likely false positives within the TESS data set. Nevertheless, the routine demonstrated a general ability to identify and disregard these false positives within this test, and these results help increase confidence with the routine.

4.4 Refinement of Routine from Testing

When the routine was tested on a wider set of data, there were two separate common cases that would cause an error in the code. These cases both had to be accounted for and the code had to be altered to cope with them.

The first error arose if there were no significant peaks in the Lomb-Scargle power spectrum. This indicates a star is not variable or its variability could not be detected in the TESS data. A check for this was implemented into the routine, and in this case an assumption is made that the star is non-variable.

The second error came from a rounding error with the implementation of PDM, wherein the code would define more intervals to investigate than were expected. A check was implemented into the code for this situation that would delete any unexpected intervals.

Once these errors were amended, the routine demonstrated a high level of accuracy during testing in its resultant frequency values. The tradeoff between accuracy and processing time established during the preliminary testing and code development was also validated by these tests, and this test allowed a degree of confidence to be ascribed to the routine.

5 Results of Routine Run-through

The routine, as described above, was then applied to the data present in TESS Cycle 1 observations, from sectors 1 through to 13. This covers the southern ecliptic hemisphere sky. In all, 38728 individual objects - represented in 79088 light curves - satisfied the pre-determined temperature parameters and were analysed with the routine. 9127 of these objects had variability according to the routine in line with the variability expected in an Ap star. This suggests approximately 24% of the objects are Ap candidate stars according to the routine, which is significantly higher than the 5-10% indicated in literature.

These candidate Ap stars are a broad selection that needs to be reduced to a more specific list. Decreasing the number of candidate objects reduces the time that follow-up observations or analysis would take. The candidate Ap list is reduced by analysing the results in multiple ways: investigating the position of candidate stars when their effective temperature is plotted against rotation period, alongside the analysis of data for stars present in multiple sectors, and manual inspection to identify light curves that the routine has not handled. Anomalous results can be identified by this aforementioned plot, shown in Figure 12, and easily investigated and removed. Further, if stars do not show consistency between multiple sectors, they are easily disregarded as non-Ap stars. This is discussed in Section 5.3. The steps performed manually here can also help to inform any future iterations of the routine.

With this plot of effective temperature against the routine's result, there are two major issues that are immediately present. Firstly, there is a large grouping of stars that are apparently demonstrating variability beyond the time scale expected with the data, including a notable clumping of stars where the routine identified a rotation period of 30-35 days. Secondly, there is a large number of apparent Ap stars present near the lower temperature cutoff, where we would instead be expecting fewer Ap stars and more variable F-type stars. Both groups of stars are followed up on.

5.1 Comparisons between Sectors

First, the results were analysed on a sector-by-sector basis. Variations in the performance of the routine between different sectors can indicate flaws in the routine or any potential issues with the TESS data. The results of the routine, separated by sectors, are demonstrated in Table 4. This shows the total number of light curves analysed per sector, as well as the breakdown of how false positives were rejected and the overall number of Ap candidate stars for which values were calculated. Table 4 presents these results as absolute values and as percentages of the total value analysed.

It must be noted that the three tests for false positive objects are performed sequentially: if non-harmonic peaks are detected, the routine will not probe the frequency of the primary peak. Similarly, if no significant peaks are detected, there is no reason to investigate harmonics.

Between 4500 and 7000 light curves were analysed per sector, with an average of 6000

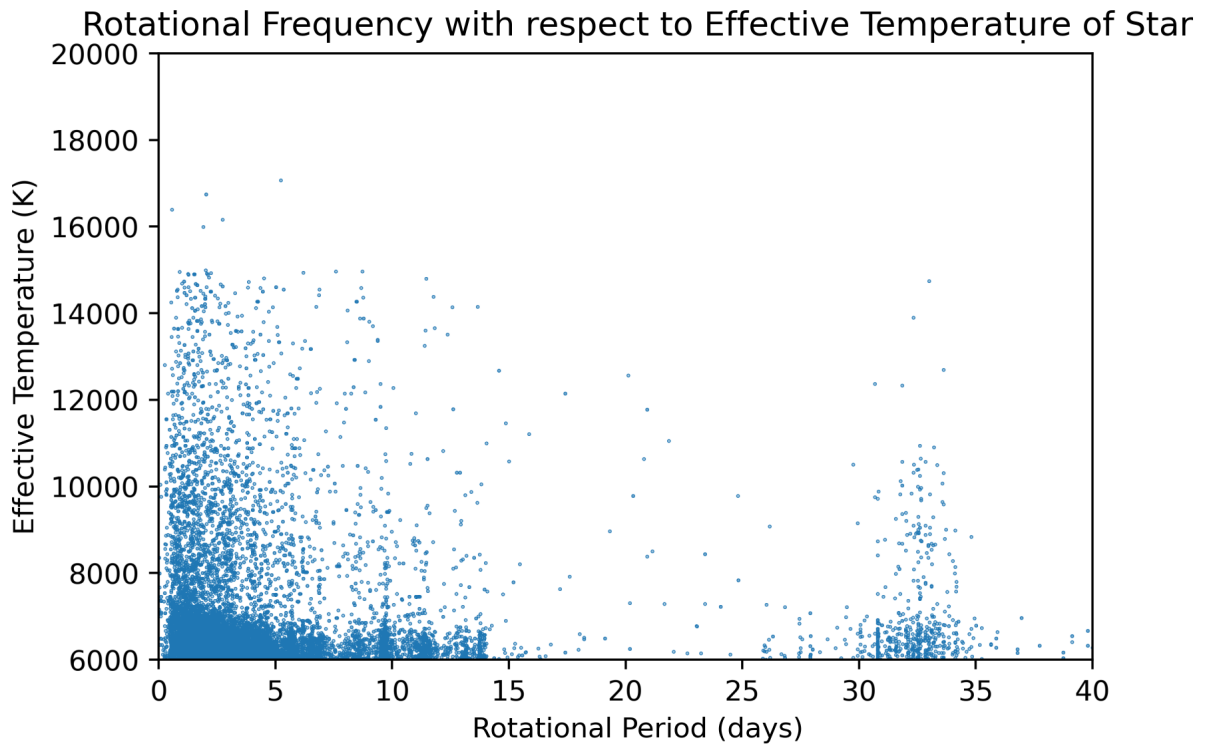


Figure 12: Period determined for the routine plotted against the effective temperature of the object, for all light curves where the routine provided a rotation period.

per sector. In most sectors, approximately 80% of these light curves were discarded as false positives. Sectors 4 and 8 present notable exceptions to this, where a significantly larger proportion of light curves were discarded by the routine for not presenting harmonic peaks. There is also a marked decrease from these sectors in the percentage of light curves with no significant peaks or a frequency that's too high.

Upon further investigation of these sectors, this appears to be due to the lower quality of the data in these sectors. Large portions of data from these sectors has been filtered out by the pre-processing pipeline, resulting in a far larger gap in the data from sector 8 and two separate pronounced gaps in sector 4 data. This is demonstrated in Figure 13, where sectors 4 and 8 can be seen compared to a more typical TESS sector.

This missing data may have made any harmonic frequencies more difficult for Lomb Scargle to identify, resulting in less defined peaks on the Lomb Scargle periodogram, and meaning the initial period does not get defined as precisely. This increases the chance of harmonics being placed out of the tolerances the routine uses and not being classed as harmonic. There is also the potential that harmonics may not have been detected or considered insignificant by the routine, which would also cause the light curve to be classified as non-harmonic. Missing data reduces the range of frequencies the routine can probe, as well as the range of data present for these frequencies.

The reduction in objects identified with a frequency that is too high is reasonable since the routine approaches the false positive checks sequentially. Discarding more light curves

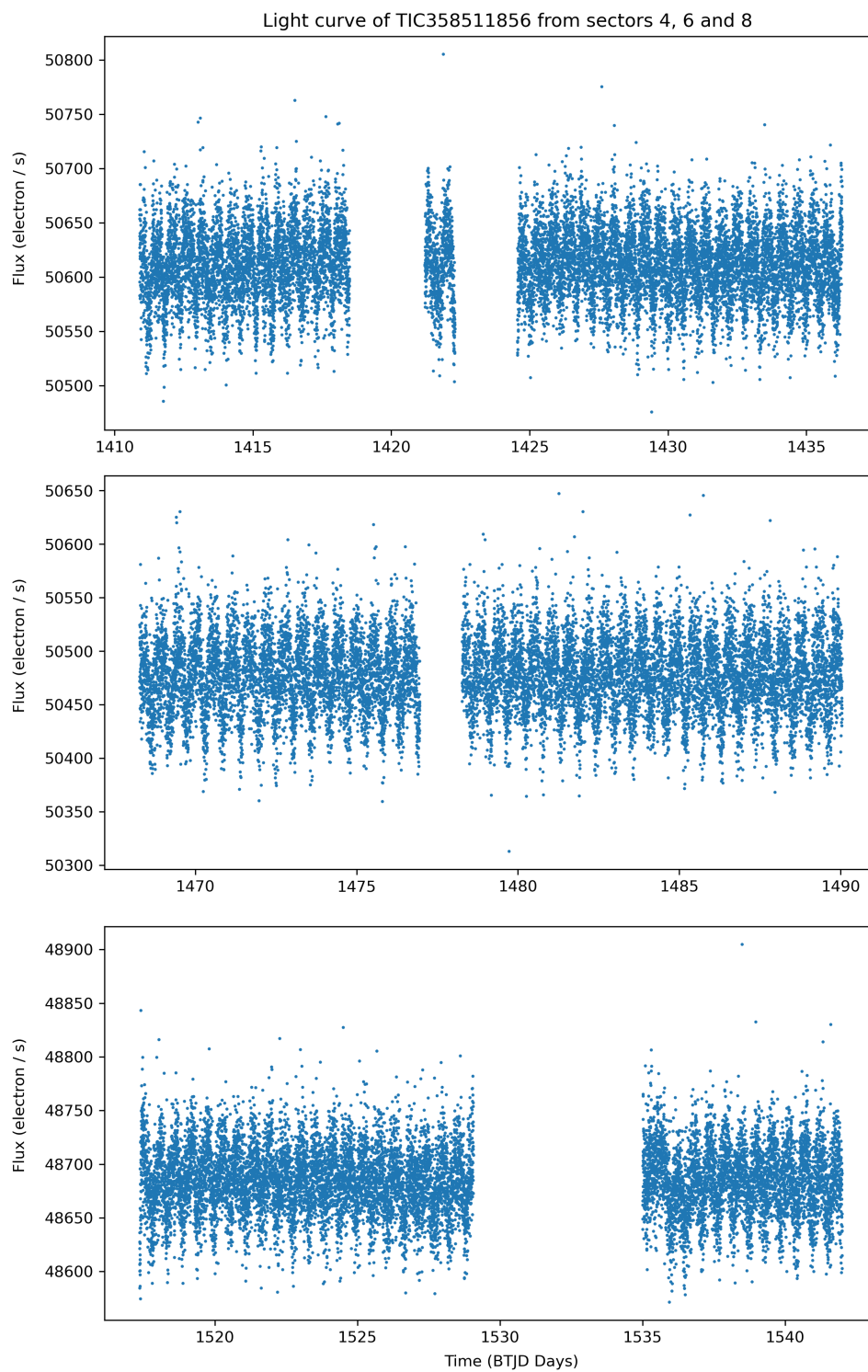


Figure 13: The light curve of TIC358511856 demonstrated in (top to bottom) sectors 4, 6 and 8. This demonstrates the larger missing gaps of data in sectors 4 and 8 that reduced their quality of data.

| Sector | 1 | 2 | 3 | 4 | 5 | 6 | 7 | 8 | 9 | 10 | 11 | 12 | 13 |
|----------------------|------|------|------|------|------|------|------|------|------|------|------|------|------|
| Total | 4630 | 4528 | 4551 | 6308 | 6521 | 6239 | 6130 | 6527 | 7131 | 7132 | 6930 | 7033 | 5428 |
| Non-Harmonic Peaks | 2859 | 2500 | 2425 | 5836 | 4058 | 3277 | 3275 | 6090 | 3853 | 4324 | 4504 | 4335 | 3122 |
| No Significant Peaks | 644 | 1100 | 1242 | 15 | 1000 | 1406 | 1504 | 217 | 1794 | 1251 | 704 | 997 | 1035 |
| Frequency Too High | 150 | 140 | 150 | 155 | 220 | 228 | 230 | 5 | 301 | 278 | 219 | 287 | 169 |
| Value Calculated | 977 | 788 | 734 | 302 | 1243 | 1328 | 1121 | 215 | 1183 | 1279 | 1503 | 1414 | 1102 |
| Non-Harmonic Peaks | 62% | 55% | 53% | 93% | 62% | 53% | 53% | 93% | 54% | 61% | 65% | 62% | 58% |
| No Significant Peaks | 14% | 24% | 27% | 0% | 15% | 23% | 25% | 3% | 25% | 18% | 10% | 14% | 19% |
| Frequency Too High | 3% | 3% | 3% | 2% | 3% | 4% | 4% | 0% | 4% | 4% | 3% | 4% | 3% |
| Value Calculated | 21% | 17% | 16% | 5% | 19% | 21% | 18% | 3% | 17% | 18% | 22% | 20% | 20% |

Table 4: The results from the routine broken down by sector, presented in absolute values and in terms of percentages.

before the frequency threshold is applied results in fewer stars being above the threshold. The reduction in light curves that show no significant peaks is more surprising, as this is checked before the harmonic check. This is likely explained as the reduced data creating more noise in the Lomb-Scargle periodogram and some of this noise passes the significance threshold. Despite this reduction in quality, the results calculated from sectors 4 and 8 can still be used to help identify Ap stars.

To further compare the sectors, the average rotation period from Ap candidate stars in each sector were also calculated. These are presented in Table 5, alongside the number of stars with a long period. Sectors 10 and 11 are notable here for having significantly higher average rotation periods than the other sectors. After inspecting the light curves within this sector, the high-frequency stars identified earlier in Figure 13 are overwhelmingly located in these two sectors. This is investigated in more depth later.

Aside from the two notable exceptions discussed here, the variation between sectors appears to be largely random and will not affect the results from the routine. Comparisons between individual objects observed within multiple sectors are made later.

5.2 Long Period Stars in the Data

The TESS data for each sector spans ~ 28 days, so Ap stars can only be identified through the presence of harmonics if they rotate on the time scale of $\lesssim 14$ days. However, as became evident when plotting the rotation of candidate Ap stars against their effective temperatures, the routine identified a number of stars to have rotation periods beyond 14 days. These stars are investigated further to determine the validity of their identified

| Sector | 1 | 2 | 3 | 4 | 5 | 6 | 7 | 8 | 9 | 10 | 11 | 12 | 13 |
|-------------------------|------|------|------|------|------|------|------|------|------|------|-------|------|------|
| Total | 4630 | 4528 | 4551 | 6308 | 6521 | 6239 | 6130 | 6527 | 7131 | 7132 | 6930 | 7033 | 5428 |
| Mean Period (days) | 4.42 | 4.20 | 3.45 | 3.35 | 4.05 | 2.85 | 3.50 | 3.48 | 3.11 | 6.98 | 12.33 | 3.29 | 4.20 |
| Long Period (>14d) | 28 | 23 | 3 | 7 | 5 | 7 | 8 | 2 | 4 | 141 | 391 | 11 | 6 |
| Very Long Period (>28d) | 13 | 8 | 0 | 3 | 0 | 1 | 0 | 0 | 0 | 136 | 376 | 0 | 0 |

Table 5: The period lengths from the routine broken down by sector. The long period stars are inclusive of the very long period stars.

rotation periods, and to look into what alterations could be made to the routine to mitigate this issue. There is also a large grouping of stars where the routine identified periods beyond 28 days - longer than the time base of the observations - meaning these periods would be impossible to identify from the TESS data set. These results can be easily excluded from the final data set, however it is still important to investigate these and determine where the routine failed.

Of the total 13189 light curves where a value was calculated, the results with periods beyond 14 days represent 636 light curves. This represents approximately 5% of the total light curves that demonstrate harmonic variability. Of these, only 99 sit between 14 and 28 days. These light curves were investigated further to determine if the routine had correctly identified a rotation period or harmonic. The other 537 light curves have a period above 28 days. Table 5 demonstrates how these long-period light curves are distributed on a sector by sector basis, where it is clear that the incorrectly identified light curves occur primarily in sectors 10 and 11.

5.2.1 Long Period Stars ($14 < P_{\text{rot}} < 28$ days)

To investigate the long period stars, their light curves, Lomb-Scargle power spectra, and the graphs of PDM analysis were investigated through inspection. Individual cases are discussed below. Most commonly these long period values are the result of the routine not investigating the correct region when evaluating the harmonics with PDM.

TIC35905913 is a roAp star discussed in Holdsworth et al (2021) that has a rotation period of 7.513(1) days. In TESS Cycle 1, it is observed in sectors 11 and 12. The routine rejects this object in sector 11 whereas it provides a value in sector 12 of 14.8(8) days - the routine identifies a subharmonic of the main frequency. Data for this star also exists in sector 38, from which the routine can correctly identify the rotation period of 7.5(2) days. In the sector 12 data, Lomb Scargle correctly identifies the rotation period around 7 days - however when the harmonics are investigated with PDM, the boundaries of the investigation do not include the full extent of the troughs. This is demonstrated in Figure 14.

TIC183802904, which was only observed in sector 2, shows a light curve that appears to demonstrate Ap star-like features at a period beyond 14 days. The routine determined it to have a period of 21.2(2) days. Through inspection of its folded light curve, in Figure 15, this is clearly incorrect. Cunha et al. (2019) identifies this star and calculates its rotation period of 19.408(17) days. The coarse Lomb-Scargle search correctly identified this as an Ap star, though gave an inaccurate period, which resulted in PDM never investigating the actual rotation period. When run through on the full range of periods, as demonstrated in Figure 16, PDM correctly identifies 19.49(17) days. This demonstrates the ability for a routine to identify rotation signatures in a limited way beyond 14 days, though not with the same degree of confidence as present in shorter periods.

Similarly, TIC170060823 also demonstrates periodic variability with the routine not identifying the actual period. Again, the routine does not investigate the correct region

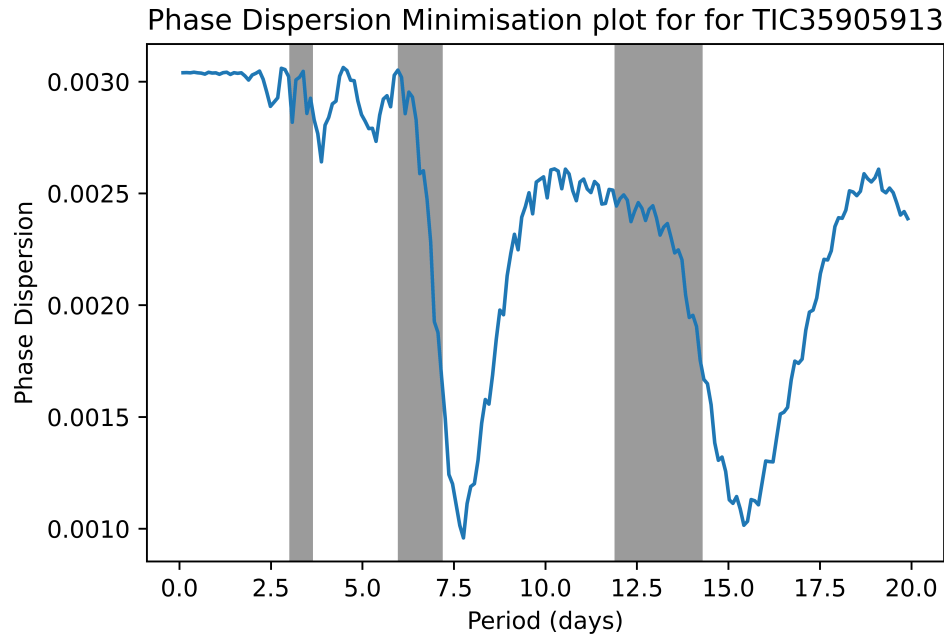


Figure 14: Phase Dispersion Minimisation for TIC35905913. The shaded regions are the regions the routine investigated with PDM.

with PDM and leads to a disjointed folded light curve, as demonstrated in Figure 17. This object only has one light curve present (from sector 12), and is not mentioned in the literature. When analysed again, running directly through PDM, the routine identifies a period of 16.4(7) days.

TIC41026067 in sector 12 demonstrates a failure in Lomb-Scargle, where the routine has detected apparent low-frequency periodic variability in a light curve where there is no clear variability. This light curve, its PDM graph, and its Lomb-Scargle power spectrum are all shown in Figure 18. As can be seen in the central plot of the figure, the minimum phase dispersion calculated from PDM on this star is ~ 2 , which indicates the graph does not fold cleanly over the fold period. An upper bounds on the phase dispersion may provide a simple way to confirm the variability of objects being analysed and reduce the number of false results, which would further improve the routine.

TIC279741942 and TIC382067804 are both examples of eclipsing binary stars, as can be seen in their light curves shown in Figure 19. These were both incorrectly identified by the routine as Ap stars in a limited number of sectors. Their periods were given as the time between two subsequent troughs, which happened to be longer than 14 days. In the majority of sectors, both these objects were identified as false positive objects by the routine, however they were miscategorised in a few cases. Eclipsing binary stars are easy to identify through inspection, however it is important to be aware the routine could still incorrectly identify eclipsing binary stars as Ap stars.

Most commonly in these cases, PDM does not investigate the correct region and investigates a downwards slope, missing the region of the graph where phase dispersion is minimised. The PDM is informed by the Lomb-Scargle search, which is a coarse search

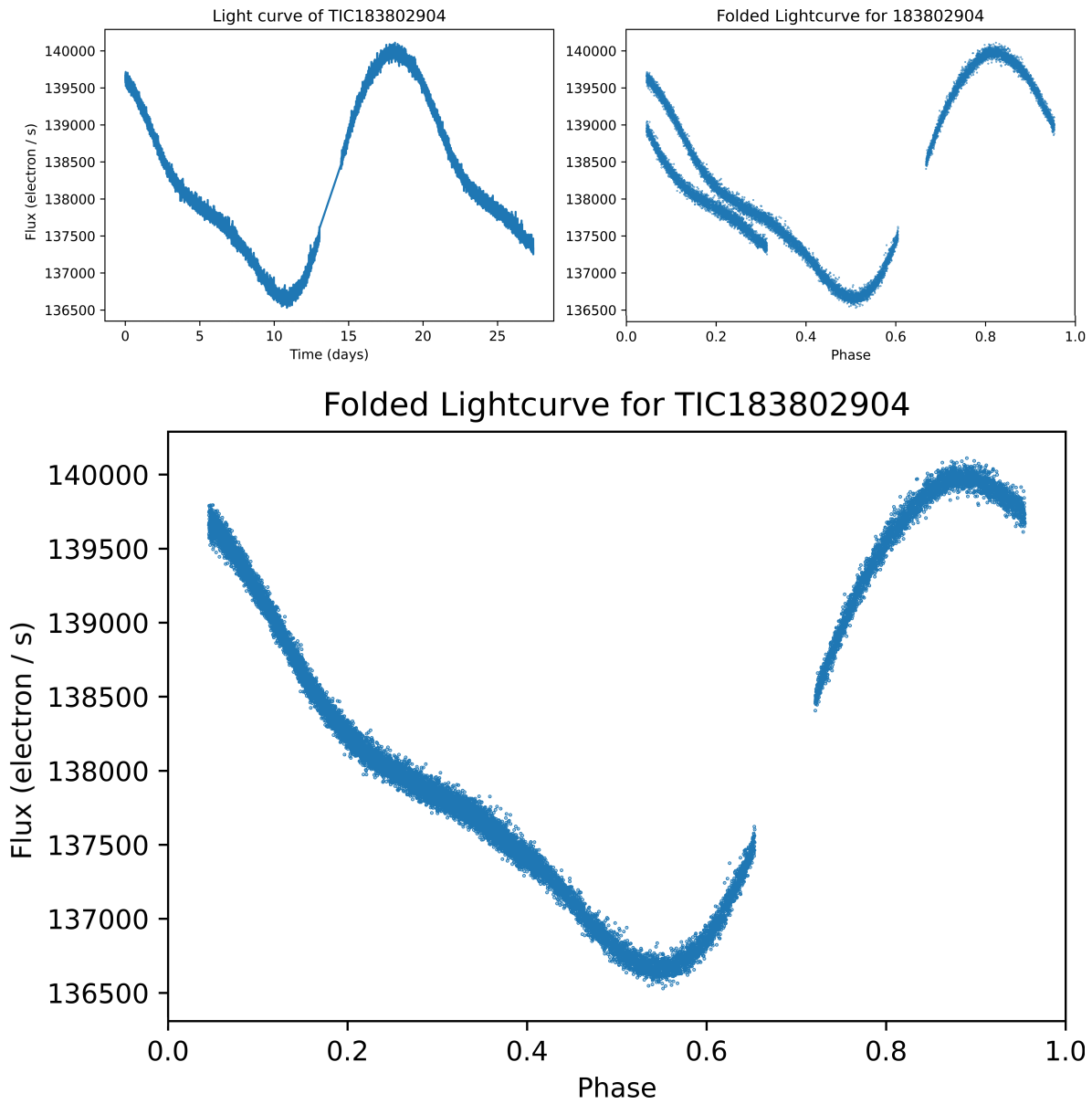


Figure 15: Top-left: light curve of TIC183802904. Top-right: folded with the routine's value of 21.2(2) days. Bottom: folded with a value of 19.49(17) days determined by a wider PDM search.

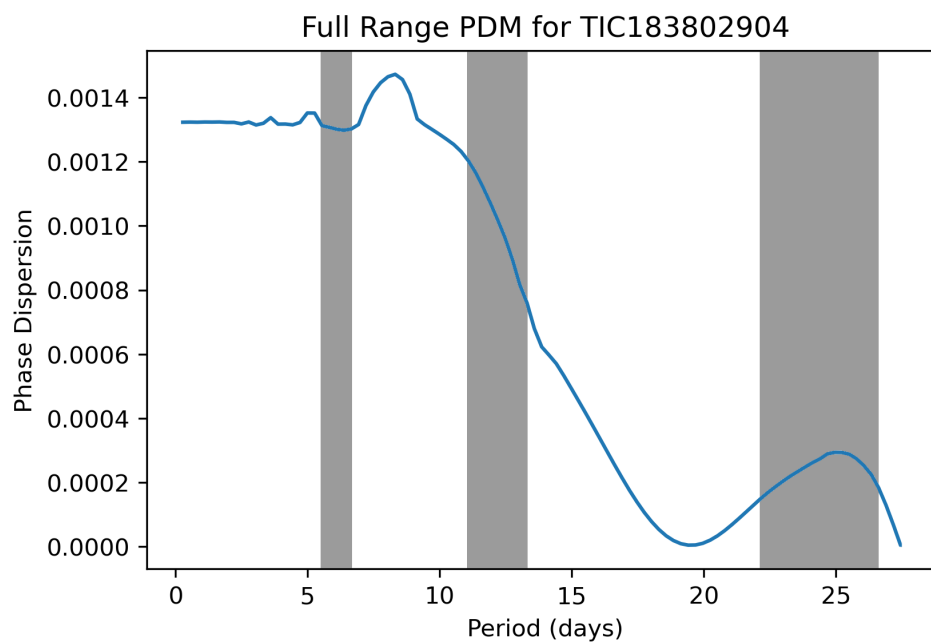


Figure 16: Phase Dispersion Minimisation for TIC183802904. The shaded regions are the regions the routine investigated with PDM.

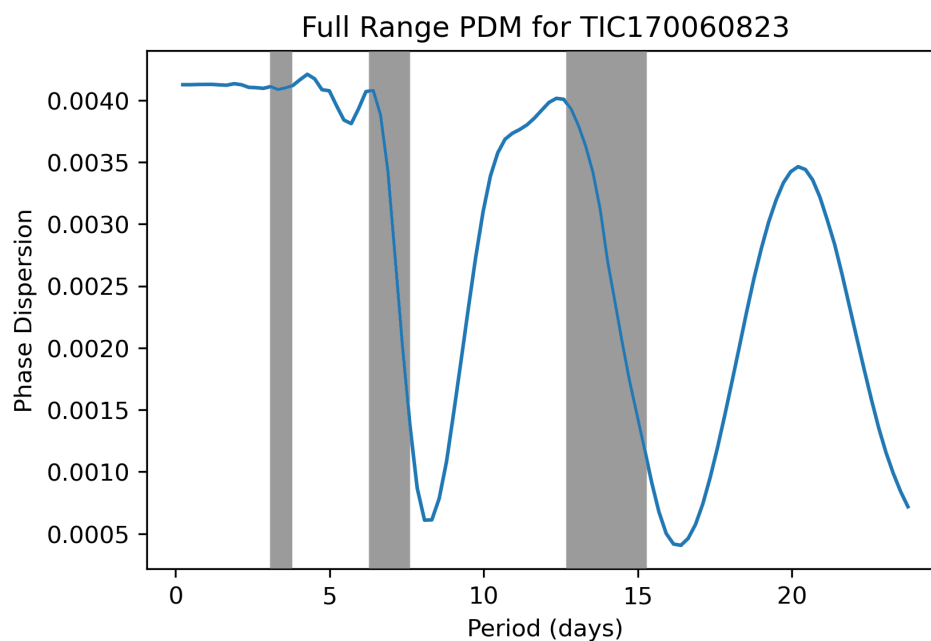


Figure 17: Phase Dispersion Minimisation for TIC170060823. The shaded regions are the regions the routine investigated with PDM.

and may not identify the exact period. The effects of this coarseness are magnified with longer period objects. This could be improved through increasing the range PDM investigates, at the cost of computation time.

Long period values of between 14 and 28 days are not direct indicators that a result is a false positive, and the routine is demonstrably capable of identifying Ap stars with periods of up to ~ 20 days. It also becomes clear from inspection of these light curves that any failures in a single sector's data are not reciprocated in other sectors for the same star. If a star passes the false positive checks and has periods in agreement determined

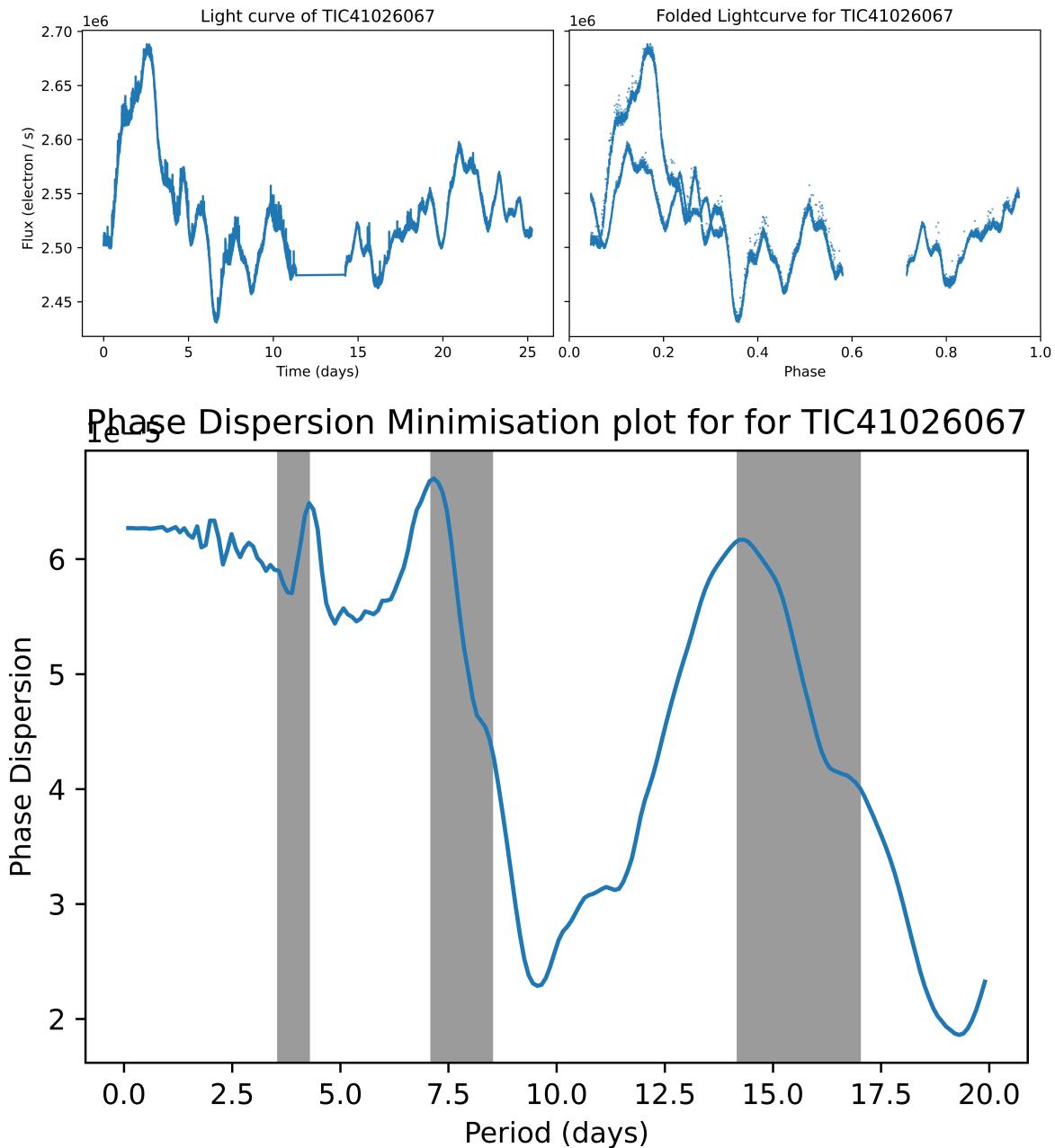


Figure 18: Top left: the unfolded light curve for TIC41026067. Top right: the folded light curve for the same object. Bottom: the PDM graph, with the regions the routine investigated highlighted. This object is not an Ap star and does not show any repetition in its light curve.

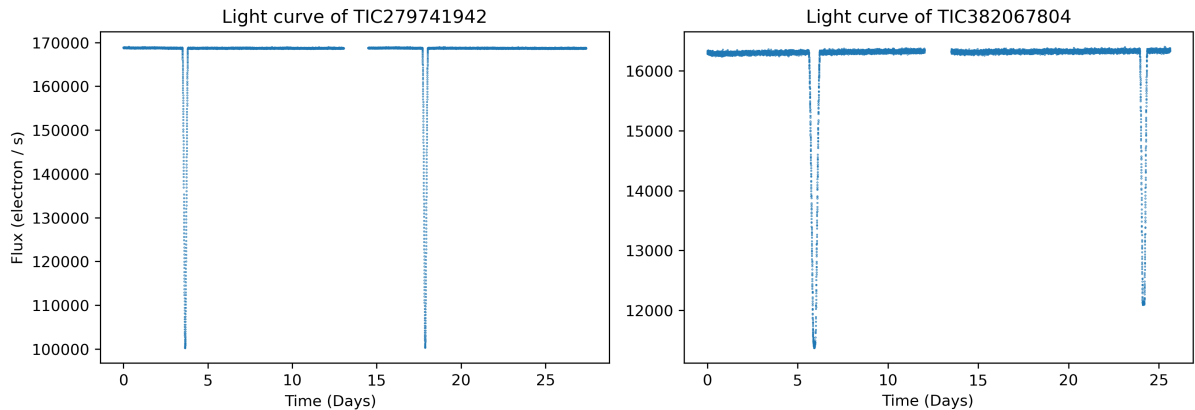


Figure 19: The unfolded light curves of TIC279741942 and TIC382067804, which the routine identified as having periods beyond 14 days in specific sectors. Upon inspection, these are eclipsing binary stars.

independently in multiple sectors of data, this demonstrates a reproducibility to the results that makes them more likely Ap candidate objects. Failing that, there needs to be a high degree of confidence in the data from a single sector, which is best gained through manual inspection.

At longer periods, the false positive detection implemented into the routine does not work to a high enough degree of confidence on its own, as the presence of harmonics cannot be tested. Ap stars can be identified at longer periods, though with less confidence compared to stars where the Lomb-Scargle periodogram demonstrates harmonics. Furthermore, the accuracy of the period identification is severely limited at longer periods. It becomes clear from this the routine is optimised for shorter period stars with periods in the range of a few days. Even so - and due to the small number of light curves with a long period - these results have been kept in the overall data set.

5.2.2 Very Long Period Stars ($28 \text{ days} < P_{\text{rot}}$)

With PDM, the light curve is folded before the analysis is performed using the period determined by Lomb-Scargle. Thus, when a period of > 28 days is analysed by PDM, it is in effect investigating the phase dispersion of the unfolded light curve. If this returns a lower value through PDM than any other investigated frequencies, it is an indicator the object does not demonstrate variability at the candidate period. It is impossible to investigate frequencies beyond 28 days with a single sector of TESS data, as that is the time base of the observations.

As established earlier, these very long period stars were primarily identified in sectors 10 and 11. A random selection of high-period light curves in these sectors were analysed. The majority of the light curves analysed demonstrated a discontinuity between two levels of flat, scattered points which likely represent pulsating stars or random noise. This discontinuity is a result of an issue in the data processing pipeline, and is demonstrated in Figure 20.

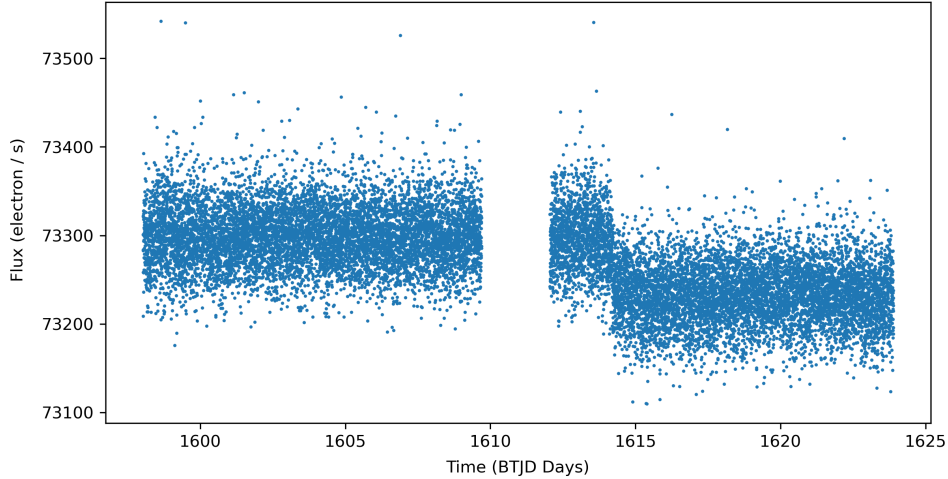


Figure 20: The unfolded light curve of TIC349647797 demonstrates the discontinuity in sector 10 and 11 data.

In these cases, there is no significant rotation period, however Lomb Scargle incorrectly identifies the point of the discontinuity as a significant frequency. This typically places the candidate period in the range of 14-18 days. Then, when the harmonics of the candidate period are analysed via PDM, the routine investigates 14-18 days, as well as half that and double that. When this is doubled to 28-36 days, it is equivalent to investigating the phase dispersion of the unfolded light curve. If the routine determines the minimum phase dispersion to be when the light curve is unfolded, this is represented as twice the period of the discontinuity that was identified by Lomb Scargle.

Any light curves that provide a rotation period over 28 days can be immediately disregarded as periods of that length cannot be analysed by the routine. However, since these results are caused by failure in the routine or in the pre-processing, the object itself cannot be disregarded using this. This allows the omission of 537 light curves, which reduces the data set by 103 Ap star candidates.

5.3 Low Temperature Stars in the Data

It is expected that there are fewer Ap stars at lower temperatures, especially below 7000K. However, Figure 12 showed instead a large grouping of stars at low temperatures. The majority of these stars are likely F-type stars which have developed shorter-lived surface spots, and had not been correctly identified as false positives.

The number of low-temperature stars (effective temperature $< 7500\text{K}$) and very low-temperature stars ($< 7000\text{K}$) within the data set are presented in Table 6 on a per-sector basis. The former category is inclusive of the latter category. There does not appear to be any significant outlying sectors.

A total of 7263 candidate Ap stars from the routine had an effective temperature below 7500K; 6763 of those were then below 7000K. This represents 80% and 74% of the light curves that the routine processed, respectively. This further demonstrates the

| Sector | 1 | 2 | 3 | 4 | 5 | 6 | 7 | 8 | 9 | 10 | 11 | 12 | 13 |
|------------------------------------|------|------|------|------|------|------|------|------|------|------|------|------|------|
| Total | 4630 | 4528 | 4551 | 6308 | 6521 | 6239 | 6130 | 6527 | 7131 | 7132 | 6930 | 7033 | 5428 |
| Low T_{eff} (<7500K) | 830 | 666 | 620 | 222 | 1048 | 999 | 793 | 192 | 895 | 991 | 1208 | 1057 | 906 |
| Very Low T_{eff} (<7000K) | 769 | 624 | 559 | 199 | 972 | 911 | 707 | 190 | 822 | 920 | 1113 | 969 | 846 |

Table 6: The low temperature results from the routine broken down by sector. Low T_{eff} is inclusive of very low T_{eff} .

disproportionately large number of stars that turned up positive from the routine, but were outside the temperature range of A-type stars. Light curves between 7000K and 7500K represent only 6% of the total Ap candidate objects, which is closer to the expected distribution.

This grouping of low temperature stars are the result of an initially optimistic temperature cutoff as opposed to an error in the data or routine. The routine was not adequately designed to handle variable F-type and G-type stars. This is compounded by the extremely limited extent of the testing in this project, which means issues like this were not identified in the testing phase and the routine was not altered to mitigate this issue.

TIC21504987 presents a clear example of a low-temperature star with evolving spots. It has an effective temperature of 6000(100) K, and an apparent rotational period of 2.26(1) days from the routine. However, as seen in Figure 21, the amplitude changes with each rotation as the spots evolve and change. The spots on Ap stars, by comparison, are stable over many rotation cycles. The routine is not set up to detect this object as a false positive; harmonics are not present in its periodogram and the routine does not investigate variation in the amplitude of the light curve over multiple rotations. Raising the temperature cutoff would remove this object, and similar F-type stars, from the data set.

By raising the temperature cutoff to 7000K, the vast majority of these low-temperature stars were removed from the data set, whilst excluding a minimal amount of Ap candidate

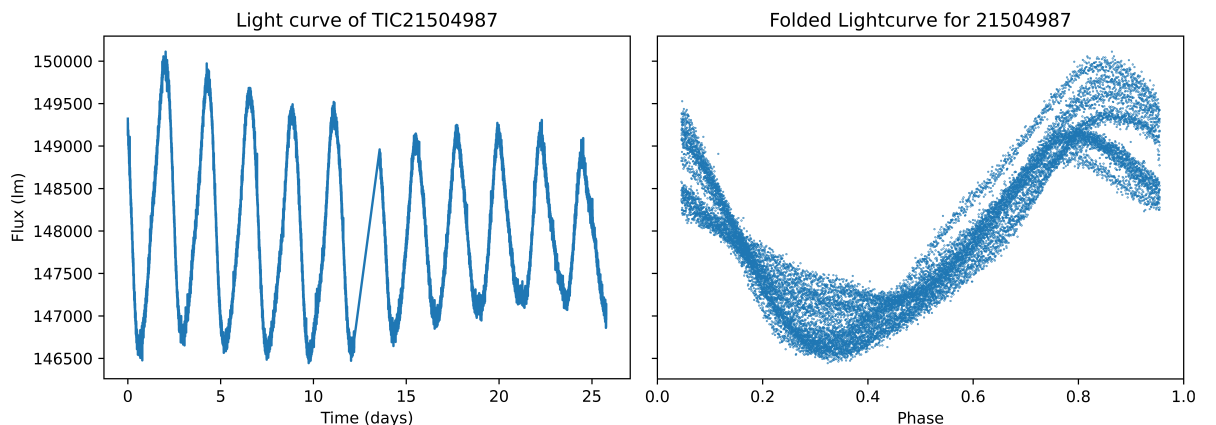


Figure 21: TIC21504987 light curve, folded over the identified rotation period of 2.26(1) days, demonstrates varying amplitude typical of a lower-temperature star.

stars. This also significantly reduces the number of candidate Ap stars by 74%.

5.4 Analysing Stars Observed in Multiple Sectors

With the temperature cutoff raised to 7000K and the high-frequency data points ($P_{\text{rot}} > 28$ days) removed, there were 2261 candidate Ap stars remaining. Of these, 1065 had been observed in multiple sectors and 558 had multiple periods calculated.

Objects were then categorised based on whether they were observed in multiple sectors, and whether the routine had detected rotation periods in multiple sectors. A short secondary routine was quickly developed to help automate and reduce the time taken for this task. Any stars observed in a single sector by the routine were passed over for this stage of analysis.

Stars observed in multiple sectors, but where a rotation period was detected in only one sector, were evaluated based on the number of sectors where the routine had identified it as a false positive. If a star was observed in 4 or more sectors and only a single sector had an identified period, it was disregarded.

For any objects where periods were identified in multiple sectors, the result from each light curve for an individual object was analysed against each other light curve. If these agreed within 5x the larger uncertainty of the two objects, the values were considered to represent the same period. Further, if the two values did not agree within this tolerance, the two closest harmonics were also investigated. The number of times two individual values agreed versus disagreed was stored by the routine.

If all the values for an individual object agreed within these tolerances, the average period and the standard deviation of results were carried forward as the object's rotation period and uncertainty. If none of the values for an individual object agreed within tolerances, the object was disregarded. In cases where some values agreed within tolerances, the values were evaluated manually.

In total, 249 objects were manually inspected. The vast majority of these values were clearly non-harmonic, with multiple periodicities identified. In 16 cases, close values were considered to be out of tolerance of one another due to the size of the uncertainties in the light curve, resulting from high frequencies and short periods. A further 30 objects were evaluated further through inspection of their light curves.

This analysis resulted in 3 separate groupings of Ap candidate stars which had demonstrated different levels of confidence. 1184 objects were identified as Ap candidate stars with a single sector's worth of data. 471 objects had multiple sectors worth of data that agreed within the defined parameters. A further 249 objects had multiple periods calculated that were not in agreement with one another. This produced a list of 1904 objects, down from the initial 4657 identified by the routine.

5.5 Manual Investigation of Data

A final, manual inspection of the light curves for these 1904 objects was performed to reduce the list down further. This involved evaluating through inspection the unfolded light curve as well as the phase-folded light curve according to the phase determined by the routine. In cases where the final rotation period was determined from the results of multiple sectors, this allowed the accuracy of that determined result to be evaluated through inspection. Further, this gave an opportunity to evaluate objects and object types where the routine was still producing incorrect results. This manual investigation was not thorough and was intended to handle any obvious non-Ap stars that the routine was not designed appropriately to handle.

Of the 1184 objects with a single sector of data, 470 of these were kept from the manual investigation for the final data set, or 39% of the objects. Of the 471 objects with multiple sectors of data, 147 were kept in the final candidate list, or 31% of these objects. None of the 249 objects where periods values disagreed were retained.

Most of the removed light curves showed scattered points and no significant frequency when folded, or were eclipsing binary systems. Evaluating the minimum value given by PDM would help discard the light curves where no significant period was detected: with the current iteration of the routine, PDM is only used for calculating a period rather than evaluating if an object is variable.

Eclipsing binary objects were not directly handled by the routine; contact binaries, which are the most commonly observed in literature, typically have periods in the range of $0.2 < P < 0.8$ days (Deb & Singh, 2011). The lower period cutoff was raised from 0.3 days (8 hours) to 0.8 days (19 hours) as a way to efficiently remove most binary systems from the data. Even so, longer period binary objects still had to be identified and removed manually.

This further reduced the list of 1904 objects down to 617. An investigation of literature was performed to determine how many of these objects had been previously identified in literature, and to provide literature values for their rotation periods where available. 90 objects were provided literature values, and a further 7 objects were removed at this stage due to literature identifying them as not-Ap stars.

This final list of 610 objects is presented in Appendix A.

6 Discussion

A non-exhaustive list of candidate Ap stars was produced from the set of data presented in Cycle 1 of TESS observations. From an initial set of 79088 light curves and 38728 objects, which was collected based on the effective temperatures of the objects, this was reduced down to 9127 objects represented by 21107 light curves by the automated routine, and then down further through multiple stages of analysis to a finalised list of 610 objects represented by 943 light curves. The routine was searching for rotation modulation; roAp stars may be present in the data though no searches for pulsations have been made in this project. The final list of candidate Ap stars are listed in Appendix A.

These 610 objects represent a set of results that are likely candidate Ap stars. They demonstrate Ap-like properties in all light curves from sectors they are observed in, with observable rotation modulation on the order expected from Ap stars. Of these 610 objects, values from literature were found for 90. These literature values are also presented in the table in Appendix A. Further discussion on a limited selection of objects is presented below.

The final results required a large amount of manual investigation, with the final list of candidate objects being reduced partially through inspection, and a number of oversights were present with the development of the routine. These principally come from the false positive detection, with potential improvements listed in Section 6.4. The routine performed well to identify a general list of rotational variable stars in the data set, however it did not run with the level of autonomy intended, and the list required a large amount of manual analysis as was discussed in Section 5. Discussion of the routine and of its efficiency is presented in Section 6.2, below.

Preliminary testing of the routine was performed as part of the project. This is covered in Section 4, and is further discussed in Section 6.3. This testing involved determination of the best period determination methods for the routine, alongside evaluation of the effectiveness of the routine.

An improved routine could build upon the current, simple routine discussed in this thesis. Improvements to the routine and the methods utilised here are discussed in Section 6.4, alongside further steps to take with the data. Further, an improved routine could be used to determine candidate Ap stars within Cycle 2 data and identify further candidates within the current Cycle 1 data.

6.1 Results

The final results of the project are presented in a table in Appendix A. This includes 610 candidate Ap stars alongside the routine's calculated rotation period and uncertainty, and the number of sectors the rotation period was determined in. Further, the effective temperature and log-g values used to construct a HR diagram are presented with their errors and, where available, literature values have also been presented.

The longest rotation period within this list is from TIC183802904, where the routine

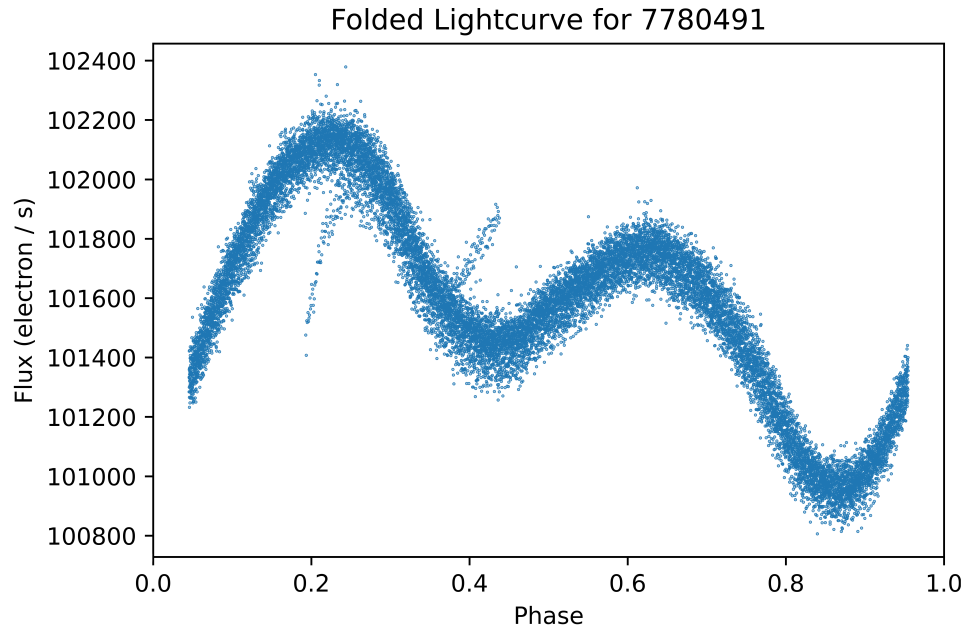


Figure 22: Folded light curve of TIC7780491 over a period of 1.87834(5) days.

discovered a period of 21.2(2) days. This object is also mentioned in Cunha et al. (2019), where its rotation period was calculated as 19.396(50) days. The shortest periods are constrained by the arbitrary lower limit of 0.8 days (~ 19 hours) applied to the results. Ap stars may have shorter periods, though these have been ignored to avoid variability from pulsation. TIC11198532 has the shortest period found in this work, with a period of 0.809(3) days.

These results demonstrate generally small errors, with the smallest errors being on the order of 10^{-5} days; these are all from objects observed in two sectors where the light curve shows minimal variation between sectors. TIC7780491 was observed in sectors 4 and 5, with the PDM agreeing on rotational values between the two sectors. This star appears to have two spots, as well as a further frequency modulating their amplitudes, resulting in a messy folded light curve for such a low uncertainty, as demonstrated in Figure 22. This may provide an indication that the standard deviation may not be an optimal source of uncertainty for situations where only two values were averaged.

Uncertainties, calculated using the method described in Section 3.5, were overall very low for the results, with only 67 objects having an uncertainty of or greater than 0.1 days. These were usually longer-period stars, typically observed in only a single sector. This is as expected. An investigation into the amplitudes of the star's light curves was not performed, though a link between uncertainties and amplitudes would be logical as a larger amplitude reduces the effect of noise in the data.

A number of the candidate Ap stars presented in the final list may be rotational variable objects, however they cannot be analysed with the detail required to determine that in this thesis.

As was demonstrated when comparing the results from the routine against values in

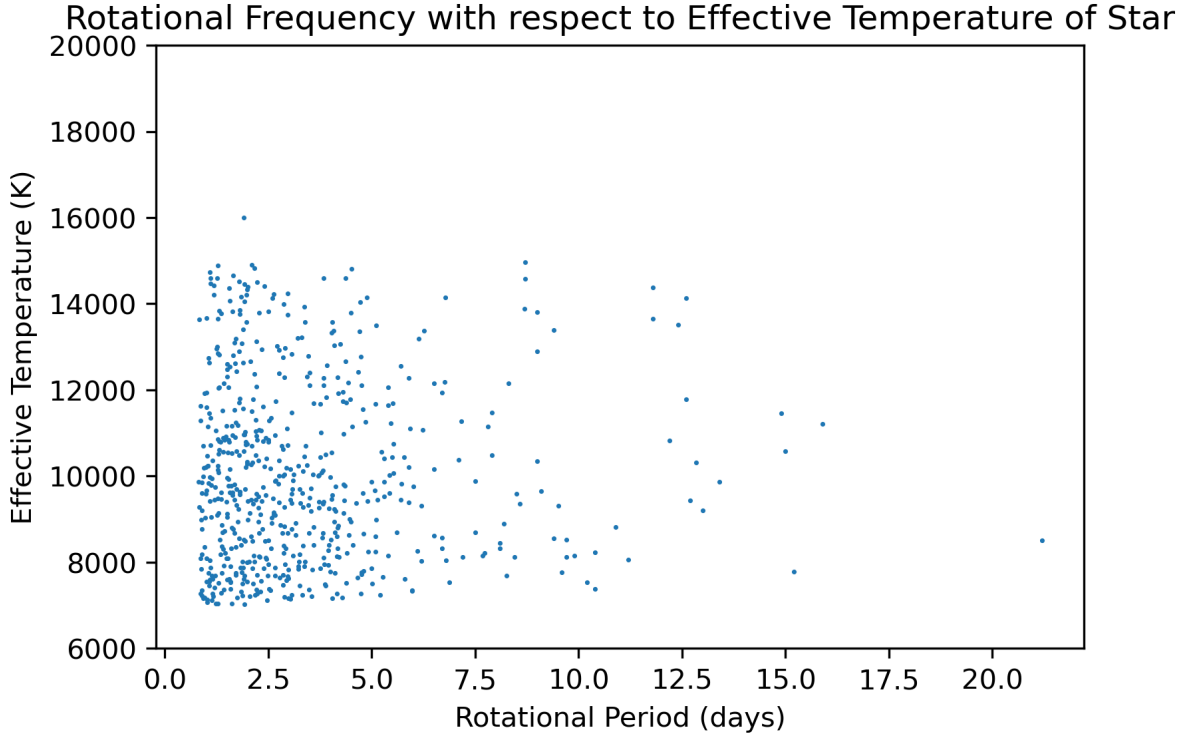


Figure 23: The plot of rotational period against effective temperature, for only the final set of 610 Ap candidate stars.

Cunha et al. (2019), the routine identifies values that are either in agreement with the literature values or twice the result. This can be demonstrated again with the results in Appendix A: 64 of the Ap stars with rotation periods given in literature agree with the routine’s values; 23 identify the first harmonic of the original rotation period. 2 objects, TIC183802904 and TIC294769049, show values that are vary significantly from literature values. These are discussed later.

The plot of rotational period against effective temperature presented at the start of Section 5 has been redone with only the final Ap candidate stars. This is presented in Figure 23.

6.1.1 Representing the Results on a HR Diagram

The spectroscopic Hertzsprung-Russell diagram allows the determination of the properties and stage of evolution for a star from spectroscopic data for the star. Plotting the effective temperature against the gravity of a star provides the spectroscopic HR diagram, from which the main sequence can be observed and the classification of stars can be determined (Langer & Kudritzki, 2014).

By plotting the effective temperature (T_{eff}) against the surface gravity ($\log g$) of a star, the results from this research can be represented in a way that is familiar to the spectroscopic HR diagram. This diagram, sometimes called a Kiel diagram, has been plotted and is presented in Figure 24, below.

This figure presents three separate plots of the Kiel diagram, clockwise from top-left: for all stars within the initial data set, for all stars where the routine returned a value, and for only the stars in the final data set. In the second plot, red points represent data that either was below the temperature cutoff or above the period cutoff.

Comparisons between the first plot and second plot give an indication into the objects the routine correctly identified and removed. The dense cluster of stars with $T_{\text{eff}} < 7000\text{K}$ is significantly reduced. No analysis was performed to determine the magnitude of this reduction, though the preliminary testing suggested 84% of results in this region would

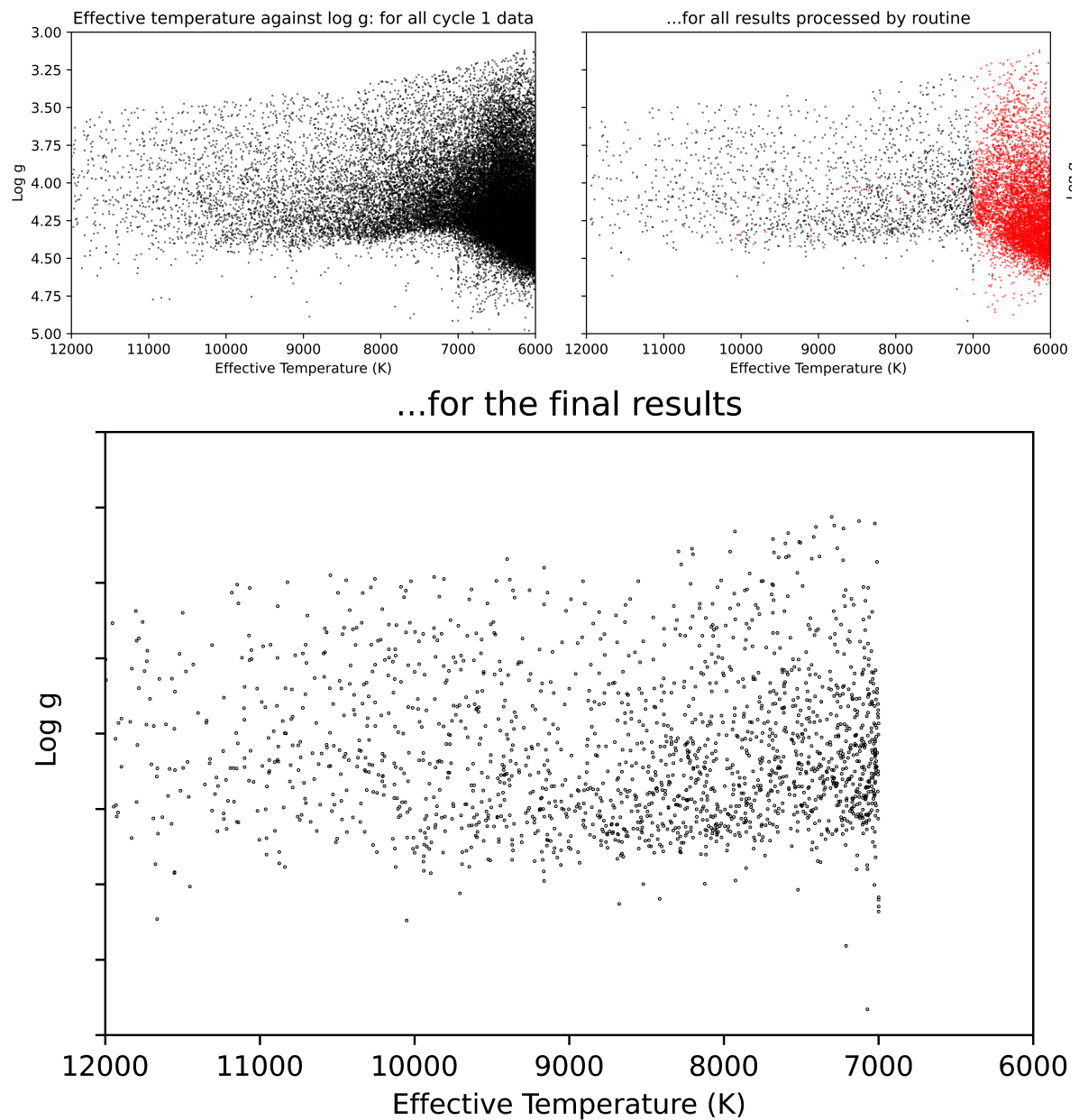


Figure 24: The Kiel diagram for the data. Clockwise from top-left: for all stars within the initial data set, for all stars where the routine returned a value, and for only the stars in the final data set.

be removed. Points with high $\log g$ values (> 4.75) are also almost all removed.

The long period stars, marked in red on the second plot with $T_{\text{eff}} > 7000$ K, are scattered approximately equally on the plot. As expected from the analysis of these stars, this indicates these results are an issue with the routine in general and the data from sectors 10 and 11, rather than any specific object type causing these results.

There is also a large number of stars visible in the top-right of the diagram which have been rejected by the routine. Objects in this region are giant stars and it can be seen they have been correctly regarded by the routine in general. The routine being able to handle giant stars means these objects didn't have to be sorted manually.

The distribution of the low temperature stars, visible in red in the second plot, demonstrates a far larger variety of $\log g$ values. A lot of these stars do not follow the general area of the graph where Ap stars are located, and many of them are likely not Ap stars.

The positions of the final results form a uniform band along the graph. The average uncertainties on the effective temperature values on this plot are ± 200 K; the average $\log g$ uncertainty is ± 0.07 .

6.1.2 Discussion of Individual Objects

A select number of objects within this set are discussed below. These are objects with unusual results, such as high numbers of observed sectors, notable uncertainties, or objects where the literature brings up discussion.

Whilst objects were observed in all 13 sectors, no objects in the data set showed agreeing values within all 13 sectors. 6 objects in the final list had values determined by the routine in 11 sectors.

TIC44889961 appears to be an Ap star with a simple spot structure, and its light curve forms a sinusoidal wave. There is likely only a single, equatorially central chemical spot on this star. The period of 5.389(1) days determined with the routine agrees with the literature value from Sikora et al. (2019). Within the data set, TIC44889961 has a relatively low uncertainty for its long period.

This object was observed in sectors 4 and 5, however the quality of its light curve varies greatly between the two sectors. As was discussed in the results analysis, sector 4 light curves displayed two discontinuities. Figure 25 demonstrates the sector 4 and 5 light curves for this object.

TIC258837989 was observed only in sector 11, where the routine determined a rotation period of 0.888(20) days. This is in agreement with the value of 0.887(1) days from Eisner et al. (2021). Eisner et al. (2021) identifies this object as an eclipsing binary star, and a candidate multiple system. The light curve for this object appears to be complex, with potentially 3 components, and may warrant further investigation. This object's folded light curve is demonstrated in Figure 26.

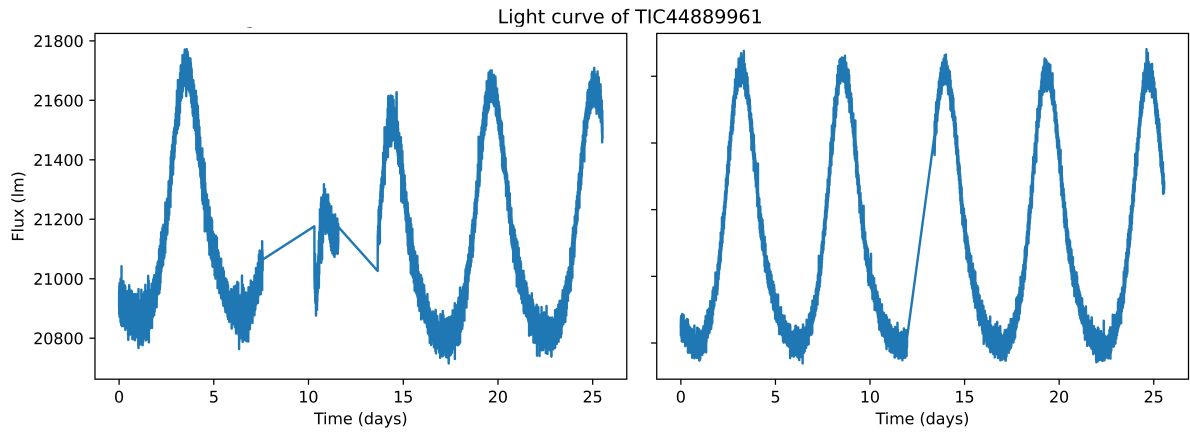


Figure 25: Left; sector 4 light curve for TIC44889961. Right, same object in sector 5.

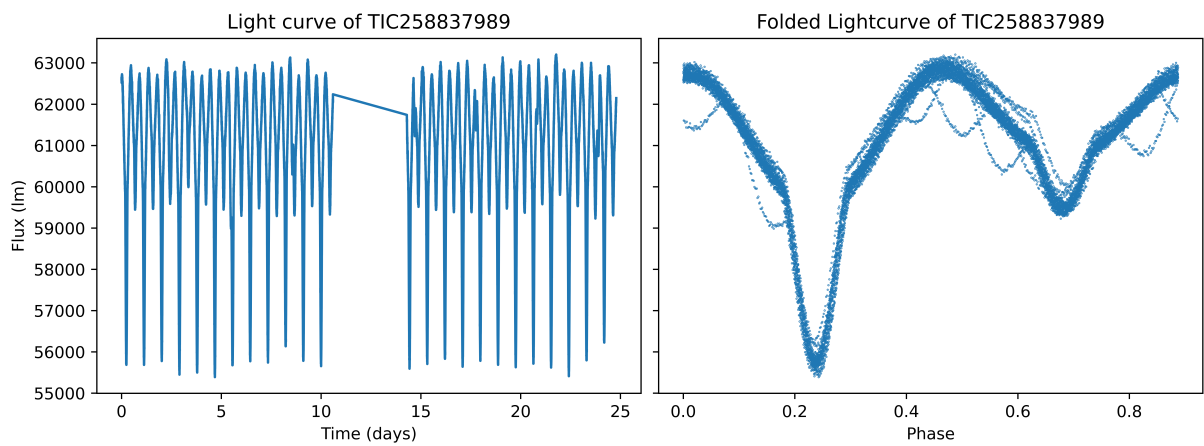


Figure 26: Left, the unfolded light curve of TIC258837989 as observed in sector 11. Right, the same light curve folded over a period of 0.888 days.

TIC405520863 is a very hot Be star that was observed in a single sector, where the routine determined its rotational period to be 1.539(3) days; in Balona and Ozuyar (2020), a value of 0.77 days is instead given. The routine again is determining a subharmonic of the rotation frequency.

Variation in the peak heights of the object appears to have given the routine difficulty when determining a periodogram, which has then meant the routine has identified the incorrect harmonic.

TIC323999777 is an Ap candidate star observed in sector 13 only, where it was determined to have a period of 12.6(6) days. This period appears to be a harmonic of the actual period of 6.32604(88) days as determined from Kochukhov et al. (2021); literature disagrees over the classification of the star, though Kochukhov et al. (2021) considers it most likely to be a magnetic Bp star. Further observations of this star could potentially reveal more about its variation and allow a more certain determination of its variability. However, the light curve from its sector 13 observation (shown in Figure 27) could be the result of variability caused by surface spots.

TIC78566138 demonstrates a period on the order of ~ 7.5 days, calculated from data in sectors 6 and 7. From inspection of its folded light curve, presented in Figure 28, it is clear the period of 7.5(1) days determined by the routine is inaccurate, likely due to a failure of the routine. This object has a clean sinusoidal light curve, indicative of a simple spot structure, as well as a relatively long rotation period compared to many of the Ap candidate stars within the TESS data. Furthermore, it has minimal high-frequency variation, indicating no observable pulsation. This object is not mentioned in literature,

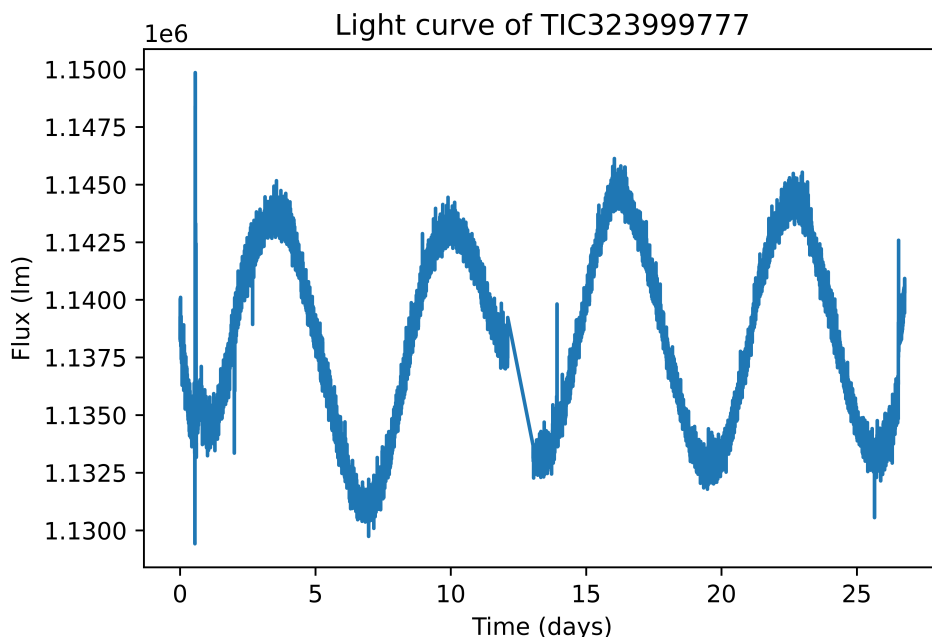


Figure 27: Light curve for TIC323999777.

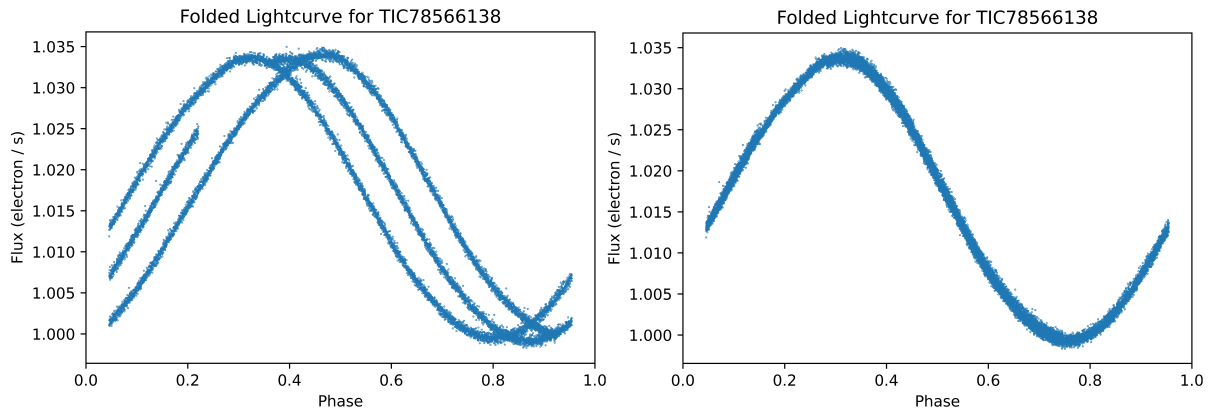


Figure 28: Left; folded light curve for TIC78566138 using the routine’s period value of 7.5(1) days. Right; same object folded over the value of 7.89(3) days from a wider PDM search.

so no comparisons can be made. Running PDM on a larger range of values provides a more reasonable rotational period of 7.89(3) days.

TIC393162912 is an object observed in sectors 11 and 12 with no values in literature. It similarly shows a sinusoidal wave, much alike the one from TIC78566138. Further, the routine has also failed to find an accurate value on the period of this object. The routine determined a value of 7.72(1) days, however a more thorough investigation with PDM returns a value of 8.0(1) days. The variation in uncertainty is because the routine’s value is determined from the standard deviation of two values; the PDM value is from analysis of a single light curve. This light curve is demonstrated in Figure 29.

TIC70525154 is an Ap candidate star discussed in Sikora et al. (2019), where a period of 0.5457(1) days was determined. The routine identified a harmonic of this, giving a final period of 1.092(6) days - in agreement with the literature value. Aside from that, this object has a more complex series of surface spots than the previously discussed objects, with the light curve not following a uniform sinusoidal wave.

TIC141127435 was observed in all 13 sectors of TESS Cycle 1. In 11 of those sectors, the routine identified it as an Ap candidate object. This object has two significant, uneven dips, indicating the star has two unequally sized star spots on its surface. This object has not been observed in literature. Further observations and analysis of this object may be useful to better determine the type of object. The folded light curve of this object is demonstrated in Figure 30.

TIC469246567 is a candidate Ap star observed by TESS in 2 sectors of Cycle 1. Its light curve, similarly, has two pronounced dips, though less equally spaced. It also displays pulsation variability, and is a known roAp star (Shi et al., 2021). The folded light curve of TIC469246567 is also demonstrated in Figure 30.

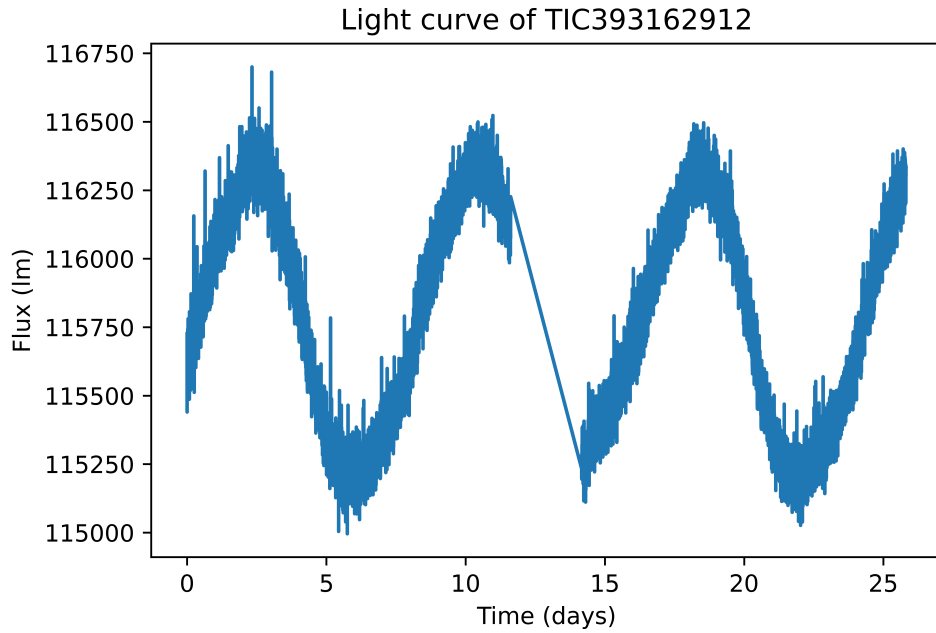


Figure 29: Light curve for TIC393162912.

TIC300744369 is a rotationally variable B star the routine identified, that was observed in 12 sectors in Cycle 1. The routine determined a period of 1.045(2) days from the average of results from 10 of those sectors. Its light curve demonstrates a small rotational modulation as identified by the routine. The large variation between data points indicates a pulsation frequency is also present in the star. This object is discussed in Balona et al. (2019) where it is similarly classified as a rotationally variable main sequence B-type star, in agreement with the routine presented here.

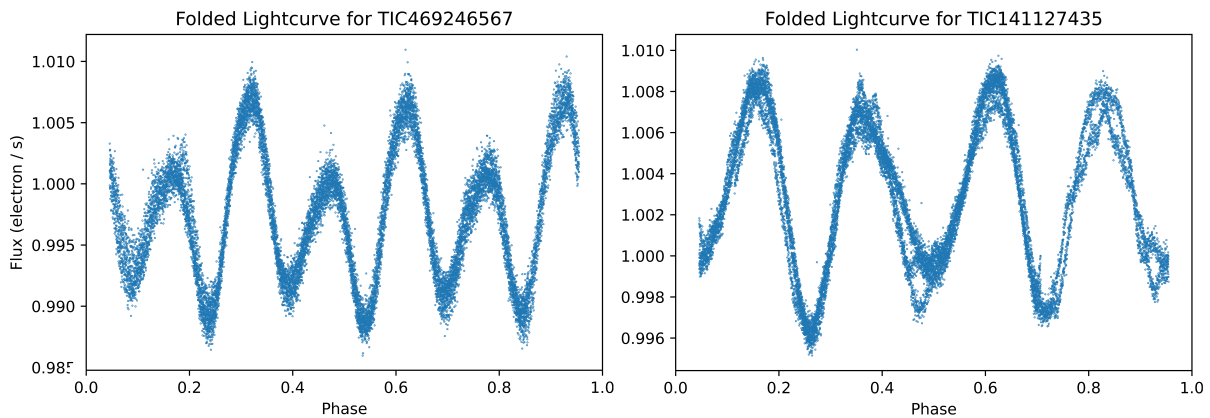


Figure 30: Folded light curves for TIC469246567, with a period of 2.050(3) days, and TIC141127435, with a period of 3.241(4) days.

6.2 Routine and Methods

The routine, in its simplest form, identified and acquired data for candidate Ap stars from TESS data on a sector by sector basis, analysed it through Lomb Scargle to aid identifying the features present in frequency space, before determining a more accurate value of the rotation period of the star. It was a compartmentalised way of handling the process that was simple to develop and test in stages.

The routine worked quickly, taking 1 day to identify and download the relevant data for a single TESS sector, and similarly 1 day to analyse the data for a single sector. This can depend drastically on the number of objects identified in a single region. The Lomb-Scargle process and identification of false positives takes on the order of seconds. The multiple run-throughs of PDM to identify a final rotation period takes 1 minute.

Despite that, the routine is currently not capable of running independently to the desired degree of competence. It requires significant human oversight still, however it has significantly aided the compilation of the list present in this document. The Python code for the routine is presented in Appendix B.

6.2.1 Identification and Acquisition of Data

The identification and acquisition of data from MAST for the routine is handled by Astroquery, and this process is discussed in Section 3.1 and 3.2 of this thesis. The identification and acquisition were broken into two separate processes. Identification of objects queried the target list for each sector, classifying each star by its listed effective temperature in the TESS Input Catalogue. This reduced list was then passed into Astroquery again, with only relevant data being downloaded.

Whilst slow for large amounts of data, this process produces a significantly reduced list of only the stars that satisfy the temperature parameters. For a whole sector of data, the identification and downloading took on the order of a day. Identification alone typically took ~ 90 minutes per sector. This is slow for the volume of data being downloaded, however this is limited by the server connection rather than the routine itself. The process described above may be able to be refined to operate quicker, though it accomplished its task and only needed to be run once per sector, which could be done far before the routine as a whole was fully developed.

The data acquisition for this project could alternately have been performed with bulk downloads of data from MAST, which are also provided. This would have likely reduced the time taken significantly as far fewer requests would be made to the server, however this method would have required more storage for the extraneous data acquired. Further, an alternate process would have been required to identify and use only the required data from the bulk download. The effective temperature of individual objects is included in their FITS headers so classifying stars by temperature would still have been possible using the bulk downloads. This alternate process may have proven more time-efficient if tested, however it was not considered due to the size of these bulk downloads.

6.2.2 Lomb Scargle and False Positive Identification

The Lomb Scargle process is used to initially analyse every light curve presented to the code, and is discussed in Section 2.3 and later, specifically about its use in the routine, in Section 3.3. This quickly and efficiently produces a power spectrum, such as is presented in Figure 9. Lomb Scargle is a commonly used process that accomplished its intended purpose in the routine. The Lomb Scargle power spectrum acquired from this process was easy to simplify for the purposes of analysing the distribution of its peaks.

The Lomb Scargle periodogram was vastly oversampled, with a rate of 30 samples per peak, when 5 or 10 is optimal (VanderPlas, 2018). Further, investigating the whole range of periods possible from the data is unnecessary; the light curve alone is unlikely to demonstrate repeatability at a period close to its own timebase. A dynamic upper period that sets itself as 0.75 of the length of the data would cover 1.5 phases of variability, identifying any rotation modulation whilst further reducing processing time for the routine.

False positive identification was performed by checking the power spectrum for non-harmonic peaks, primary peaks of too high frequency, and no significant peaks. These are defined in more detail in Section 3.3. These cases describe the most common indicators that a light curve is not of an Ap star. Overall, these checks provided simplistic ways to eliminate a number of light curves, however they did not cover all possible cases. Eclipsing binaries and exoplanets often were incorrectly handled by the routine.

The non-harmonic peaks check was the most common indicator the routine used to exclude objects. However, in cases where the power spectrum only had a single significant peak, this check was skipped over. This meant any object with a single significant peak below the frequency threshold from the Lomb Scargle analysis would be automatically assumed to be an Ap candidate star.

The checks in the routine were effective for false positive identification. The limits on these check may need adjusting. The non-harmonic peaks check could often detect non-harmonic peaks in power spectrum where manual analysis would conclude otherwise. Similarly, the lowest period accepted by the routine was 0.8 days, which means the most rapidly rotating Ap stars may have been cut out of the data. This was ultimately done to reduce the number of false positives in the final data set.

Further checks could have been implemented into the code to ensure the false positive detection was more robust. The maximum gradient of object light curves, folded or unfolded, could have been evaluated, which would eliminate exoplanets, some binary systems and pulsating stars. The routine is generally good for ignoring exoplanets however this would provide a secondary check. Further, the difference between maximum and minimum luminosity values could be checked and this could be evaluated against the noise of the data. This would further indicate whether a star is variable.

Though the Lomb Scargle transformation was a vital step in light curve evaluation, further methods - that do not rely on the peaks present in the Lomb Scargle power spectrum - could have also been implemented to identify false positives. These adjustments

could be made to future implementations of this routine or a similar routine.

6.2.3 Phase Dispersion Minimisation

The implementation of PDM in the routine was custom, and worked as intended and as expected when tested. This custom implementation was tested both in the preliminary investigation of period methods (discussed later) and in its later implementation into the routine. It was scaleable and able to identify known rotation periods in Ap stars to within uncertainty. PDM is a slow method, and the quality of its searches were drastically decreased in order to speed up the process.

Investigation of Harmonics The harmonics of the identified periods were then investigated using the PDM. The ranges investigated for these harmonics are informed through the earlier Lomb-Scargle investigation. This is primarily to avoid cases where the main peak in Lomb Scargle is half the rotation period, or twice the rotation period. Given the Lomb Scargle is a coarse search, this was a possibility.

The range over which the PDM searched for this investigation was limited to again reduce the time PDM was being calculated. However, this meant PDM could often not investigate the correct region at all. This is covered in Section 5.2.1, as a common error that would happen to longer period stars. This issue means some of the results from the routine will have significantly larger uncertainties than calculated by the routine - especially at the longer period values.

This issue could have been avoided by investigating larger regions with PDM, or performing another PDM search in cases where the lowest value discovered is at the end of the array of test periods. Further, a finer Lomb-Scargle search earlier around the period determined could have yielded a more accurate test period for the harmonics to be based on.

Further, it was possible for this harmonic investigation to investigate regions outside the time base of the observations, which would accomplish nothing. A check to ensure this doesn't happen should have been included in the routine.

Results from PDM The final results from the routine were also derived using PDM, performing a fine search on the region identified as the most likely candidate period by the previous PDM run. Since this was a repeat of the methods employed in the rest of Section 6.2.3, the major benefits and drawbacks are as mentioned earlier. Results were typically as expected, and were tested to be within uncertainty of literature values in the majority of cases.

An amendment to the final run of PDM may have been to check the value of the lowest phase dispersion value, and apply a cutoff to that. This would have cut out many objects where PDM was not able to find a period, such as non-variable data and any cases where PDM was not investigating the correct region.

Errors were determined using an altered equation from Montgomery and Odonoghue

(1999). The errors were often in agreement with values from literature, though were typically an order of magnitude larger. In cases where the routine did not work correctly, these errors were usually inflated though still significantly smaller than expected. This is seen with TIC294769049, where the routine value's uncertainty is only ± 0.2 days, even though the routine underestimated the period by ~ 0.8 days. This is similarly true in TIC183802904. In situations where an object had multiple calculated periods in agreement, the average and standard deviation of these values was instead used as the period and error. This provided an appropriate uncertainty in most cases, however in cases where there were only two or three calculated periods, it could result in an uncertainty that was significantly lower than the individual uncertainties of the object.

6.2.4 Analysis of Data and Reduction of Ap Candidate List

Significant manual analysis of the data from this routine was performed to produce a more accurate list of candidate Ap stars. Portions of this analysis are discussed in chapter 5.

From the analysis comparing sectors in Section 5.2.1, differences in the quality of data between sectors - notably sectors 4 and 8 - were noted. The gaps in data for these justify the use of period determination methods that could operate in unevenly spaced time data. The routine could still run with larger gaps in data, though it reduced the number of identified candidate Ap stars in the region.

Reducing the data set depending on their calculated period (Section 5.2.2) and effective temperature (Section 5.2.3) was a trivial matter that reduced the amount of candidate Ap stars from 9127 to 2261. These reductions were changes in the future that could be handled automatically by the routine. The effective temperature cut-off was optimistically low when identifying and acquiring data, and the large number of low temperature stars made it clear the routine was not as effective at correctly identifying and ignoring variable F- and G-type stars. The calculated period could have been avoided with checks during either running of PDM, or by limiting Lomb Scargle so the test period could not exceed 14 days.

Data collected with multiple TESS sectors has been noted in the final object list. These objects have a greater confidence. This was simply calculated as the average of frequencies in cases where all values agree. In situations where the values did not all agree, the values and their errors were saved to a list for manual investigation. This was done manually as it was quicker for the ~ 200 values from this thesis than defining robust cutoffs and amending the routine to perform this manually. This process could be automated entirely for future routines, however this would require some further investigation on limits to impose on this.

To verify the 1904 results, the light curves of the individual objects were manually investigated via inspection, alongside the same light curves folded against the calculated value. This allowed the light curves to be quickly analysed and any outlying light curves to be removed. This included a large number of eclipsing binary objects the routine had ignored, alongside non-variable objects, and objects that showed very minor rotational

variability. The list was reduced by 68%, with this process significantly increasing the percentage chance of any given star being an Ap star. When literature values were searched for these last set of objects, 90 values were found with a further 7 objects being listed in literature as δ Sct, γ Dor or eclipsing binary objects. From this self-selecting sample of 97 objects, it can be said tentatively that $\sim 92\%$ of the objects in this final list are likely Ap stars. The actual value is likely significantly lower though this cannot be probed without further investigation.

6.3 Preliminary Testing

Before assembling the final routine, a number of preliminary testing methods were employed to inform decisions about the routine and its methods, as well as to determine the effectiveness of the routine before its running and identify any major issues.

This included the investigating of period determination, covered in Section 2, and the evaluation of the efficiency of the routine, covered in Section 4.2 and 4.3, which are both discussed below. The preliminary testing aided in determining the best process for efficient and generally accurate results, however the testing of false positive identification was limited with small data sets. Furthermore, the investigation of the routine's ability to identify F-type and G-type variable stars was flawed as it included a potentially large number of other types of stars.

6.3.1 Testing of Period Searching Methods

The period searching methods investigated, as described in Section 2, cover the most common forms of period determination. However, as became clear with the routine, the capabilities and limits of the tested methods were not investigated to the degree that was required. These tests were performed with a very limited number of objects, discussed in Section 4.1, that were all known to demonstrate specific forms of variability that the routine would be able to process. There was no consideration taken to how the routine could handle discontinuities such as those found in sectors 10 and 11, nor how the coarse Lomb Scargle search would affect the accuracy of the PDM in longer-period objects.

The overall decision to use Lomb Scargle for a coarse search over Box Least Squares was reasonable for reducing the complexity of the routine and allowing dominant periodic frequencies to be identified more easily. The difference between the Lomb Scargle power spectra versus the BLS spectra, as discussed in Section 2, and demonstrated in Figure 8, meant for cleaner peaks within lower-frequency data.

If the Fourier method could work with the TESS data, and could be tested against Box Least Squares and Lomb Scargle, it would provide an interesting comparison. Lomb Scargle is based on Fourier, so it is comparatively unlikely that Fourier would prove outright more effective than Lomb Scargle for the routine. Furthermore, determining why the Fourier method did not appear to work with the data may be able to offer some form of insight into the data or the routine.

As was also demonstrated during this preliminary testing, the most effective ways to get higher quality results came from longer computation times: from higher autoperiod or samples per peak for BLS or Lomb Scargle; or from a greater number of test periods and a larger time base for PDM. This preliminary testing may have been aided by investigating the best balance between computation time and quality of results, especially for PDM - as discussed in Section 5.2, a number of the failures observed in the longer period results came from the PDM code not investigating the correct regions.

6.3.2 Preliminary Testing of the Routine

Preliminary testing was performed with the routine to evaluate its performance with both known Ap stars from literature and non-Ap stars that could provide convincing false positive objects for the routine. This testing performed on the routine against data present in literature, as presented in Section 4.2 and 4.3, was limited to a few hundred data points. These false positive objects were introduced in Section 1.3 of this thesis.

6.3.3 Accuracy of PDM

The testing against Cunha et al. (2019) in Section 4.2 demonstrated overall positive results. Figure 11 was plotted using the results from this test. This investigation validated that PDM and the routine could identify the correct period to within a reasonable degree of uncertainty in the majority of cases presented to it. This set of data included only 82 stars, which represented 377 total light curves thanks to data repeating in multiple sectors. This, whilst still a substantial set of data to prove PDM, was not a large enough set of data to identify the cases where the routine failed to investigate the minima of the PDM plot, and entirely missed the rotation period of the object. These cases, whilst minimal, are still a sign of an error in the routine that could have been entirely avoided if this preliminary investigation was more substantial.

If any cases such as described above presented themselves during this preliminary test, then they were not investigated. With the two trend lines plotted and the clear correlation between literature value and the routine's own value demonstrated, the results were not analysed further as the routine had demonstrated agreement with literature. Further analysis may have been time-consuming, though would have identified this issue earlier in the process.

The only harmonic present on Figure 11 was for results where the routine had identified twice the literature value. This is likely the routine calculating twice the rotation period, though there is a non-zero chance that a given literature value is for half the rotation period. It's a positive sign for the routine that the values are generally limited to the rotation period or twice this period. This means the results presented in this thesis are unlikely to represent any other harmonics of the star's light curve.

However, no further steps were taken to try reduce the rate the routine incorrectly identified harmonics. This preliminary test suggested $\sim 15\%$ of final values would be incorrectly identified in this way. A finer search of the harmonics via PDM would likely

reduce this percentage, which could potentially be performed after a final value had been determined.

6.3.4 False Positive Identification

The testing in Section 4.3 was limited in terms of scope of objects observed and of the number of objects tested. The routine was 96% accurate at identifying binary stars in that test, though the 27 light curves tested were representative of only 10 objects. Similarly, SPBs, δ Sct, γ Dor and non-variable stars were tested with similar numbers of light curves from similar numbers of objects. The routine showed promising ability at identifying these objects, however a more thorough test of these objects, using hundreds of objects rather than 10, would create more confidence in the routine.

Detection of SPBs, δ Sct, γ Dor, binary stars and non-variable stars is inbuilt into the design of the routine. As discussed in Section 1.3, SPB and γ Dor stars are identified through non-harmonic peaks, δ Sct stars show dominant pulsations that are shorter than Ap star rotation, and non-variable stars show no significant peaks. Binary stars have predictable light curves though the routine was not designed adequately to handle these; instead it relied on these objects generally having shorter periods than the cutoff.

The experiment in Section 4.3 also showed a 84% accuracy with identifying and correctly discounting F-type and G-type variable stars, however these F-type and G-type stars were not collated from literature. Rather, they were a small sampling of objects with an effective temperature below an arbitrary 7500K cutoff. This means the random selection of stars likely also contained red giant stars that the routine is capable of handling, as well as low temperature Ap stars that the routine needs to keep. Considering the massive number of low-temperature stars that were rejected from the final data set, there is little to suggest the routine is much better than random chance at identifying F-type and G-type variable stars.

Due to the fact data from individual stars was analysed for each sector it was present in, a single star could be represented numerous times in this testing. The overall effectiveness of the routine for identifying false positives may have been exaggerated if one or more of the stars present in the data provided abnormally easy to identify.

6.4 Future Work

This project provides numerous points for improvement and refinement of the routine, as well as the continuation of its processes to further improve knowledge of the Ap stars observable with the TESS data.

6.4.1 Sectors from Cycle 2 Onwards

The results in this thesis cover only the data from the first cycle of TESS - sectors 1 through to 13, which image only the southern ecliptic hemisphere. As part of TESS'

prime mission, Cycle 2 performed observations on the same scale as Cycle 1, with objects in the northern ecliptic hemisphere. These observations were not analysed for this thesis.

With the routine in place, performing the same analysis on Cycle 2 data is a trivial matter. Candidate Ap stars in the northern ecliptic hemisphere can be identified, and these can be observed from ground-based telescopes located in the northern hemisphere - such as the Jeremiah Horrocks Institute's Moses Holden Telescope. Most analysis of TESS data for Ap stars focuses on the earlier sectors. Cycle 2 will present more previously unknown Ap stars.

Further, TESS Cycles 3 and 4 - as part of the TESS extended mission - are repeating observations of the same regions as Cycles 1 and 2. Data from Cycles 3 and 4 can be used to identify new Ap stars that were not targets in the satellite's prime mission, as well as further validate the Ap stars that have been identified in Cycle 1. TESS is a continuing mission, and with an effective and efficient automated routine in place, analysis can continue to take place with the new data from each sector and Ap candidate stars can continue to be observed with increased confidence.

6.4.2 Further Analysis of Objects Observed in Multiple Sectors

Data of stars present in multiple sectors has been used in this project only for validating the rotation periods of Ap stars which rotate on the order of days. It is potentially possible to stitch together and use multiple sectors of TESS data to investigate candidate Ap stars with periods on the order of months. Theoretically, polar objects with a period of up to ~ 6 months could be observed and identified as Ap stars, and their rotation periods could be determined from this.

An example plot of TIC358459933, a polar star which was observed in all 13 sectors of Cycle 1, is presented in Figure 31. This plot was constructed by taking time and flux data from all 13 sectors and plotting it on the same axis. There are a few clear challenges before this could be utilised for period determination. There are discontinuities present between all sectors of data, where the average luminosity of the object shifts massively between sectors. This is a result of the pre-processing pipeline, and would have to be tackled either by adjusting light curves based on their mean flux values, or using unprocessed data. With the former, this then causes issues as any process to accomplish this have to differentiate between data issues and actual long-term periodic variation. The latter means development of alternative pre-processing for the data. Either would be possible.

6.4.3 Utilising TESS Full Frame Images

Furthermore, TESS data is also released in the form of Full Frame Images (as mentioned in Section 1). These are images of the entire observation field taken in Cycle 1 and 2 for each sector with a cadence of 30 minutes, and 10 minutes for each sector in Cycles 3 and 4. Photometry can be collected for any objects within the frame, on which a search for variability can be performed. Tools, such as TESScut (Brasseur, Phillip, Fleming, Mullally, & White, 2019), have been developed to perform this with TESS. To use this

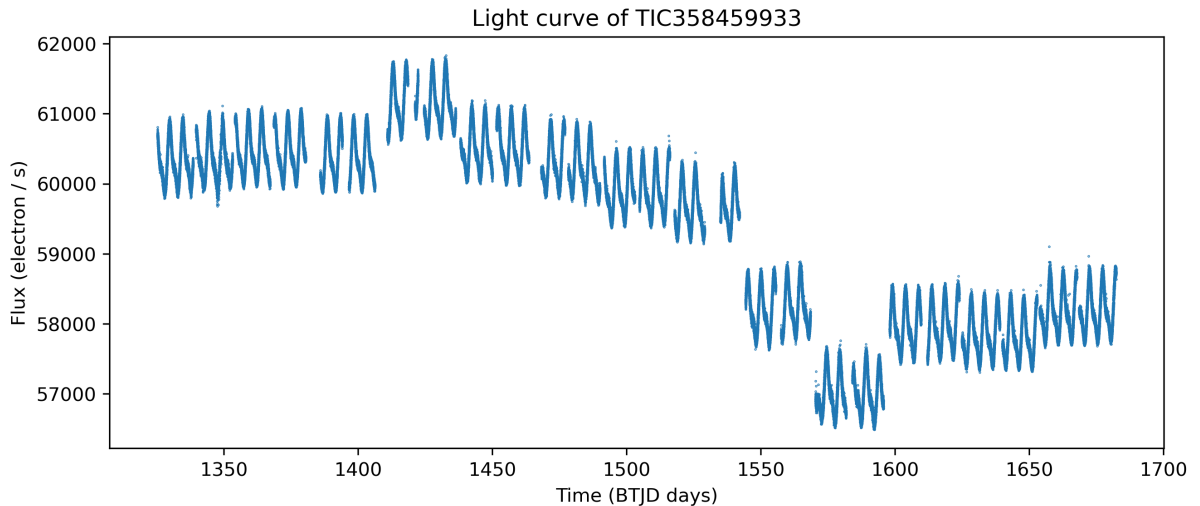


Figure 31: Sectors 1-13 data for TIC358459933 plotted on the same axis. This demonstrates how data could potentially be stitched together from multiple sectors to provide a longer time base, though also demonstrates the issue with discontinuities that comes up when trying this.

TESS full frame image data, the routine would have to be adjusted and added to, and be able to use a tool such as TESScut to extract luminosity values for individual objects from the full frame images.

This would mean the investigation is not limited to data from stars targeted by TESS directly, and would vastly increase the number of potential Ap candidate stars that could be identified by the routine, though with less confidence than with the TESS light curve data.

This flat field data is not processed through the same pipeline as the data used for this thesis, and is minimally processed. This involves flat field corrections, background subtractions and cleaning of cosmic rays. A separate pre-processing pipeline would have to be made and implemented into the routine before the resulting light curves could be processed through the routine. The 30 minutes cadence for these full frame images limits the minimum period this data can probe, however is still far shorter than the shortest period of any known Ap stars.

6.4.4 Follow-up Observations

As mentioned in the introduction, Ap stars are identified observationally through their chemical composition. The results presented from this thesis are representative only of candidate Ap stars, many of which are known. Follow-up observations with spectroscopy would allow the investigation of the chemical compositions of these candidate Ap stars to determine whether they demonstrate the overabundances characteristic of Ap stars.

These were initially considered for the scope of the project, to be performed at the Jeremiah Horrocks Institute's Moses Holden Telescope (MHT). These observations were not performed for this thesis for two reasons. As mentioned earlier, the objects identified in this thesis are all present in the southern hemisphere. Therefore, for the MHT located

53.8 degrees north, these objects are not observable. Time limitations meant that stars in the northern hemisphere, from TESS Cycle 2 as discussed earlier, were not identified during this project. Most importantly, the MHT does not have a working spectrograph to perform these observations with due to a delay in acquisition.

The Ap candidate stars identified from this and other research can be followed up on with separate observations to validate, or otherwise, their chemical peculiarities.

6.4.5 Changes and Adjustments to the Routine

The issues brought up about the routine earlier in this discussion all provide ample points of improvement for the routine in future work. They also provide clear examples of common issues that need to be avoided and considered in future work. Before performing any form of expanded investigation of Ap stars with the routine developed in this thesis, a number of alterations and improvements would be advisable to increase the accuracy of the periods and the confidence of the routine for identifying Ap stars.

The false positive detection utilised for the routine was not comprehensive: low-temperature F-type and G-type stars with varying star spots were often wrongly identified by the routine; eclipsing binaries were not considered; and a number of non-variable stars appeared to be incorrectly handled by the routine. The checks for Ap stars included from Lomb-Scargle are valid and effective with a wide range of objects, however further checks made with the folded light curve, or with the PDM plot, could increase the effectiveness of the routine.

Further, a higher quality search with PDM would be advisable. Situations where the routine entirely missed the true period can be reduced by analysing a wider range of points for the coarse search, or by dynamically expanding the size of the PDM search when the lowest phase dispersion results from a point at the boundary of the range.

A number of general optimisations not identified in this discussion likely could also be made to the code.

With a more robust routine, the Cycle 1 TESS data could be investigated to a greater degree of confidence. The potential region of Ap stars with periods between 12 and 20 hours is ignored due to how many false positive objects are located in these regions. This was justified in this version of the routine as the routine wasn't designed to pick up every Ap star - rather, it was intended to discard any non-Ap stars. However more Ap candidate stars are very likely to be present in the TESS Cycle 1 data.

7 Conclusion

A routine was developed for identifying candidate Ap stars and determining their rotational frequencies. This routine utilised Lomb-Scargle for a coarse evaluation of an object's given light curve and Phase Dispersion Minimisation for the determination of rotational frequencies. This routine was tested against light curves of objects presented in literature before being applied to data from Cycle 1 of the TESS mission. From these tests, the routine is estimated to have an accuracy of $\sim 80\%$.

610 candidate Ap stars were identified and listed, of which 90 have rotational periods from literature. These 610 candidate objects have significant observable frequencies within the range expected of Ap star rotation, alongside harmonic frequencies where applicable. This list has been further reduced based on effective temperature and manual inspection of their folded and unfolded light curves. The finalised list has been presented in this thesis.

The routine has significant potential improvements to be made to improve its effectiveness, and to reduce the reliance on manual reduction of the results to exclude eclipsing binary objects, δ Sct, γ Dor stars and objects with no significant rotational modulation in their light curves. Furthermore, the scope of the analysis could be expanded for future work. However, this routine serves to demonstrate the possible automation of Ap star identification.

Acknowledgements I would like to thank Daniel Holdsworth for supervising this project. I would also like to thank the universe for tolerating me this long.

References

- Antoci, V., Cunha, M. S., Bowman, D. M., Murphy, S. J., Kurtz, D. W., Bedding, T. R., ... et al. (2019). The first view of delta scuti and gamma doradus stars with the tess mission. *MNRAS*, *490*(3), 4040–4059. Retrieved from <http://dx.doi.org/10.1093/mnras/stz2787> doi: 10.1093/mnras/stz2787
- Aurière, M., Wade, G. A., Silvester, J., Lignières, F., Bagnulo, S., Bale, K., ... Toqué, N. (2007). Weak magnetic fields in Ap/Bp stars. Evidence for a dipole field lower limit and a tentative interpretation of the magnetic dichotomy. *A&A*, *475*(3), 1053-1065. doi: 10.1051/0004-6361:20078189
- Babel, J., & North, P. (1997). Discovery of a very large magnetic field in three AP stars. *A&A*, *325*, 195-202.
- Bagnulo, S., Landstreet, J. D., Lo Curto, G., Szeifert, T., & Wade, G. A. (2003). Discovery of a 14.5 kG magnetic field in the NGC 2516 star HD 66318. *A&A*, *403*, 645-651. doi: 10.1051/0004-6361:20030376
- Balona, L. A., Handler, G., Chowdhury, S., Ozuyar, D., Engelbrecht, C. A., Mirouh, G. M., ... Cantiello, M. (2019). Rotational modulation in TESS B stars. *MNRAS*, *485*(3), 3457-3469. doi: 10.1093/mnras/stz586

- Balona, L. A., Holdsworth, D. L., & Cunha, M. S. (2019). High frequencies in TESS A–F main-sequence stars. *MNRAS*, *487*(2), 2117–2132. Retrieved from <https://doi.org/10.1093/mnras/stz1423> doi: 10.1093/mnras/stz1423
- Balona, L. A., & Ozuyar, D. (2020, 03). Pulsation among TESS A and B stars and the Maia variables. *MNRAS*, *493*(4), 5871–5879. doi: 10.1093/mnras/staa670
- Bognár, Z., Kawaler, S. D., Bell, K. J., Schrandt, C., Baran, A. S., Bradley, P. A., ... Zong, W. (2020). TESS first look at evolved compact pulsators. Known ZZ Ceti stars of the southern ecliptic hemisphere as seen by TESS. *A&A*, *638*, A82. doi: 10.1051/0004-6361/202037470
- Braithwaite, J., & Spruit, H. C. (2004). A fossil origin for the magnetic field in a stars and white dwarfs. *Nature*, *431*(7010), 819–821. Retrieved from <http://dx.doi.org/10.1038/nature02934> doi: 10.1038/nature02934
- Brasseur, C. E., Phillip, C., Fleming, S. W., Mullally, S. E., & White, R. L. (2019). *Astrocut: Tools for creating cutouts of TESS images*.
- Caldwell, D. A., Tenenbaum, P., Twicken, J. D., Jenkins, J. M., Ting, E., Smith, J. C., ... Burke, C. (2020). TESS Science Processing Operations Center FFI Target List Products. *RNAAS*, *4*(11), 201. doi: 10.3847/2515-5172/abc9b3
- Cantiello, M., & Braithwaite, J. (2011). Magnetic spots on hot massive stars. *A&A*, *534*, A140. doi: 10.1051/0004-6361/201117512
- Cooley, J. W., & Tukey, J. W. (1965). An algorithm for the machine calculation of complex fourier series. *Mathematics of Computation*, *19*(90), 297–301. Retrieved from <http://www.jstor.org/stable/2003354>
- Cunha, M. S., Antoci, V., Holdsworth, D. L., Kurtz, D. W., Balona, L. A., Bognár, Z., ... Weiss, W. W. (2019). Rotation and pulsation in Ap stars: first light results from TESS sectors 1 and 2. *MNRAS*, *487*(3), 3523–3549.
- David-Uraz, A., Neiner, C., Sikora, J., Bowman, D. M., Petit, V., Chowdhury, S., ... Collaboration, M. (2019). Magnetic OB[A] Stars with TESS: probing their Evolutionary and Rotational properties (MOBSTER) – I. First-light observations of known magnetic B and A stars. *MNRAS*, *487*(1), 304–317. Retrieved from <https://doi.org/10.1093/mnras/stz1181> doi: 10.1093/mnras/stz1181
- Deb, S., & Singh, H. P. (2009). Light curve analysis of variable stars using Fourier decomposition and principal component analysis. *A&A*, *507*(3), 1729–1737. doi: 10.1051/0004-6361/200912851
- Deb, S., & Singh, H. P. (2011). Physical parameters of 62 eclipsing binary stars using the All Sky Automated Survey-3 data - I. *MNRAS*, *412*(3), 1787–1803. doi: 10.1111/j.1365-2966.2010.18016.x
- Eisner, N. L., Barragán, O., Lintott, C., Aigrain, S., Nicholson, B., Boyajian, T. S., ... Hoffman, T. (2021). Planet Hunters TESS II: findings from the first two years of TESS. *MNRAS*, *501*(4), 4669–4690. doi: 10.1093/mnras/staa3739
- Fausnaugh, M. M., Caldwell, D. A., Jenkins, J. M., Smith, J. C., Twicken, J. D., Vanderspek, R., ... Villaseñor, J. S. (2018). TESS Data Release Notes: Sector 1, DR1.

- Fedurco, M., Paunzen, E., Hümmerich, S., Bernhard, K., & Parimucha, Š. (2020). Pulsational properties of ten new slowly pulsating B stars. *A&A*, *633*, A122. doi: 10.1051/0004-6361/201935478
- Feroz, F., Hobson, M. P., & Bridges, M. (2009). Multinest: an efficient and robust bayesian inference tool for cosmology and particle physics. *MNRAS*, *398*(4), 1601–1614. Retrieved from <http://dx.doi.org/10.1111/j.1365-2966.2009.14548.x> doi: 10.1111/j.1365-2966.2009.14548.x
- Folsom, C. P., Bagnulo, S., Wade, G. A., Alecian, E., Landstreet, J. D., Marsden, S. C., & Waite, I. A. (2012). Chemical abundances of magnetic and non-magnetic Herbig Ae/Be stars. *MNRAS*, *422*(3), 2072–2101. doi: 10.1111/j.1365-2966.2012.20718.x
- Ginsburg, A., Sipócz, B. M., Brasseur, C. E., Cowperthwaite, P. S., Craig, M. W., Deil, C., ... a subset of astropy Collaboration (2019). astroquery: An Astronomical Web-querying Package in Python. *AJ*, *157*(3), 98. doi: 10.3847/1538-3881/aafc33
- Graczyk, D. (2003). Light-curve solutions for bright detached eclipsing binaries in the Small Magellanic Cloud: absolute dimensions and distance indicators. *MNRAS*, *342*, 1334–1338.
- Groenewegen, M. A. T. (2017). Variable stars in the gaia era: Mira, rr lyrae, delta and type-ii cepheids. *Proceedings of the International Astronomical Union*, *12*(S330), 287–296. Retrieved from <http://dx.doi.org/10.1017/S1743921317005506> doi: 10.1017/s1743921317005506
- Hümmerich, S., Paunzen, E., & Bernhard, K. (2020). A plethora of new, magnetic chemically peculiar stars from lamost dr4. *A&A*, *640*, A40. Retrieved from <http://dx.doi.org/10.1051/0004-6361/202037750> doi: 10.1051/0004-6361/202037750
- Holdsworth, D. L., Cunha, M. S., Kurtz, D. W., Antoci, V., Hey, D. R., Bowman, D. M., ... Vanderspek, R. (2021). TESS cycle 1 observations of roAp stars with 2-min cadence data. *MNRAS*, *506*(1), 1073–1110. Retrieved from <https://doi.org/10.1093/mnras/stab1578> doi: 10.1093/mnras/stab1578
- Hubrig, S., North, P., & Mathys, G. (2000). Magnetic AP Stars in the Hertzsprung-Russell Diagram. *ApJ*, *539*(1), 352–363. doi: 10.1086/309189
- Hubrig, S., North, P., Schöller, M., & Mathys, G. (2006). Evolution of magnetic fields in stars across the upper main sequence: I. catalogue of magnetic field measurements with fors 1 at the vlt. *Astron. Nachr.*, *327*(4), 289–297. Retrieved from <http://dx.doi.org/10.1002/asna.200610535> doi: 10.1002/asna.200610535
- Jenkins, J. M., Twicken, J. D., McCauliff, S., Campbell, J., Sanderfer, D., Lung, D., ... Vanderspek, R. (2016). The TESS science processing operations center. , *9913*, 99133E. doi: 10.1117/12.2233418
- Kepler, S. O., Giovannini, O., Kanaan, A., Wood, M. A., & Claver, C. F. (1995). Non-Variable Stars Inside the ZZ Ceti. *Balt. Astron.*, *4*, 157–165. doi: 10.1515/astro-1995-0212
- Kirk, B., Conroy, K., Prša, A., Abdul-Masih, M., Kochoska, A., Matijević, G., ...

- Borucki, W. (2016). Kepler Eclipsing Binary Stars. VII. The Catalog of Eclipsing Binaries Found in the Entire Kepler Data Set. *AJ*, *151*(3), 68. doi: 10.3847/0004-6256/151/3/68
- Kochukhov, O. (2011). The spots on Ap stars. , *273*, 249-255. doi: 10.1017/S1743921311015328
- Kochukhov, O., & Bagnulo, S. (2006). Evolutionary state of magnetic chemically peculiar stars. *A&A*, *450*(2), 763-775. doi: 10.1051/0004-6361:20054596
- Kochukhov, O., Khalack, V., Kobzar, O., Neiner, C., Paunzen, E., Labadie-Bartz, J., & David-Uraz, A. (2021). TESS survey of rotational and pulsational variability of mercury-manganese stars. *MNRAS*, *506*(4), 5328-5344. doi: 10.1093/mnras/stab2107
- Kovács, G., Zucker, S., & Mazeh, T. (2002). A box-fitting algorithm in the search for periodic transits. *A&A*, *391*, 369-377. doi: 10.1051/0004-6361:20020802
- Kurtz, D. W. (1990). Rapidly oscillating AP stars. *RAA*, *28*, 607-655.
- Langer, N., & Kudritzki, R. P. (2014). The spectroscopic hertzsprung-russell diagram. *A&A*, *564*, A52. Retrieved from <http://dx.doi.org/10.1051/0004-6361/201423374> doi: 10.1051/0004-6361/201423374
- Liu, W.-M., & Chen, W.-C. (2014). Magnetic braking of Ap/Bp stars: an alternative formation mechanism of compact intermediate-mass binary pulsars. *MNRAS*, *441*(4), 3615-3621. doi: 10.1093/mnras/stu823
- Lomb, N. R. (1976). Least-Squares Frequency Analysis of Unequally Spaced Data. *ApSS*, *39*(2), 447-462. doi: 10.1007/BF00648343
- Martins, B. L. C., Gomes, R. L., Messias, Y. S., de Lira, S. R., Leão, I. C., Almeida, L. A., ... Medeiros, J. R. D. (2020). A search for rotation periods in 1000 TESS objects of interest. *The Astrophysical Journal Supplement Series*, *250*(1), 20. Retrieved from <https://doi.org/10.3847/1538-4365/aba73f> doi: 10.3847/1538-4365/aba73f
- Mathys, G. (2004). Rotation and Properties of A- and B-Type Chemically Peculiar Stars (Invited Review). , *215*, 270.
- Mathys, G., Kurtz, D. W., & Holdsworth, D. L. (2020). Long-period ap stars discovered with tess data. *A&A*, *639*, A31. Retrieved from <http://dx.doi.org/10.1051/0004-6361/202038007> doi: 10.1051/0004-6361/202038007
- Mathys, G., Romanyuk, I. I., Hubrig, S., Kudryavtsev, D. O., Landstreet, J. D., Schöller, M., ... Yakunin, I. A. (2019). Variation of the magnetic field of the Ap star HD 50169 over its 29-year rotation period. *A&A*, *624*, A32. doi: 10.1051/0004-6361/201834706
- Montgomery, M. H., & Odonoghue, D. (1999). A derivation of the errors for least squares fitting to time series data. *DSSN*, *13*, 28.
- Mortensen, D., Eisner, N., IJspeert, L., Kochoska, A., & Prsa, A. (2021). TESS Eclipsing Binary Data Validation. In *American astronomical society meeting abstracts* (Vol. 53, p. 530.01).

- Neilson, H. R., & Ignace, R. (2015). Period change and stellar evolution of beta Cephei stars. *A&A*, *584*, A58. doi: 10.1051/0004-6361/201526836
- Renson, P., & Manfroid, J. (2009). Catalogue of ap, hgmn and am stars*. *A&A*, *498*(3), 961-966. Retrieved from <https://doi.org/10.1051/0004-6361/200810788> doi: 10.1051/0004-6361/200810788
- Ricker, G. R., Winn, J. N., Vanderspek, R., Latham, D. W., Bakos, G. ., Bean, J. L., ... et al. (2014). Transiting exoplanet survey satellite. *JATIS*, *1*(1), 014003. Retrieved from <http://dx.doi.org/10.1117/1.JATIS.1.1.014003> doi: 10.1117/1.jatis.1.1.014003
- Rusomarov, N., Kochukhov, O., & Piskunov, N. (2014). Magnetic fields of Ap stars from full Stokes spectropolarimetric observations. In G. Mathys, E. R. Griffin, O. Kochukhov, R. Monier, & G. M. Wahlgren (Eds.), *Putting a stars into context: Evolution, environment, and related stars* (p. 380-385).
- Scargle, J. D. (1982). Studies in astronomical time series analysis. II. Statistical aspects of spectral analysis of unevenly spaced data. *ApJ*, *263*, 835-853. doi: 10.1086/160554
- Shi, F., Kurtz, D. W., Holdsworth, D. L., Saio, H., Cunha, M. S., Zhang, H., ... Handler, G. (2021). Discovery of multiple p-mode pulsation frequencies in the roAp star, HD 86181. *MNRAS*, *506*(4), 5629-5639. doi: 10.1093/mnras/stab2144
- Shin, M.-S., & Byun, Y.-I. (2004). Efficient Period Search for Time Series Photometry. *JKAS*, *37*(2), 79-85. doi: 10.5303/JKAS.2004.37.2.079
- Shultz, M. E., Wade, G. A., Rivinius, T., Neiner, C., Alecian, E., Bohlender, D., ... BinaMIcS Collaboration (2018). The magnetic early B-type stars I: magnetometry and rotation. *MNRAS*, *475*(4), 5144-5178. doi: 10.1093/mnras/sty103
- Sikora, J., David-Uraz, A., Chowdhury, S., Bowman, D. M., Wade, G. A., Khalack, V., ... Paunzen, E. (2019). MOBSTER – II. Identification of rotationally variable A stars observed with TESS in sectors 1–4. *MNRAS*, *487*(4), 4695-4710.
- Stellingwerf, R. F. (1978). Period determination using phase dispersion minimization. *ApJ*, *224*, 953-960. doi: 10.1086/156444
- Stepien, K. (1998). Why are magnetic AP stars slowly rotating? *Contributions of the Astronomical Observatory Skalnaté Pleso*, *27*(3), 205-212.
- VanderPlas, J. T. (2018). Understanding the Lomb-Scargle Periodogram. *ApJS*, *236*(1), 16. doi: 10.3847/1538-4365/aab766
- Vio, R., Andreani, P., & Biggs, A. (2010). Unevenly-sampled signals: a general formalism for the Lomb-Scargle periodogram. *A&A*, *519*, A85. doi: 10.1051/0004-6361/201014079

Appendices

A Final List of Candidate Ap Stars

The complete list of candidate Ap stars determined as part of this project are presented here. Total sectors is representative of the sectors where the object has been observed in TESS Cycle 1. Sectors with Value is representative of how many sectors the routine determined a rotation period for the object in. T_{eff} and $\log(g)$ values are from the TESS Input Catalog, which are congruent with the objects' FITS headers. Literature values are presented wherever available. [1] are values from (Sikora et al., 2019); [2] (Holdsworth et al., 2021); [3] (Cunha et al., 2019); [4] (Balona et al., 2019); [5] (David-Uraz et al., 2019); [6] (Balona, Holdsworth, & Cunha, 2019); [7] (Shi et al., 2021); [8] (Kochukhov et al., 2021); [9] (Martins et al., 2020); [10] (Eisner et al., 2021); [11] (Balona & Ozuyar, 2020); [12] (Mathys et al., 2020).

| TICID | Period (days) | Error (days) | Total Sectors | Sectors with value | $T_{eff}(K)$ | $\log(g)$ | Literature Value (days) |
|----------|---------------|--------------|---------------|--------------------|--------------|-----------|-------------------------|
| 4070682 | 1.048 | 0.002 | 1 | 1 | 9840 | 4.0907 | 1.046(1) [12] |
| 4616407 | 6.78 | 0.04 | 2 | 2 | 14150 | nan | |
| 5506314 | 8.26 | 0.07 | 1 | 1 | 7692 | 3.53808 | |
| 7780491 | 1.87834 | 0.00005 | 2 | 2 | 8006 | 3.96261 | 1.8763(3) [1] |
| 9355205 | 7.9 | 0.2 | 1 | 1 | 11478.8 | 3.79405 | 3.99912(90) [8] |
| 9459162 | 1.11 | 0.006 | 1 | 1 | 7874 | nan | |
| 9460388 | 4.8 | 0.1 | 1 | 1 | 8667 | 4.19836 | |
| 9521568 | 2.47 | 0.03 | 1 | 1 | 7120 | 4.28036 | |
| 10863314 | 2.13 | 0.01 | 1 | 1 | 9353 | 3.92879 | 2.1345(6) [1] |
| 11198532 | 0.809 | 0.003 | 1 | 1 | 9864 | 3.74561 | |
| 11646496 | 2.178 | 0.005 | 1 | 1 | 7245 | 3.91195 | |
| 12358411 | 1.280 | 0.008 | 1 | 1 | 7038 | 4.35962 | |
| 12359289 | 3.07 | 0.01 | 1 | 1 | 12830 | nan | 3.0644(5) [1] |
| 12377940 | 1.53 | 0.01 | 1 | 1 | 9772 | 4.03522 | |
| 12393823 | 2.85 | 0.03 | 1 | 1 | 10011 | 4.38211 | 1.4237(6) [1] |
| 13257370 | 6.8 | 0.3 | 1 | 1 | 8050 | 4.32194 | |
| 16580177 | 2.56 | 0.03 | 1 | 1 | 8323 | nan | |
| 17676722 | 1.602 | 0.005 | 1 | 1 | 8321 | 4.21989 | 1.5995(3) [2] |
| 20500037 | 2.86 | 0.03 | 1 | 1 | 7463 | 3.88852 | |
| 24662382 | 4.92 | 0.03 | 2 | 2 | 8242 | 4.18628 | |
| 25424318 | 0.875 | 0.003 | 1 | 1 | 8987 | 4.20606 | |
| 25784722 | 12.6 | 0.2 | 1 | 1 | 11783 | nan | |
| 27985664 | 1.815 | 0.008 | 1 | 1 | 11792 | 4.0378 | 1.8144(3) [1] |
| 28974483 | 6.2 | 0.1 | 1 | 1 | 9310 | 3.76336 | |
| 29628184 | 4.78 | 0.01 | 2 | 2 | 11553 | 3.98404 | |
| 29666185 | 2.12 | 0.01 | 1 | 1 | 8490 | 4.12712 | 1.0594(5) [1] |
| 29755072 | 6.2 | 0.2 | 1 | 1 | 8033 | 3.70828 | 6.180(4) [1] |
| 29781099 | 2.874 | 0.005 | 12 | 10 | 8214 | 4.01467 | 2.8749(9) [1] |

| | | | | | | | |
|----------|--------|--------|----|----|---------|---------|--------------------|
| 29928131 | 4.16 | 0.08 | 1 | 1 | 7272 | 4.11004 | |
| 30982266 | 4.73 | 0.08 | 1 | 1 | 7276 | 4.17551 | |
| 31313111 | 1.991 | 0.009 | 10 | 1 | 7555.45 | nan | |
| 31770408 | 1.060 | 0.004 | 1 | 1 | 12745 | nan | |
| 32035258 | 2.230 | 0.003 | 9 | 9 | 14498 | nan | 2.23047(4) [5] |
| 32593293 | 4.51 | 0.03 | 1 | 1 | 14812 | nan | |
| 32651174 | 2.522 | 0.009 | 1 | 1 | 11291 | 4.20044 | |
| 33007731 | 3.097 | 0.009 | 1 | 1 | 9902 | 4.09997 | |
| 33525286 | 1.92 | 0.01 | 1 | 1 | 14457 | nan | |
| 33601621 | 2.66 | 0.01 | 1 | 1 | 7877 | 3.81907 | 2.661 [6] |
| 34199198 | 2.57 | 0.02 | 1 | 1 | 11356 | 4.16896 | |
| 34369597 | 1.715 | 0.005 | 1 | 1 | 11235 | 4.26484 | |
| 35241809 | 1.68 | 0.02 | 1 | 1 | 11540 | nan | |
| 36344653 | 1.81 | 0.02 | 1 | 1 | 9632 | nan | |
| 36451007 | 3.07 | 0.02 | 1 | 1 | 9587 | 3.92797 | |
| 36936064 | 2.20 | 0.01 | 1 | 1 | 10485 | 3.82483 | |
| 37002569 | 2.083 | 0.005 | 1 | 1 | 9448 | 4.16044 | |
| 37296503 | 1.906 | 0.006 | 1 | 1 | 10584 | 3.81208 | |
| 38030046 | 4.24 | 0.09 | 1 | 1 | 13065 | nan | |
| 38586082 | 2.837 | 0.004 | 9 | 8 | 8669 | nan | 2.8349(2) [1] |
| 40535825 | 0.998 | 0.004 | 1 | 1 | 10206 | 4.14137 | |
| 41259805 | 1.716 | 0.003 | 12 | 10 | 8359 | 4.24426 | 1.714489(6) [2] |
| 41331819 | 1.402 | 0.002 | 10 | 6 | 10880.9 | 4.04316 | |
| 41557467 | 8.7 | 0.2 | 1 | 1 | 14964 | nan | |
| 41659964 | 2.97 | 0.02 | 1 | 1 | 8682 | 3.86542 | |
| 41939370 | 1.912 | 0.009 | 1 | 1 | 8518 | 4.05142 | |
| 42055368 | 2.32 | 0.01 | 1 | 1 | 7563 | 4.01917 | 2.3120(4) [1] |
| 42829820 | 1.99 | 0.01 | 1 | 1 | 10742 | 4.28574 | |
| 42884620 | 1.179 | 0.002 | 1 | 1 | 14211 | nan | |
| 43900848 | 1.69 | 0.01 | 1 | 1 | 12618 | nan | |
| 44889961 | 5.389 | 0.001 | 2 | 2 | 8157 | 4.04866 | 5.3818(9) [1] |
| 46435334 | 2.83 | 0.02 | 1 | 1 | 10705 | 3.70539 | |
| 47344320 | 5.6 | 0.2 | 1 | 1 | 8690 | 3.697 | |
| 47550162 | 2.50 | 0.02 | 1 | 1 | 10797 | 3.95122 | |
| 47985275 | 2.220 | 0.006 | 1 | 1 | 12081 | nan | |
| 49067821 | 1.953 | 0.005 | 1 | 1 | 10793 | 3.85341 | |
| 49182849 | 1.5432 | 0.0002 | 2 | 2 | 12066 | nan | |
| 49297078 | 4.37 | 0.02 | 1 | 1 | 12663 | nan | |
| 49381769 | 1.3133 | 0.0008 | 2 | 2 | 10601 | 4.06613 | |
| 49956074 | 9.7 | 0.2 | 1 | 1 | 8522 | 3.97173 | |
| 50650112 | 2.661 | 0.007 | 1 | 1 | 10944 | 4.0143 | |
| 51036653 | 2.709 | 0.009 | 1 | 1 | 13023 | nan | |
| 51251212 | 6.23 | 0.08 | 1 | 1 | 11075 | nan | |
| 52367945 | 1.739 | 0.008 | 1 | 1 | 7184 | 4.25675 | |
| 52368859 | 1.569 | 0.004 | 1 | 1 | 9617 | 3.75683 | 1.57052(9) [1] |
| 53446257 | 2.576 | 0.007 | 1 | 1 | 8911 | 3.49474 | |
| 53601805 | 1.554 | 0.003 | 2 | 2 | 14366 | nan | |
| 53691410 | 1.194 | 0.005 | 1 | 1 | 9445 | 4.23878 | |
| 53748370 | 4.4769 | 0.0001 | 2 | 2 | 11783 | 3.84884 | |

| | | | | | | | |
|----------|-------|--------|----|---|---------|---------|---------------|
| 54415101 | 1.806 | 0.004 | 1 | 1 | 9566 | 3.68761 | |
| 55060474 | 1.727 | 0.002 | 1 | 1 | 10569 | 3.66319 | |
| 55111103 | 6.1 | 0.2 | 1 | 1 | 8255 | 3.82674 | |
| 55452563 | 1.769 | 0.002 | 12 | 8 | 8940 | 4.19025 | |
| 56043194 | 5.7 | 0.1 | 1 | 1 | 12556 | nan | |
| 56597571 | 2.095 | 0.006 | 1 | 1 | 14896 | nan | |
| 56777828 | 1.634 | 0.004 | 1 | 1 | 10955 | 4.17509 | |
| 59127116 | 2.03 | 0.02 | 1 | 1 | 8017 | 4.29823 | |
| 59353886 | 0.965 | 0.005 | 1 | 1 | 11914 | nan | |
| 59504074 | 2.794 | 0.004 | 1 | 1 | 8854 | 3.97753 | |
| 59586057 | 0.890 | 0.002 | 1 | 1 | 9194 | nan | |
| 60464650 | 8.2 | 0.1 | 1 | 1 | 8894 | 4.16711 | |
| 61399368 | 2.875 | 0.0003 | 2 | 2 | 8389 | 3.97149 | |
| 61542962 | 4.72 | 0.06 | 1 | 1 | 14037 | nan | |
| 62121499 | 2.454 | 0.005 | 1 | 1 | 10399 | 3.65447 | |
| 63763073 | 1.973 | 0.006 | 1 | 1 | 13573 | nan | |
| 66425085 | 5.11 | 0.07 | 1 | 1 | 8989 | 3.55384 | |
| 66646031 | 4.47 | 0.02 | 1 | 1 | 9000 | 3.85079 | 4.4751(4) [1] |
| 67650835 | 5.09 | 0.01 | 1 | 1 | 8241 | 4.03356 | 5.0979(5) [1] |
| 67978974 | 1.137 | 0.005 | 1 | 1 | 7120 | 3.69488 | |
| 68431895 | 1.87 | 0.01 | 1 | 1 | 7495 | 4.00107 | |
| 69285076 | 1.79 | 0.01 | 1 | 1 | 14521 | nan | |
| 70525154 | 1.092 | 0.006 | 1 | 1 | 9977 | 3.91832 | 0.5457(1) [1] |
| 70911570 | 2.26 | 0.02 | 1 | 1 | 8943 | 4.39323 | |
| 71010540 | 3.60 | 0.06 | 1 | 1 | 8819 | 4.07431 | |
| 71110143 | 1.81 | 0.01 | 1 | 1 | 13760 | nan | |
| 71624373 | 11.8 | 0.2 | 1 | 1 | 14381 | nan | |
| 72586907 | 1.894 | 0.005 | 1 | 1 | 13400 | nan | |
| 73191506 | 5.72 | 0.05 | 1 | 1 | 9812 | 3.77604 | |
| 73298259 | 3.88 | 0.05 | 1 | 1 | 7455 | 4.18039 | |
| 73441863 | 3.84 | 0.08 | 1 | 1 | 8108 | 4.28686 | |
| 73614905 | 10.4 | 0.1 | 1 | 1 | 7382.33 | 3.41257 | |
| 73699931 | 1.340 | 0.004 | 1 | 1 | 10788 | 4.03862 | |
| 74048154 | 5.4 | 0.1 | 2 | 1 | 12054 | nan | |
| 74095252 | 3.526 | 0.008 | 1 | 1 | 9710 | 3.90576 | |
| 75672455 | 2.85 | 0.01 | 1 | 1 | 12752 | nan | |
| 78566138 | 7.5 | 0.1 | 2 | 2 | 9888 | nan | |
| 78902000 | 4.847 | 0.003 | 2 | 2 | 11255 | nan | |
| 78957734 | 3.591 | 0.004 | 2 | 2 | 11689 | 4.28118 | |
| 79602105 | 1.435 | 0.005 | 1 | 1 | 8717 | 3.83288 | |
| 80379078 | 9.7 | 0.3 | 1 | 1 | 8118 | 3.61637 | |
| 81350817 | 3.43 | 0.03 | 1 | 1 | 12301 | nan | |
| 81933335 | 1.993 | 0.007 | 1 | 1 | 10336 | 3.53343 | |
| 86629981 | 1.067 | 0.005 | 1 | 1 | 11453 | 4.50723 | |
| 89060881 | 1.268 | 0.005 | 1 | 1 | 9095 | 4.31495 | |
| 89240674 | 2.85 | 0.01 | 1 | 1 | 10621 | 4.10147 | |
| 89305963 | 1.940 | 0.006 | 1 | 1 | 11018 | 3.85064 | |
| 89327422 | 2.37 | 0.001 | 3 | 2 | 10806 | 4.15854 | |
| 91074100 | 1.51 | 0.01 | 1 | 1 | 7586.6 | 3.54408 | |
| 92705248 | 4.32 | 0.03 | 1 | 1 | 9142 | 4.33498 | 2.1576(2) [1] |

| | | | | | | | |
|-----------|--------|--------|---|---|---------|---------|----------------|
| 93206724 | 2.50 | 0.01 | 1 | 1 | 10839 | 4.44214 | |
| 93315654 | 1.687 | 0.005 | 1 | 1 | 9800 | 3.83103 | |
| 94036886 | 3.82 | 0.07 | 1 | 1 | 10128 | 4.38152 | |
| 94859894 | 1.298 | 0.003 | 1 | 1 | 10088 | 4.11646 | |
| 97833468 | 2.29 | 0.02 | 1 | 1 | 8122 | 4.09504 | |
| 98672610 | 2.96 | 0.02 | 1 | 1 | 13737 | nan | |
| 98909020 | 1.022 | 0.004 | 1 | 1 | 7138 | 4.40389 | |
| 100112815 | 1.644 | 0.001 | 1 | 1 | 12802 | nan | |
| 100391630 | 11.8 | 0.2 | 1 | 1 | 13654 | nan | |
| 101225771 | 1.113 | 0.002 | 1 | 1 | 9795 | 4.03435 | |
| 101325986 | 1.51 | 0.01 | 1 | 1 | 9053 | 4.05275 | |
| 106195671 | 1.366 | 0.004 | 1 | 1 | 9625 | 4.24495 | |
| 106337931 | 2.88 | 0.03 | 1 | 1 | 12287 | nan | |
| 106633011 | 3.53 | 0.05 | 1 | 1 | 9192 | 3.72115 | |
| 108749808 | 8.7 | 0.2 | 1 | 1 | 14586 | nan | |
| 110798661 | 1.911 | 0.009 | 1 | 1 | 15996 | nan | |
| 111866978 | 2.634 | 0.009 | 1 | 1 | 9114 | 4.17494 | |
| 113059506 | 1.003 | 0.003 | 1 | 1 | 11593 | 4.20669 | |
| 113244828 | 3.59 | 0.05 | 1 | 1 | 8392 | 4.21496 | |
| 113454452 | 3.89 | 0.04 | 1 | 1 | 10501 | 4.34841 | |
| 114648049 | 5.5 | 0.2 | 1 | 1 | 10437 | 4.32608 | |
| 115150623 | 1.503 | 0.002 | 1 | 1 | 9126 | 4.27242 | 1.50048(5) [3] |
| 117646499 | 4.15 | 0.07 | 1 | 1 | 8603.76 | 4.05598 | |
| 117765777 | 1.1005 | 0.0006 | 2 | 2 | 11345 | 3.95701 | |
| 117925262 | 1.202 | 0.005 | 1 | 1 | 7405 | 3.31436 | |
| 118803698 | 3.39 | 0.04 | 1 | 1 | 8004 | nan | |
| 119020352 | 4.73 | 0.03 | 1 | 1 | 12768 | nan | |
| 119024163 | 1.029 | 0.001 | 1 | 1 | 10474 | 4.22336 | |
| 119444396 | 4.697 | 0.009 | 2 | 2 | 13365 | nan | |
| 119635231 | 7.9 | 0.1 | 1 | 1 | 10477 | 4.13455 | |
| 121161014 | 7.5 | 0.2 | 1 | 1 | 8698 | nan | 3.7700(16) [8] |
| 121714050 | 4.16 | 0.03 | 1 | 1 | 8139 | 3.67511 | |
| 121849312 | 3.3 | 0.04 | 1 | 1 | 13218 | nan | |
| 122613463 | 2.2643 | 0.0009 | 2 | 2 | 9528 | 4.14516 | |
| 124807364 | 1.099 | 0.005 | 1 | 1 | 14591 | nan | |
| 125115524 | 3.07 | 0.02 | 1 | 1 | 11468 | 4.09399 | |
| 125200110 | 1.683 | 0.007 | 1 | 1 | 13101 | nan | |
| 125262673 | 2.44 | 0.006 | 1 | 1 | 9561 | nan | |
| 125296407 | 4.76 | 0.04 | 1 | 1 | 7771 | 3.604 | |
| 126361418 | 2.58 | 0.02 | 1 | 1 | 9030 | 3.90295 | |
| 126776787 | 3.83 | 0.01 | 1 | 1 | 14593 | nan | |
| 127256815 | 1.312 | 0.001 | 1 | 1 | 13833 | nan | |
| 127376588 | 0.855 | 0.002 | 1 | 1 | 11281 | 4.14525 | |
| 128800217 | 1.755 | 0.005 | 1 | 1 | 11172 | 4.11469 | |
| 135369080 | 1.267 | 0.002 | 1 | 1 | 14600 | nan | |
| 136843852 | 1.858 | 0.006 | 1 | 1 | 7757 | 4.02537 | 1.8595(1) [1] |
| 139548413 | 10.9 | 0.5 | 1 | 1 | 8811 | 4.04238 | |
| 139553214 | 4.80 | 0.07 | 1 | 1 | 7799 | 3.81963 | |
| 139575644 | 1.168 | 0.006 | 1 | 1 | 7213 | 4.36932 | |
| 140044682 | 0.921 | 0.002 | 1 | 1 | 9985 | 4.37588 | 0.92045(5) [1] |

| | | | | | | | |
|-----------|---------|---------|----|----|---------|---------|----------------|
| 140204398 | 13.4 | 0.3 | 1 | 1 | 9873 | 3.67938 | 6.795(1) [1] |
| 140288359 | 2.766 | 0.004 | 2 | 2 | 10000 | 3.79498 | |
| 140388186 | 2.36 | 0.01 | 1 | 1 | 8776 | 3.89994 | |
| 141045993 | 3.37 | 0.06 | 1 | 1 | 7896 | 4.33964 | |
| 141127435 | 3.241 | 0.004 | 13 | 11 | 8011 | 3.75019 | |
| 141691538 | 1.71 | 0.01 | 1 | 1 | 7698 | 4.13826 | |
| 142110536 | 2.236 | 0.003 | 11 | 9 | 7702 | 3.86196 | |
| 142391542 | 0.834 | 0.002 | 1 | 1 | 9281 | 4.2632 | |
| 143615305 | 6.14 | 0.07 | 1 | 1 | 13183 | nan | |
| 144374241 | 3.73 | 0.01 | 1 | 1 | 9398 | 4.01761 | |
| 146983358 | 4.025 | 0.006 | 2 | 2 | 13330 | nan | |
| 147174421 | 5.42 | 0.003 | 2 | 2 | 10023 | 3.49442 | |
| 147634959 | 1.89 | 0.01 | 1 | 1 | 11572 | 4.29898 | |
| 147958908 | 1.500 | 0.009 | 1 | 1 | 12303 | nan | |
| 148096708 | 4.037 | 0.001 | 2 | 2 | 7160 | 3.83374 | |
| 148398963 | 3.960 | 0.002 | 2 | 2 | 9250 | 3.8017 | |
| 148466573 | 1.9773 | 0.0002 | 2 | 2 | 14211 | nan | |
| 151516273 | 1.1800 | 0.0002 | 2 | 2 | 14417 | nan | |
| 152484511 | 1.78 | 0.01 | 1 | 1 | 9225 | 4.28293 | |
| 152486380 | 0.893 | 0.003 | 1 | 1 | 8763 | 4.3057 | |
| 153742460 | 3.37 | 0.02 | 1 | 1 | 13925 | nan | 3.3639(4) [1] |
| 155514798 | 4.01 | 0.07 | 1 | 1 | 8528 | 4.31124 | |
| 156886111 | 6.874 | 0.007 | 2 | 2 | 7537 | 3.90684 | 6.858(3) [2] |
| 156918577 | 1.93 | 0.02 | 2 | 1 | 14049 | nan | |
| 157046764 | 1.62964 | 0.00004 | 2 | 2 | 9563 | 3.85797 | |
| 157076761 | 1.8938 | 0.0002 | 2 | 2 | 12632 | nan | |
| 157787615 | 0.929 | 0.002 | 1 | 1 | 7163 | 4.07123 | |
| 158106048 | 1.588 | 0.008 | 3 | 1 | 7525 | 4.26059 | |
| 158671360 | 1.832 | 0.002 | 2 | 2 | 7872 | 3.94408 | |
| 160992329 | 4.18 | 0.04 | 1 | 1 | 8797 | 3.68612 | |
| 161270578 | 1.58 | 0.01 | 1 | 1 | 7900 | nan | 0.7910(7) [1] |
| 161334416 | 3.06 | 0.03 | 1 | 1 | 8773 | 3.86573 | 1.5264(4) [1] |
| 162246786 | 1.72 | 0.01 | 1 | 1 | 7756 | 4.3546 | |
| 163377314 | 1.430 | 0.005 | 1 | 1 | 7920 | 4.24055 | |
| 164029492 | 2.39 | 0.02 | 1 | 1 | 7861 | 4.29389 | |
| 166236309 | 3.16 | 0.01 | 1 | 1 | 8636 | 3.5734 | |
| 167045028 | 3.031 | 0.003 | 12 | 11 | 7145.79 | nan | 3.039 [4] |
| 169534653 | 5.9 | 0.2 | 1 | 1 | 12274 | nan | 2.9327(11) [8] |
| 169957259 | 3.872 | 0.005 | 1 | 1 | 7485 | 4.01422 | |
| 170060823 | 15.9 | 0.7 | 1 | 1 | 11206 | nan | |
| 170343327 | 4.53 | 0.03 | 1 | 1 | 11151 | 4.1159 | |
| 171737389 | 9.0 | 0.3 | 1 | 1 | 10342 | 3.63254 | |
| 172512694 | 1.68 | 0.01 | 1 | 1 | 9445 | 3.78937 | |
| 173884686 | 6.7 | 0.1 | 1 | 1 | 8571 | 4.21751 | |
| 175220800 | 2.15 | 0.01 | 1 | 1 | 8149 | 3.7984 | |
| 175971765 | 2.076 | 0.007 | 1 | 1 | 10272 | 3.7942 | |
| 176522518 | 2.89 | 0.04 | 1 | 1 | 9280 | 4.10582 | |
| 176663783 | 1.142 | 0.007 | 1 | 1 | 9941 | 4.40624 | |
| 177067315 | 9.0 | 0.3 | 1 | 1 | 12894 | nan | |
| 177592452 | 2.233 | 0.007 | 1 | 1 | 10832 | 3.99942 | |

| | | | | | | | |
|-----------|---------|---------|---|---|---------|---------|----------------|
| 177810502 | 4.04 | 0.02 | 1 | 1 | 13576 | nan | |
| 177847847 | 2.16 | 0.01 | 1 | 1 | 14828 | nan | |
| 177961519 | 1.448 | 0.004 | 1 | 1 | 10840 | 3.99872 | |
| 178379696 | 5.00 | 0.07 | 1 | 1 | 9865 | nan | |
| 178480690 | 6.5 | 0.1 | 1 | 1 | 12152 | nan | |
| 178575480 | 4.76 | 0.02 | 1 | 1 | 7718 | 4.25041 | 4.7788(5) [2] |
| 178823687 | 1.94 | 0.01 | 1 | 1 | 9700 | 4.27164 | |
| 181084080 | 4.118 | 0.008 | 1 | 1 | 9760 | nan | |
| 183802904 | 21.2 | 0.2 | 1 | 1 | 8500 | 3.59373 | 19.396(5) [3] |
| 185548147 | 2.20 | 0.01 | 1 | 1 | 9451 | 3.76106 | |
| 185827241 | 4.03 | 0.02 | 2 | 1 | 10548 | 3.84968 | |
| 187454730 | 2.27 | 0.01 | 1 | 1 | 11067 | 3.75644 | |
| 193195241 | 3.90 | 0.02 | 1 | 1 | 11829 | 3.7848 | |
| 194440256 | 5.70 | 0.02 | 2 | 2 | 9454 | nan | |
| 199752613 | 1.68 | 0.01 | 1 | 1 | 8678 | 4.56472 | |
| 200441087 | 5.09 | 0.07 | 1 | 1 | 8595 | 4.10703 | 5.094(2) [1] |
| 201731557 | 3.254 | 0.008 | 1 | 1 | 9695 | 4.31367 | |
| 201923258 | 4.78 | 0.09 | 1 | 1 | 9601 | 3.66712 | 2.396(2) [1] |
| 204645314 | 3.97 | 0.02 | 1 | 1 | 8390 | 3.81704 | |
| 204673811 | 1.494 | 0.007 | 1 | 1 | 8081 | 4.31297 | |
| 205913291 | 1.277 | 0.003 | 1 | 1 | 10853 | 3.95836 | |
| 207208753 | 2.046 | 0.002 | 3 | 3 | 9136 | 4.12254 | 2.0436(4) [1] |
| 207235278 | 3.580 | 0.006 | 3 | 3 | 10029 | nan | 1.792 [4] |
| 209396749 | 2.22 | 0.02 | 1 | 1 | 7370 | 3.89386 | |
| 209971455 | 1.2097 | 0.0007 | 1 | 1 | 7681 | 3.50798 | |
| 211041913 | 2.41 | 0.02 | 1 | 1 | 10216 | 3.93931 | |
| 213106455 | 1.037 | 0.004 | 1 | 1 | 10242 | 4.1963 | |
| 213441251 | 2.94 | 0.01 | 1 | 1 | 10192 | 3.75537 | |
| 214176362 | 2.318 | 0.007 | 1 | 1 | 11054 | 3.75297 | |
| 214176395 | 1.088 | 0.005 | 1 | 1 | 7600 | nan | |
| 214213463 | 2.88 | 0.01 | 1 | 1 | 8837 | 3.8946 | |
| 215110637 | 9.4 | 0.1 | 1 | 1 | 13385 | nan | |
| 215256883 | 5.3 | 0.1 | 1 | 1 | 9525.46 | 4.28122 | |
| 217813958 | 3.26 | 0.02 | 1 | 1 | 8184 | 3.95297 | |
| 218094872 | 3.50 | 0.05 | 1 | 1 | 12106 | nan | |
| 218377930 | 4.07 | 0.04 | 1 | 1 | 13378 | nan | |
| 218449155 | 12.4 | 0.3 | 1 | 1 | 13514 | nan | |
| 218658640 | 11.2 | 0.6 | 1 | 1 | 8061 | 4.19078 | |
| 219118940 | 1.584 | 0.009 | 1 | 1 | 7383 | 4.28934 | 0.7927(1) [1] |
| 219166334 | 6.5 | 0.2 | 6 | 1 | 8616 | 3.74147 | |
| 219213742 | 0.97828 | 0.00007 | 4 | 3 | 9036 | 4.25174 | |
| 219967673 | 0.860 | 0.002 | 1 | 1 | 8084 | 4.27417 | |
| 219990936 | 1.4289 | 0.0006 | 2 | 2 | 7370 | 4.20914 | 0.7140(1) [1] |
| 220035931 | 2.206 | 0.001 | 3 | 3 | 13124 | nan | 2.20280(9) [1] |
| 220617441 | 1.92 | 0.02 | 2 | 1 | 7025 | 4.13202 | |
| 221026292 | 4.88 | 0.07 | 1 | 1 | 14140 | nan | |
| 221674070 | 5.92 | 0.07 | 1 | 1 | 11103 | 3.91553 | |
| 222206460 | 5.14 | 0.03 | 1 | 1 | 9455 | nan | |
| 224244458 | 3.83 | 0.05 | 1 | 1 | 12106 | nan | 1.916 [4] |
| 229811530 | 0.874 | 0.003 | 1 | 1 | 7847 | nan | |

| | | | | | | | |
|-----------|--------|--------|----|----|---------|---------|----------------|
| 231380072 | 8.1 | 0.1 | 1 | 1 | 8444 | 4.12726 | |
| 231385237 | 2.410 | 0.007 | 1 | 1 | 14405 | nan | |
| 231404835 | 1.91 | 0.01 | 1 | 1 | 10963 | 4.25082 | |
| 231665881 | 1.157 | 0.006 | 1 | 1 | 7268.27 | 3.86772 | |
| 231672529 | 3.38 | 0.02 | 1 | 1 | 13573 | nan | |
| 231897483 | 3.23 | 0.05 | 1 | 1 | 10244 | 4.3929 | |
| 232066526 | 2.918 | 0.002 | 2 | 2 | 8325 | 4.06892 | 2.9195(2) [1] |
| 232173498 | 3.47 | 0.02 | 1 | 1 | 9332 | 3.76877 | |
| 234505545 | 1.0542 | 0.0002 | 2 | 2 | 7749 | 3.49393 | |
| 234561914 | 8.1 | 0.2 | 1 | 1 | 8321 | 3.83259 | |
| 234634235 | 2.002 | 0.003 | 1 | 1 | 14395 | nan | |
| 237322105 | 1.62 | 0.01 | 1 | 1 | 7039 | 4.06309 | |
| 237336864 | 4.20 | 0.02 | 1 | 1 | 8116 | 4.37489 | 4.2006(1) [2] |
| 237338677 | 3.86 | 0.05 | 1 | 1 | 7945 | 3.98581 | |
| 238571811 | 1.2761 | 0.0004 | 3 | 2 | 12848 | nan | |
| 238613894 | 1.5028 | 0.0004 | 3 | 2 | 9963 | 4.3215 | |
| 241361373 | 1.249 | 0.007 | 1 | 1 | 12956 | nan | |
| 241483053 | 2.601 | 0.005 | 1 | 1 | 14138 | nan | |
| 242939970 | 0.863 | 0.003 | 1 | 1 | 7273.87 | 4.20717 | |
| 243141437 | 2.55 | 0.03 | 1 | 1 | 7343 | 4.35024 | |
| 243321910 | 1.507 | 0.008 | 1 | 1 | 12474 | nan | |
| 245035219 | 1.2735 | 0.0008 | 1 | 1 | 13644 | nan | |
| 245947677 | 3.57 | 0.06 | 1 | 1 | 7819 | 3.99727 | |
| 246322977 | 1.423 | 0.002 | 1 | 1 | 12147 | nan | |
| 246693262 | 5.24 | 0.06 | 1 | 1 | 10554 | 4.10845 | |
| 247388097 | 2.01 | 0.01 | 1 | 1 | 9425 | 4.07546 | |
| 247919395 | 5.30 | 0.05 | 1 | 1 | 10414 | 3.77407 | |
| 248396674 | 5.53 | 0.08 | 1 | 1 | 10740 | 4.02706 | 5.5347(10) [8] |
| 249027325 | 6.7 | 0.2 | 1 | 1 | 11932 | nan | |
| 249037663 | 5.9 | 0.1 | 1 | 1 | 10209 | 4.15824 | |
| 253153987 | 5.2 | 0.1 | 1 | 1 | 7242 | 3.6381 | |
| 253305687 | 4.10 | 0.05 | 1 | 1 | 13028 | nan | |
| 253689414 | 1.73 | 0.01 | 1 | 1 | 9325 | 4.12167 | |
| 254852764 | 4.00 | 0.04 | 1 | 1 | 9971 | 3.76923 | |
| 255045871 | 9.1 | 0.3 | 1 | 1 | 9647 | 3.5548 | |
| 255567700 | 2.773 | 0.002 | 6 | 3 | 7640 | 3.88626 | |
| 255759671 | 2.678 | 0.004 | 7 | 2 | 9904 | 4.38272 | |
| 257775193 | 2.13 | 0.01 | 1 | 1 | 11783 | 3.68402 | |
| 258498944 | 1.390 | 0.001 | 1 | 1 | 11513 | 4.18917 | |
| 258837989 | 0.888 | 0.002 | 1 | 1 | 9855 | 4.24119 | 0.887(1) [10] |
| 259027194 | 1.292 | 0.001 | 1 | 1 | 12037 | nan | |
| 259915804 | 2.23 | 0.01 | 1 | 1 | 7270 | 4.23856 | |
| 259998358 | 1.078 | 0.006 | 1 | 1 | 7455 | 4.09492 | |
| 260194124 | 1.257 | 0.003 | 1 | 1 | 13004 | nan | |
| 261399435 | 0.962 | 0.002 | 13 | 10 | 7181 | 4.05098 | |
| 262089167 | 1.227 | 0.002 | 1 | 1 | 11061 | 4.05711 | |
| 262553765 | 9.9 | 0.2 | 1 | 1 | 8157 | 3.58407 | |
| 262935843 | 1.365 | 0.004 | 1 | 1 | 13771 | nan | |
| 263345261 | 6.5 | 0.1 | 1 | 1 | 10166 | 3.63818 | |
| 264014201 | 1.003 | 0.004 | 1 | 1 | 13663 | nan | |

| | | | | | | | |
|-----------|--------|--------|----|----|-------|---------|----------------|
| 264679929 | 1.922 | 0.004 | 1 | 1 | 7690 | 4.12145 | |
| 266845051 | 1.4692 | 0.0007 | 2 | 2 | 10911 | 3.99221 | |
| 268460597 | 15.0 | 0.5 | 1 | 1 | 10577 | nan | |
| 268760378 | 1.2861 | 0.0001 | 3 | 2 | 10141 | 4.34907 | |
| 269438290 | 3.748 | 0.003 | 2 | 2 | 10432 | nan | |
| 269857621 | 1.1253 | 0.0002 | 9 | 8 | 9054 | 4.43585 | 1.12324(2) [1] |
| 270165435 | 2.99 | 0.02 | 1 | 1 | 7161 | 3.57242 | |
| 270304671 | 15.2 | 0.3 | 1 | 1 | 7786 | 3.9565 | 7.8132(7) [3] |
| 270761386 | 1.928 | 0.003 | 2 | 1 | 10965 | 3.91259 | |
| 271308027 | 2.67 | 0.01 | 1 | 1 | 9875 | 3.65029 | |
| 271365430 | 2.76 | 0.03 | 1 | 1 | 12388 | nan | |
| 271979372 | 1.523 | 0.005 | 1 | 1 | 10547 | 3.99717 | |
| 272113696 | 1.508 | 0.003 | 1 | 1 | 12599 | nan | |
| 274000097 | 1.369 | 0.005 | 1 | 1 | 7751 | 4.07968 | |
| 277688819 | 8.45 | 0.03 | 1 | 1 | 8113 | 4.16007 | 8.4464(9) [1] |
| 277748932 | 4.45 | 0.06 | 1 | 1 | 8634 | 4.09539 | 4.4501(19) [3] |
| 278413303 | 1.8440 | 0.0007 | 3 | 3 | 8398 | 4.29932 | |
| 278804454 | 2.503 | 0.006 | 1 | 1 | 8507 | 3.91832 | 2.5062(2) [5] |
| 280051467 | 8.69 | 0.07 | 3 | 2 | 13884 | nan | 4.369 [8] |
| 280095777 | 1.7880 | 0.0005 | 4 | 4 | 8556 | 4.29362 | 1.7862(1) [1] |
| 280198016 | 2.855 | 0.009 | 1 | 1 | 7708 | 4.09316 | 2.8517(2) [2] |
| 280667311 | 1.630 | 0.003 | 2 | 1 | 9622 | 4.10003 | |
| 280965566 | 1.220 | 0.003 | 1 | 1 | 9749 | 3.90702 | |
| 281408198 | 2.097 | 0.004 | 2 | 2 | 11500 | 3.59933 | |
| 281668790 | 3.948 | 0.003 | 1 | 1 | 8277 | 4.08788 | 3.951(3) [5] |
| 282352354 | 4.04 | 0.02 | 1 | 1 | 9558 | nan | |
| 282804121 | 2.09 | 0.01 | 1 | 1 | 8592 | 4.15152 | |
| 283091451 | 4.00 | 0.05 | 1 | 1 | 7781 | 3.58376 | |
| 284022899 | 3.791 | 0.007 | 1 | 1 | 10088 | 3.82842 | |
| 286852895 | 3.75 | 0.04 | 1 | 1 | 7850 | 3.52168 | |
| 289912168 | 2.753 | 0.007 | 1 | 1 | 10357 | 4.05464 | |
| 290409509 | 0.961 | 0.002 | 2 | 1 | 8350 | 4.07117 | |
| 290682018 | 12.2 | 0.4 | 2 | 1 | 10822 | 3.49774 | |
| 291479498 | 1.728 | 0.004 | 1 | 1 | 9699 | 3.74071 | |
| 292718727 | 9.0 | 0.2 | 1 | 1 | 13803 | nan | |
| 294100968 | 3.801 | 0.003 | 2 | 2 | 8575 | 3.73058 | |
| 294769049 | 9.6 | 0.2 | 2 | 1 | 7761 | 4.17282 | 10.4641(7) [2] |
| 295464123 | 1.300 | 0.003 | 1 | 1 | 10519 | 4.23536 | |
| 295744368 | 1.790 | 0.007 | 1 | 1 | 12895 | nan | |
| 295820243 | 5.10 | 0.05 | 1 | 1 | 13502 | nan | |
| 296638064 | 1.412 | 0.002 | 2 | 2 | 10566 | 4.04647 | |
| 297967252 | 2.348 | 0.002 | 2 | 2 | 12942 | nan | 1.128(14) [9] |
| 298703043 | 2.375 | 0.002 | 2 | 2 | 9736 | 3.76366 | |
| 299099849 | 7.2 | 0.2 | 1 | 1 | 8121 | 4.0389 | |
| 299100030 | 2.97 | 0.03 | 1 | 1 | 7666 | 4.25676 | |
| 299370787 | 2.50 | 0.02 | 1 | 1 | 7946 | 4.13209 | |
| 300162713 | 1.621 | 0.003 | 12 | 4 | 8804 | 4.25776 | 1.623(2) [1] |
| 300329728 | 2.432 | 0.003 | 12 | 11 | 10881 | 4.0923 | 2.433 [4] |
| 300353152 | 3.22 | 0.02 | 1 | 1 | 7848 | 4.23142 | |
| 300400510 | 2.01 | 0.01 | 1 | 1 | 8986 | 4.07297 | |

| | | | | | | | |
|-----------|--------|--------|----|----|---------|---------|--------------------|
| 300744369 | 1.045 | 0.002 | 13 | 10 | 11149 | 4.29246 | |
| 301040555 | 4.11 | 0.06 | 1 | 1 | 8688 | 3.95615 | |
| 301098674 | 2.161 | 0.004 | 1 | 1 | 12372 | nan | |
| 301286582 | 4.68 | 0.08 | 1 | 1 | 12418 | nan | |
| 301323571 | 1.564 | 0.002 | 2 | 1 | 14063 | nan | |
| 301481939 | 2.20 | 0.01 | 1 | 1 | 11310 | 4.25528 | 2.2051(5) [1] |
| 301868089 | 1.513 | 0.005 | 4 | 2 | 8092 | 3.95983 | |
| 302001037 | 1.41 | 0.02 | 3 | 2 | 8298 | 4.01512 | |
| 303441920 | 0.9192 | 0.0001 | 4 | 4 | 10703 | 4.23012 | |
| 303478699 | 3.09 | 0.01 | 1 | 1 | 8148 | 3.93561 | |
| 303860976 | 1.276 | 0.001 | 3 | 3 | 10237 | 3.69193 | |
| 304101379 | 3.217 | 0.001 | 2 | 2 | 7910 | 4.01019 | 3.2123(4) [1] |
| 304458680 | 1.0405 | 0.0001 | 2 | 2 | 10234 | 4.13601 | |
| 304471319 | 3.07 | 0.04 | 1 | 1 | 9369 | 4.369 | |
| 305004624 | 5.4 | 0.1 | 1 | 1 | 11643 | nan | |
| 305425566 | 1.91 | 0.01 | 2 | 1 | 7611.01 | 3.78855 | |
| 305946666 | 2.98 | 0.02 | 2 | 1 | 7833 | 3.46859 | |
| 306350710 | 2.48 | 0.03 | 1 | 1 | 7684 | 3.90153 | |
| 306523989 | 3.12 | 0.02 | 2 | 1 | 10031 | 4.25036 | |
| 306573201 | 4.895 | 0.009 | 13 | 11 | 9414 | 4.13517 | 4.88938(63) [3] |
| 306578324 | 1.2973 | 0.0001 | 13 | 3 | 7514.23 | nan | |
| 306982803 | 4.29 | 0.08 | 2 | 1 | 7170 | 3.88259 | |
| 307488085 | 1.007 | 0.004 | 6 | 1 | 8084 | nan | |
| 307990280 | 2.314 | 0.002 | 3 | 3 | 7313 | 4.02824 | |
| 308007965 | 3.47 | 0.04 | 1 | 1 | 12779 | nan | |
| 308156531 | 3.33 | 0.05 | 4 | 1 | 10117 | 3.64006 | |
| 308244519 | 1.3735 | 0.0002 | 2 | 2 | 8857.47 | 3.91824 | |
| 308452159 | 3.778 | 0.002 | 10 | 2 | 11004 | 4.35219 | |
| 308751185 | 1.3619 | 0.0006 | 9 | 2 | 7286.95 | 3.30963 | |
| 310815859 | 1.656 | 0.001 | 2 | 2 | 14650 | nan | |
| 311419022 | 10.2 | 0.5 | 2 | 1 | 7525 | nan | |
| 312102715 | 0.992 | 0.001 | 1 | 1 | 9584 | 3.91246 | |
| 314265097 | 2.272 | 0.008 | 1 | 1 | 8683 | 4.14682 | |
| 316652732 | 4.324 | 0.007 | 2 | 2 | 10980 | 3.71062 | |
| 316913639 | 2.348 | 0.001 | 2 | 2 | 9420 | 4.16391 | 2.34691(26) [3] |
| 318045130 | 1.439 | 0.006 | 1 | 1 | 10875 | 4.39281 | |
| 319540841 | 1.621 | 0.001 | 1 | 1 | 11168 | 4.22591 | |
| 319931414 | 1.075 | 0.003 | 1 | 1 | 12624 | nan | |
| 321302667 | 4.423 | 0.002 | 2 | 2 | 12175 | nan | |
| 322732889 | 2.91 | 0.01 | 1 | 1 | 7943 | 4.10413 | 2.9114(2) [2] |
| 323972890 | 2.740 | 0.004 | 3 | 2 | 9826 | 3.66861 | |
| 323999777 | 12.6 | 0.6 | 1 | 1 | 14137 | nan | 6.32604(88) [8] |
| 324048193 | 4.298 | 0.007 | 2 | 2 | 11953 | 3.63342 | 4.2953(1) [2] |
| 324437240 | 1.652 | 0.007 | 1 | 1 | 8773 | 3.67007 | |
| 324502498 | 1.152 | 0.005 | 1 | 1 | 7606.39 | 3.86533 | |
| 324889453 | 3.25 | 0.02 | 1 | 1 | 7454 | 3.6398 | |
| 325596252 | 2.90 | 0.03 | 1 | 1 | 12974 | nan | |

| | | | | | | | |
|-----------|---------|---------|----|----|---------|---------|---------------------|
| 326185137 | 1.945 | 0.004 | 1 | 1 | 8495 | 4.27331 | 1.9451(2) [1] |
| 327036874 | 2.88924 | 0.00003 | 2 | 2 | 7187 | 3.98316 | |
| 327529554 | 2.97 | 0.02 | 1 | 1 | 14245 | nan | |
| 327597288 | 1.789 | 0.001 | 1 | 1 | 11702 | 4.10152 | 1.786898(58) [3] |
| 328311189 | 1.319 | 0.003 | 1 | 1 | 12064 | nan | |
| 334620634 | 1.4569 | 0.0007 | 2 | 2 | 8219 | 4.17674 | |
| 334623414 | 2.13 | 0.02 | 1 | 1 | 7496 | 4.17539 | |
| 334789806 | 3.48 | 0.04 | 1 | 1 | 7367.51 | 4.01213 | |
| 336731635 | 2.76 | 0.03 | 1 | 1 | 12921 | nan | 2.77342(219) [3] |
| 337348104 | 2.95 | 0.02 | 1 | 1 | 11099 | 4.08159 | |
| 339673256 | 2.964 | 0.003 | 6 | 5 | 10723 | 3.73446 | 2.9607(2) [1] |
| 339897938 | 2.26 | 0.01 | 1 | 1 | 9264 | 4.07899 | |
| 340006157 | 7.68 | 0.04 | 7 | 4 | 8158 | 4.12799 | 7.6805 [6] |
| 340559753 | 1.001 | 0.003 | 4 | 1 | 11934 | 4.01683 | |
| 340718004 | 3.43 | 0.03 | 1 | 1 | 10256 | 3.89687 | |
| 340963903 | 4.323 | 0.008 | 2 | 2 | 9811 | 3.48712 | |
| 341849173 | 2.758 | 0.003 | 3 | 2 | 9384 | 3.48918 | |
| 343089422 | 4.333 | 0.003 | 3 | 2 | 9434 | nan | |
| 344140081 | 3.398 | 0.006 | 3 | 2 | 10706 | 3.86964 | |
| 344797718 | 2.66 | 0.01 | 1 | 1 | 9098 | 4.17397 | |
| 347602406 | 2.680 | 0.009 | 1 | 1 | 11734 | 3.97022 | |
| 347773211 | 2.20 | 0.02 | 1 | 1 | 11041 | 4.16035 | |
| 348558406 | 4.39 | 0.01 | 1 | 1 | 11711 | 3.8845 | |
| 348898673 | 5.01 | 0.01 | 13 | 9 | 7505.57 | 3.36692 | 2.50142(8) [3] |
| 349309442 | 1.586 | 0.001 | 11 | 8 | 7553 | 3.99962 | |
| 349409844 | 0.8323 | 0.0002 | 11 | 9 | 13641 | nan | 0.831(3) [3] |
| 349419996 | 1.947 | 0.007 | 1 | 1 | 10730 | 4.26946 | |
| 349484595 | 4.659 | 0.007 | 12 | 5 | 7646 | 3.41603 | |
| 349923015 | 8.3 | 0.3 | 3 | 3 | 12148 | nan | |
| 350146296 | 2.666 | 0.004 | 13 | 11 | 7683 | 4.30152 | 2.66387(2) [2] |
| 350178194 | 1.857 | 0.001 | 1 | 1 | 13079 | nan | |
| 350519062 | 4.023 | 0.005 | 13 | 10 | 9458 | 3.95164 | 4.0232(4) [1] |
| 355313904 | 1.83686 | 0.00005 | 3 | 2 | 14169 | nan | |
| 355855205 | 5.509 | 0.003 | 3 | 3 | 11693 | nan | |
| 356299294 | 4.18 | 0.01 | 2 | 2 | 12292 | nan | 4.1880(11) [8] |
| 356837404 | 0.9448 | 0.0007 | 3 | 3 | 10195 | 4.07564 | |
| 357310008 | 3.717 | 0.003 | 3 | 3 | 9257 | 3.52435 | |
| 357610207 | 1.991 | 0.002 | 2 | 2 | 10280 | 3.70523 | |
| 357727232 | 2.0935 | 0.0002 | 2 | 2 | 10693 | 3.60831 | |
| 357877850 | 3.8244 | 0.0009 | 2 | 2 | 9358 | 3.98441 | |
| 357895419 | 5.462 | 0.009 | 2 | 2 | 11222 | nan | |
| 358467700 | 1.948 | 0.001 | 7 | 5 | 10205 | 4.14039 | 1.9460(2) [5] |
| 358508391 | 1.317 | 0.007 | 7 | 1 | 10801 | 4.10451 | |
| 360060767 | 2.87 | 0.01 | 1 | 1 | 13994 | nan | |
| 361565504 | 4.76 | 0.09 | 1 | 1 | 12099 | nan | |
| 361794454 | 3.32 | 0.01 | 1 | 1 | 7236.85 | nan | |
| 361962650 | 0.8617 | 0.0001 | 2 | 2 | 11631 | 4.27752 | |
| 362153865 | 1.6189 | 0.0009 | 2 | 2 | 10528 | 4.20188 | |

| | | | | | | | |
|-----------|--------|--------|----|----|---------|---------|---------------------|
| 362332215 | 5.08 | 0.09 | 1 | 1 | 9665 | 4.38844 | |
| 362475180 | 7.16 | 0.07 | 1 | 1 | 11277 | nan | |
| 362674459 | 4.184 | 0.005 | 2 | 2 | 11926 | 4.27496 | |
| 363716787 | 5.98 | 0.05 | 1 | 1 | 7334 | 3.95267 | 5.966(1) [2] |
| 364424408 | 1.557 | 0.003 | 12 | 11 | 7608.46 | 3.59361 | 1.55632(6) [1] |
| 367217076 | 1.807 | 0.001 | 1 | 1 | 9633 | 4.17161 | |
| 367660534 | 1.379 | 0.003 | 1 | 1 | 8371 | 4.0262 | |
| 369124135 | 2.284 | 0.005 | 1 | 1 | 13796 | nan | |
| 369775632 | 4.09 | 0.04 | 1 | 1 | 8936 | 4.14487 | |
| 370111235 | 0.890 | 0.003 | 1 | 1 | 8178 | 4.29268 | |
| 370676773 | 1.802 | 0.003 | 2 | 1 | 13858 | nan | |
| 371992866 | 3.32 | 0.05 | 1 | 1 | 9605 | 4.33837 | |
| 372480369 | 7.8 | 0.2 | 1 | 1 | 11143 | 4.03243 | |
| 372537235 | 3.28 | 0.01 | 1 | 1 | 9373 | 4.0544 | |
| 373026963 | 6.26 | 0.09 | 1 | 1 | 13366 | nan | 3.13164(30) [8] |
| 373312390 | 3.91 | 0.07 | 1 | 1 | 12563 | nan | |
| 373420253 | 1.336 | 0.003 | 1 | 1 | 8177 | 4.25068 | |
| 375583232 | 3.840 | 0.005 | 2 | 2 | 12275 | nan | |
| 377058286 | 4.10 | 0.03 | 1 | 1 | 9237 | 3.90785 | |
| 381096836 | 2.626 | 0.007 | 1 | 1 | 14220 | nan | |
| 382376381 | 3.34 | 0.01 | 1 | 1 | 9280 | 4.05262 | |
| 382497314 | 4.36 | 0.02 | 1 | 1 | 14588 | nan | |
| 382512330 | 0.8927 | 0.0002 | 7 | 6 | 7227.47 | 3.31992 | 0.89113(1) [3] |
| 382750794 | 1.150 | 0.003 | 1 | 1 | 10366 | 4.07966 | |
| 383472561 | 2.108 | 0.006 | 1 | 1 | 10317 | 4.08006 | |
| 384388565 | 2.55 | 0.02 | 2 | 1 | 10168 | 3.93246 | |
| 384476577 | 3.212 | 0.002 | 2 | 2 | 13211 | nan | |
| 386308705 | 2.506 | 0.005 | 1 | 1 | 13814 | nan | |
| 387115314 | 5.26 | 0.08 | 1 | 1 | 7655 | 4.05722 | 5.264(2) [2] |
| 387176295 | 1.8980 | 0.0007 | 2 | 2 | 7870 | 3.84494 | |
| 388179664 | 1.979 | 0.009 | 4 | 1 | 8001 | 3.80702 | |
| 388244501 | 2.115 | 0.001 | 3 | 3 | 7854 | 3.6355 | |
| 389008939 | 3.82 | 0.03 | 1 | 1 | 8681 | nan | |
| 389051511 | 3.37 | 0.01 | 1 | 1 | 10447 | 4.06674 | |
| 389213034 | 3.03 | 0.03 | 1 | 1 | 10167 | 3.72053 | |
| 390549095 | 1.8692 | 0.0001 | 2 | 2 | 7228 | nan | |
| 391635191 | 1.384 | 0.009 | 1 | 1 | 8698 | 3.60808 | |
| 391942460 | 13.0 | 0.5 | 1 | 1 | 9206 | nan | |
| 392761412 | 2.158 | 0.002 | 2 | 2 | 8016 | 3.94035 | 2.1558(2) [1] |
| 393162912 | 7.72 | 0.01 | 2 | 2 | 8207 | 3.38654 | |
| 394272819 | 2.985 | 0.002 | 2 | 2 | 7631 | 4.09268 | 1.479334(69) [2] |
| 394308408 | 5.432 | 0.001 | 2 | 2 | 9597 | 3.91616 | |
| 396592990 | 7.1 | 0.1 | 2 | 1 | 10375 | 3.64888 | |
| 397156705 | 1.573 | 0.002 | 1 | 1 | 10165 | 3.74844 | |
| 397361078 | 2.21 | 0.02 | 1 | 1 | 9594 | 4.32568 | |
| 397732137 | 3.16 | 0.02 | 2 | 1 | 8905 | 4.18821 | |
| 398906730 | 8.5 | 0.1 | 1 | 1 | 9595 | 3.86164 | |
| 399619535 | 4.19 | 0.02 | 1 | 1 | 8845 | 3.63491 | |

| | | | | | | | |
|-----------|--------|--------|---|---|---------|---------|----------------|
| 399813950 | 1.133 | 0.003 | 1 | 1 | 7684 | 3.59948 | |
| 400445441 | 1.100 | 0.003 | 1 | 1 | 14475 | nan | |
| 400802343 | 9.4 | 0.1 | 1 | 1 | 8547 | 3.85169 | |
| 400861216 | 1.483 | 0.003 | 1 | 1 | 9404 | 4.13329 | |
| 401677968 | 1.567 | 0.002 | 1 | 1 | 12541 | nan | |
| 402222378 | 2.42 | 0.02 | 1 | 1 | 8484 | 4.23501 | |
| 402383273 | 1.357 | 0.002 | 1 | 1 | 9459 | 4.20185 | |
| 402447670 | 4.353 | 0.008 | 2 | 2 | 9768 | 3.6235 | |
| 402463418 | 4.30 | 0.05 | 1 | 1 | 11732 | 3.76041 | |
| 402517183 | 5.78 | 0.06 | 1 | 1 | 10443 | 3.49147 | |
| 402804150 | 3.03 | 0.03 | 1 | 1 | 9455 | 4.35027 | |
| 402971434 | 1.722 | 0.005 | 1 | 1 | 12424 | nan | |
| 403320518 | 3.76 | 0.02 | 1 | 1 | 11667 | 4.14224 | |
| 403506500 | 3.483 | 0.009 | 1 | 1 | 8675 | 4.10169 | |
| 405219270 | 1.546 | 0.006 | 1 | 1 | 10788 | 3.94419 | |
| 405520863 | 1.539 | 0.003 | 1 | 1 | 10842 | nan | 1.298 [11] |
| 407045410 | 4.54 | 0.05 | 1 | 1 | 8404 | 3.89058 | |
| 407774530 | 3.50 | 0.04 | 1 | 1 | 12395 | nan | |
| 407825808 | 3.06 | 0.03 | 2 | 1 | 7242 | 4.27762 | |
| 407880289 | 1.6083 | 0.0002 | 2 | 2 | 9776 | 4.12953 | |
| 408045700 | 1.070 | 0.004 | 1 | 1 | 7543 | 4.20417 | |
| 409087713 | 1.534 | 0.002 | 1 | 1 | 9924 | 3.92297 | |
| 410666544 | 3.50 | 0.02 | 1 | 1 | 9490 | 3.62994 | |
| 413154622 | 1.79 | 0.01 | 1 | 1 | 10485 | 4.05494 | |
| 413373814 | 3.08 | 0.05 | 1 | 1 | 9701 | 3.78779 | |
| 413395842 | 0.899 | 0.002 | 1 | 1 | 7351 | 4.15456 | |
| 415152477 | 1.316 | 0.002 | 1 | 1 | 12816 | nan | |
| 418188386 | 1.84 | 0.01 | 2 | 1 | 7313 | 3.79373 | |
| 418718010 | 3.95 | 0.03 | 1 | 1 | 7927 | 3.62112 | |
| 421047795 | 4.39 | 0.07 | 1 | 1 | 7513.25 | 3.36414 | |
| 421348273 | 3.7262 | 0.0006 | 2 | 2 | 10013 | 3.9146 | |
| 421438914 | 2.89 | 0.01 | 1 | 1 | 10041 | 3.77361 | |
| 422033239 | 2.067 | 0.008 | 1 | 1 | 12659 | nan | |
| 422692360 | 1.493 | 0.004 | 1 | 1 | 11160 | nan | |
| 423663684 | 4.62 | 0.02 | 1 | 1 | 9365 | 4.03855 | 4.633(1) [1] |
| 425210920 | 6.7 | 0.2 | 1 | 1 | 8313 | 4.31334 | |
| 425276653 | 1.69 | 0.01 | 1 | 1 | 10903 | 4.32253 | |
| 425871448 | 1.098 | 0.003 | 1 | 1 | 10708 | 4.21551 | |
| 425949279 | 3.70 | 0.02 | 1 | 1 | 9998 | 3.66244 | |
| 431380369 | 10.39 | 0.08 | 3 | 2 | 8227 | 3.90936 | 5.2434(26) [3] |
| 434362248 | 2.27 | 0.02 | 1 | 1 | 8138 | 4.24879 | |
| 437776976 | 4.172 | 0.004 | 2 | 2 | 8324 | 3.57648 | |
| 440537642 | 1.0785 | 0.0007 | 2 | 2 | 14730 | nan | |
| 443316662 | 5.0 | 0.2 | 1 | 1 | 7855 | 4.28847 | |
| 443969553 | 2.46 | 0.01 | 1 | 1 | 8074 | 3.56947 | |
| 443995718 | 6.77 | 0.08 | 1 | 1 | 12188 | nan | |
| 445325141 | 8.576 | 0.008 | 3 | 2 | 9351 | nan | |
| 446207699 | 1.710 | 0.001 | 2 | 2 | 13183 | nan | |
| 446846414 | 5.53 | 0.02 | 2 | 2 | 10070 | nan | |
| 446954324 | 4.50 | 0.01 | 1 | 1 | 13798 | nan | |

| | | | | | | | |
|-----------|---------|---------|---|---|-------|---------|---------------|
| 448652897 | 1.011 | 0.005 | 1 | 1 | 7541 | 4.17458 | |
| 448696047 | 4.13 | 0.06 | 1 | 1 | 9183 | 4.21532 | |
| 448727889 | 4.396 | 0.003 | 2 | 2 | 8216 | 3.64937 | |
| 448806252 | 1.2747 | 0.0004 | 2 | 2 | 9485 | 3.66579 | |
| 449650980 | 1.281 | 0.002 | 1 | 1 | 14893 | nan | |
| 450506529 | 2.21 | 0.02 | 1 | 1 | 10932 | 3.70491 | |
| 450737411 | 12.7 | 0.2 | 2 | 1 | 9440 | 4.27421 | |
| 451282261 | 1.33568 | 0.00004 | 2 | 2 | 8515 | nan | |
| 451507272 | 2.633 | 0.005 | 2 | 2 | 9162 | 3.44965 | |
| 452554783 | 1.9870 | 0.0006 | 3 | 3 | 14332 | nan | |
| 452731705 | 5.79 | 0.03 | 1 | 1 | 7604 | 3.82907 | |
| 452786194 | 1.0197 | 0.0009 | 1 | 1 | 7068 | 3.70121 | |
| 452976515 | 6.0 | 0.2 | 1 | 1 | 9757 | 4.28242 | |
| 453573291 | 2.37 | 0.02 | 1 | 1 | 11612 | nan | |
| 453943903 | 2.606 | 0.001 | 2 | 2 | 9478 | 3.67145 | |
| 453978573 | 3.836 | 0.003 | 2 | 2 | 9409 | nan | |
| 454024432 | 3.34 | 0.02 | 1 | 1 | 8387 | 3.86335 | |
| 454534617 | 4.11 | 0.05 | 1 | 1 | 7750 | 3.99788 | |
| 454676199 | 1.0825 | 0.0004 | 2 | 2 | 8041 | 3.5142 | |
| 454748017 | 0.8966 | 0.0002 | 2 | 2 | 9601 | 3.91989 | |
| 455035702 | 2.94 | 0.04 | 1 | 1 | 7576 | 4.20157 | |
| 455069902 | 2.52 | 0.03 | 1 | 1 | 7383 | nan | |
| 456011440 | 2.256 | 0.006 | 1 | 1 | 10359 | nan | |
| 456610411 | 2.31 | 0.01 | 1 | 1 | 9101 | 3.86574 | |
| 459407365 | 14.9 | 0.4 | 1 | 1 | 11461 | 3.64788 | |
| 460796730 | 5.97 | 0.02 | 2 | 2 | 7340 | nan | |
| 462877348 | 12.84 | 0.06 | 2 | 2 | 10316 | 4.12491 | |
| 463064259 | 3.55 | 0.05 | 1 | 1 | 7208 | 4.3196 | |
| 463507016 | 0.9988 | 0.0002 | 2 | 2 | 9672 | 4.2343 | |
| 464326149 | 1.634 | 0.001 | 2 | 2 | 13825 | nan | |
| 464886060 | 1.0831 | 0.0002 | 2 | 2 | 9424 | 4.12056 | |
| 465512201 | 9.51 | 0.05 | 2 | 1 | 9309 | nan | |
| 466131406 | 1.232 | 0.006 | 1 | 1 | 7031 | 3.86112 | |
| 467965257 | 5.9 | 0.1 | 1 | 1 | 9384 | 4.27059 | |
| 468158572 | 2.434 | 0.003 | 2 | 2 | 8111 | 4.07817 | |
| 468888280 | 4.5 | 0.1 | 1 | 1 | 8946 | 4.18713 | |
| 469022401 | 5.09 | 0.01 | 1 | 1 | 11676 | 4.43279 | |
| 469246567 | 2.050 | 0.003 | 2 | 2 | 7205 | 3.97582 | 2.051 [7] |
| 469815594 | 5.3 | 0.1 | 1 | 1 | 9867 | 4.31167 | |
| 469948764 | 1.303 | 0.006 | 1 | 1 | 9143 | 4.3521 | 1.3006(7) [1] |

B Routine Code

For posterity, the main pieces of code used to form the routine and process objects for this project are presented here. These include, in order: the object identification code, file download code, main body of the routine, data sorting code, and sector comparison code. The code isn't designed for readability nor efficiency.

Object Identification Code. The following code is a preliminary part of the routine to investigate the temperatures of objects within each TESS sector. This outputs three lists of TICID sectors sorted by whether they are within given temperature parameters.

```
#investigating astroquery.mast
import astroquery.mast as astroquery
import simplejson
import time

#set the minimum and maximum temperatures we are looking for
Teff_min =
Teff_max =

#the following code selects all the light curves we need

sector =      #change to query another region

observations = astroquery.Observations.query_criteria(sequence_number=f"{
    sector}",
                                                    dataproduct_type="
                                                    TIMESERIES",
                                                    obs_collection="TESS
                                                    ")

TIC = observations["target_name"]
right_ascension = observations["s_ra"]
declination = observations["s_dec"]

#below we create a few blank/empty values for use in the following for-loop
. it's not the most efficient code but it works.
No_Temperature = []
Valid_Temperature = []
Invalid_Temperature = []
n = 0      #this n value is essentially preserving index

for i in TIC:
    try:
        ra = right_ascension[n]
        dec = declination[n]
        catalog_data = astroquery.Catalogs.query_criteria(catalog="TIC", ID
            =i)
        ID_value = catalog_data["ID"]
```

```

if Teff_min < catalog_data["Teff"] < Teff_max:    #categorising
    stars by temp
    Valid_Temperature.append(ID_value[0])
elif Teff_min > catalog_data["Teff"] or Teff_max < catalog_data["
Teff"]:
    Invalid_Temperature.append(ID_value[0])
else:
    No_Temperature.append(ID_value[0])
except:
    time.sleep(10)

```

#the following code creates lists of objects that satisfy or do not satisfy the temperature cutoffs, or do not have temperature data

```

f = open(f'Valid_Temperature {sector}.txt', 'w')
simplejson.dump(Valid_Temperature, f)
f.close()

```

```

f = open(f'Invalid_Temperature {sector}.txt', 'w')
simplejson.dump(Invalid_Temperature, f)
f.close()

```

```

f = open(f'No_Temperature {sector}.txt', 'w')
simplejson.dump(No_Temperature, f)
f.close()

```

File Download Code. This second portion of code is to download the data from a given list. This is intended to have the resultant list from the previous section of code fed into it.

```

import astroquery.mast as astroquery
import astropy

sector = #set this to the sector being involved

#read in data
f = open(f"Valid_Temperature {sector}")
fx = f.read().split(",")
f.close()

#clean up data;
fx = " ".join(fx).replace("'", '').split()
fx = " ".join(fx).replace("[", "").split()
fx = " ".join(fx).replace("]", "").split()

obs_total = astropy.table.MaskedColumn(fx)

for x in obs_total:
    obsid = f"TIC{x}"
    print(obsid)

```

```

observations = astroquery.Observations.query_criteria(
    objectname = obsid,
                                                                    dataproduct_type
                                                                    =
                                                                    "
                                                                    TIMESERIES
                                                                    ",
    obs_collection
                                                                    =
                                                                    "TESS
                                                                    ",
    sequence_number
                                                                    =
                                                                    f"{
                                                                    sector
                                                                    }")

data_products = astroquery.Observations.get_product_list(
    observations)
download_list = astropy.table.Table()
for y in data_products:
    if "s_lc.fits" in y["productFilename"] and x in y["obs_id
    "]: #validating the file is correct using its
    filename
        download_list = astropy.table.Table(y)
        manifest = astroquery.Observations.download_products(
            download_list)
    else:
        pass
print(f"done {sector}!")

```

Main Body of the Routine. This is the main part of the routine, to identify and remove false positive results, and determine the rotation frequency of any Ap candidate stars identified. This is a slightly altered version to the final routine, and is altered to only handle a single light curve file at a time. It can be easily modified to automatically run through a list of files.

```

#Read in required packs
from astropy.io import fits
import matplotlib.pyplot as plt
import numpy as np
from sigfig import round
from astropy.timeseries import LombScargle
import os

file = #point this towards the light curve fits file or files that need
to be analysed by the routine

try:
    with fits.open(f"{file}.fits") as hdu:
        tigid = hdu['PRIMARY'].header['TICID']
        dt = hdu['LIGHTCURVE'].header['TIMEDEL']
        sector = hdu['PRIMARY'].header['SECTOR']

```

```

time = hdu['LIGHTCURVE'].data['TIME']
flux = hdu['LIGHTCURVE'].data['PDCSAP_FLUX']

#Truncate data.
t = time
y_b = flux

y = np.vstack((t, y_b)).T
not_nan = y[~np.isnan(y).any(axis=1)]

#remove nan values here
t_split = np.hsplit(not_nan, 2)[0]
y_split = np.hsplit(not_nan, 2)[1]

t_2d = t_split.T
y_2d = y_split.T

t_1d = t_2d.flatten()
y_1d = y_2d.flatten()

y_mean = np.mean(y_1d)

t_1d_proper = t_1d - t_1d[0]    #final time axis values
y_1d_proper = y_1d            #final luminosity axis

#performing a quick calculation for the sake of PDM later
fv_x_bar = np.mean(y_1d_proper)    #the mean x-value
fv_x_i_minus_mean = y_1d_proper - fv_x_bar    #x_i subtract the
mean
fv_x_i_squ = fv_x_i_minus_mean * fv_x_i_minus_mean #the above value
squared
fv_x_i_sum = sum(fv_x_i_squ)        #summing the above;
this is the numerator of the equation
N_minus_1 = len(y_1d_proper) - 1    # N - 1; the
denominator of the sigma-squared value
sigma_squared_value = fv_x_i_sum/N_minus_1    #this is the final
value which is used at the very end to determine Theta

bin_a = 100                        #number of bins for PDM

#Defining PDM.
def PDM_runthrough(start_value, end_value, desired_increments):
    global minima_array
    global increments
    global minimum_values_y

    increments = (end_value - start_value)/(desired_increments+1)    #
        this spaces out the test periods

```

```

test_periods = np.arange(start_value , end_value , increments) #
    calculates test periods using above

if len(test_periods) > (desired_increments + 1):
    test_periods = np.delete(test_periods , -1)
else:
    pass

data_values = np.column_stack([t_1d_proper , y_1d_proper])
#then fold based on this.

#now, defining bins: I'm treating N_c "covers" of bins as equal to
1
#this simplifies the code for now, though is an obvious point of
improvement

#and now defining an empty array to dump our resulting values in
theta_array = np.arange(0,0,1)

#for loop: this first part folds the data
for j in range (1, desired_increments+1):
    data_values = np.column_stack([t_1d_proper , y_1d_proper])
    for i in data_values:
        while (i[0]) > test_periods[j]:
            i[0] = i[0] - test_periods[j]

    data_values_sorted = data_values[data_values[:,0].argsort()]

#now defining the width of bins based on bin_a value earlier up
bin_width = test_periods[j]/bin_a
bin_boundaries = np.arange(0, test_periods[j], bin_width)

#and defining two further empty arrays for later loops
variance_vals = np.arange(0,0,1)
n_j_values = np.arange(0,0,1)

#the following goes through each defined bin; determines values
within the bin
#then calculates the individual variance for each bin as well as
its
for k in bin_boundaries:
    current_data = np.arange(0,0,1) #
    resets current_data array
    for l in data_values_sorted:
        if k < l[0] < k+bin_width: #
            searches for data in bin
            current_data = np.append(current_data , l[1]) #
            classifies the data as being in the bin

```

```

N_value = (len(current_data)) #
    counts how many data points are in the bin
if N_value != 0: #
    validates bin isn't empty and won't cause "division by
    zero" errors
    mean = sum(current_data)/N_value #
        the following is just calculating then saving the
        variance; same method as earlier
    data_minus_mean = current_data - mean
    data_minus_mean_squ = data_minus_mean * data_minus_mean
    sigma_squ = sum(data_minus_mean_squ)/(N_value-1)
    n_j_values = np.append(n_j_values , N_value)
    variance_vals = np.append(variance_vals , sigma_squ)

#variance_vals is representative of the s_j_squared value in
equation (2) of Stellingwerf, 1978
n_j_product_var = (n_j_values - 1) * variance_vals

sum_var = sum(n_j_product_var)
sum_M = (sum(n_j_values)) - bin_a

s_squared = sum_var / sum_M

theta_value = s_squared / sigma_squared_value
theta_array = np.append(theta_array , theta_value)

#then just defining an arbitrary x-axis (this can be changed later)
and plot:
test_periods = np.delete(test_periods , 0)
plt.plot(test_periods , theta_array)
minimum_y = np.argmin(theta_array)
minimum_y_value = np.min(theta_array)
minimum_value = (test_periods[minimum_y])
if minimum_y_value < minimum_values_y[0]:
    minimum_values_y = [minimum_y_value , minimum_value]
else:
    pass

#Lomb Scargle.
LS = LombScargle(t_1d_proper , y_1d_proper)
frequency , power = LS.autopower(samples_per_peak=30, maximum_frequency
    =30)
significance = LS.false_alarm_probability(power.max())

max_num = np.argmax(power)
max_freq = frequency[max_num]
inform = np.empty(3)
index_value = 0
sig_values = 0

```

```

#make a list of all points where the Lomb Scargle periodogram has a
    significant point
for n in power:
    significance = LS.false_alarm_probability(n)
    if significance < 0.001:
        value_info = [index_value , frequency[index_value] , power[
            index_value]]
        inform = np.vstack((inform , value_info))
        sig_values += 1
    else:
        pass
    index_value += 1

#check for significant figures
if sig_values > 0:
    max_power = max(inform[:,2])
    threshold = max_power*0.2
    inform_2 = np.empty(3)

    for n in inform:
        if n[2] > threshold:
            inform_2 = np.vstack((inform_2 , n))
        else:
            pass

    index_value = 0.5
    power_value = 0
    deleted_values = 0
    absolute_value = 0
    inform_3 = np.empty(3)

#goes through and removes any significant points directly
    neighbouring a more significant point
for n in inform_2:
    if n[0] == index_value + 1:
        if n[2] > power_value:
            inform_2 = np.delete(inform_2 , int(absolute_value -
                deleted_values) , axis=0)
            gradient = 1
        else:
            inform_2 = np.delete(inform_2 , int(absolute_value -
                deleted_values) , axis=0)
            if gradient == 1:
                deleted_values -= 0
                gradient = 0
                inform_3 = np.vstack((inform_3 , n))
            else:
                pass

```

```

        deleted_values += 1
    else:
        pass
    index_value = n[0]
    power_value = n[2]
    absolute_value += 1

inform_3 = np.delete(inform_3, 0, axis=0)

#check for harmonics
if len(inform_3) == 1:
    if inform_3[0][1] < 2:
        candidate_frequency = n[1]
    else:
        candidate_frequency = "frequency too high"
else:
    harmonics = 0
    for n in range(1, len(inform_3)):
        lower_lim = (n+1)*0.95*inform_3[0][1]
        upper_lim = (n+1)*1.05*inform_3[0][1]
        if lower_lim < inform_3[n][1] < upper_lim:
            harmonics += 1
        else:
            pass
    if harmonics == len(inform_3)-1:
        candidate_frequency = inform_3[1][1]
    else:
        candidate_frequency = "non-harmonic peaks"

#if significance > 0.1, that's probably insignificant enough to
count out
#thus this is the first cutoff

if type(candidate_frequency) == np.float64:
    final_period = [1/candidate_frequency*2, 1/candidate_frequency,
1/candidate_frequency*0.5]

    minimum_values_y = [1, 1]

#coarse search using PDM
for n in range(0,3):
    lower_boundary = final_period[n] - 0.1*final_period[n]
    upper_boundary = final_period[n] + 0.1*final_period[n]

    PDM_runthrough(lower_boundary, upper_boundary, 20)

    minimum_value = (minimum_values_y[1])

#prints out the three searches for PDM.

```

```

plt.title("Phase Dispersion Minimisation plots for a coarse
search")
plt.xlabel("Period (days)")
plt.ylabel("Phase Dispersion")
plt.show()

lower_boundary = minimum_value - 0.05*minimum_value
upper_boundary = minimum_value + 0.05*minimum_value

minimum_values_y = [1,1]

#fine search using PDM
PDM_runthrough(lower_boundary , upper_boundary , 20)

minimum_values = minimum_values_y[1]    #sets the most likely
period from the search

#prints out the final PDM search
plt.title("Phase Dispersion Minimisation plot for a fine search
")
plt.xlabel("Period (days)")
plt.ylabel("Phase Dispersion")
plt.show()

#plots out the Lomb Scargle Periodogram
plt.plot(frequency , power)
plt.title("Lomb-Scargle plot for initial search")
plt.xlabel("Frequency (days-1)")
plt.ylabel("Power")
plt.show()

#folds the light curve over the determined period then plots it out
lc = (t_1d_proper , y_1d_proper)
lc = np.empty(2)
for n in range(len(t_1d_proper)):
    lc = np.vstack((lc , (t_1d_proper[n] , y_1d_proper[n])))
lc = np.delete(lc , 0 , axis=0)
for n in lc:
    while n[0] > minimum_values:
        n[0] -= minimum_values
plt.scatter(lc[:,0] , lc[:,1])
plt.title("Folded Light curve")
plt.xlabel("Phase")
plt.ylabel("Normalised Flux")
plt.show()

#calculates the error from the folded light curve
max_argument = np.argmin(lc[:,1])
min_argument = np.argmax(lc[:,1])
total_max = lc[-1,0]

```

```

l_l_frequency = lc [min_argument, 0] - 0.005*total_max
l_h_frequency = lc [min_argument, 0] + 0.005*total_max
h_l_frequency = lc [max_argument, 0] - 0.005*total_max
h_h_frequency = lc [max_argument, 0] + 0.005*total_max
low_test = []
high_test = []
for n in lc:
    if l_l_frequency < n[0] < l_h_frequency:
        low_test = np.append(low_test, n[1])
    elif h_l_frequency < n[0] < h_h_frequency:
        high_test = np.append(high_test, n[1])
    else:
        pass
scatter_low_test = max(low_test) - min(low_test)
scatter_high_test = max(high_test) - min(high_test)
mean_scatter = (scatter_high_test + scatter_low_test)/2

T_val = time[-1] - time[0]
N_val = len(lc[:, 0])
a_val = max(lc[:, 1]) - min(lc[:, 1])

freq_error = (6/N_val)**(1/2) * 1/T_val * mean_scatter/a_val *
    10 #extra factor of 10 for caution

percentage_error = freq_error/(1/minimum_values)
period_error = minimum_values * percentage_error

final_result = round(float(minimum_values), uncertainty=float(
    period_error))

FinalResult = f"{tucid}, {sector} = {final_result} days"

else:
    FinalResult = f"{tucid}, {sector} = {candidate_frequency}"
else:
    FinalResult = f"{tucid}, {sector} = no significant peaks"

except:
    FinalResult = f"ERROR IN {tucid}"

print(FinalResult)

```

Data Sorting Code. The fourth presented piece of code takes the final results from the previous code (stored in a file called Results.txt), fetches their effective temperatures and log g values, and stores them in a list.

```

import astroquery.mast as astroquery

#import results in from main stage of routine
f = open("Results.txt", "r")

```

```

fx = f.readlines()

for x in fx:
    try:
        #clean up the input values; fetch results from the final result in
        #the previous code
        y = x.split("=")
        y2 = y[0].split(",")
        TICID = y2[0]
        SECTOR = y2[1].replace(' ', '')

        y3 = y[1].split(",")

        if len(y3) == 2:
            RESULT = y3[0].replace(" (", "")
            UNCERTAINTY = y3[1].replace(") days", "").replace(" ", "")
        else:
            RESULT = y3[0].replace(" ", "")
            UNCERTAINTY = "nan"

        #fetch catalog data for object
        catalog_data = astroquery.Catalogs.query_criteria(catalog="TIC", ID
            =TICID)
        TEFF = catalog_data["Teff"][0]
        dTEFF = catalog_data["e_Teff"][0]
        LOGG = catalog_data["logg"][0]
        eLOGG = catalog_data["e_logg"][0]

        RESULT = RESULT.replace("\n", "")
        UNCERTAINTY = UNCERTAINTY.replace("\n", "")

        result = [TICID, SECTOR, RESULT, UNCERTAINTY, TEFF, dTEFF, LOGG,
            eLOGG]

        #write in the results to the file
        f = open('OrganisedDataSectorSort.txt', 'a')
        f.write(f'{result}\n')
        f.close()
    except:
        pass

```

Sector Comparison Code. The final piece of code presented here is to calculate final values for objects with multiple periods calculated and organise the results. It assumes the data has been organised into a dictionary, which contains the TICID, values and uncertainties for each unique object. This is a different input than the output of the previous code, however acquiring a dictionary of results from the sorted results is trivial.

```

import sigfig
import numpy as np
import astroquery.mast as astroquery

```

```

import time as tm

#read in file
file = open("DictionaryDataOrgList.txt", "r")
contents = file.readlines()

#setting up a number of empty arrays and values
FinalerResults2 = []
FinalerResults = []
numb = 0
one = 0
two = 0
three = 0
four = 0

#clean up lines that were read in
for x in contents:
    y = x.split("[")
    TIC = y[0]
    RES = y[1]
    TICID = TIC.replace(",","").replace(" ","") #gives ticid
    RESU = RES.replace("]","").replace(" ","")
    RESULT = RESU.split(",") #gives an array of results

    try:
        #queries effective temperature quickly, since that's not included
        in DictionaryDataOrgList.txt
        catalog_data = astroquery.Catalogs.query_criteria(catalog="TIC", ID
        =TICID)
        TEFF = catalog_data["Teff"][0]
    except:
        tm.sleep(10)
    if TEFF < 7000: #remove low-temperature results
        pass
    else:
        if len(RESULT) == 1: #processing light curves observed in a
            single sector
            RESULT = RESULT[0].replace("\n","").replace("[","").replace
            ("]","")
            z = str(RESULT)
            if z == "nosignificantpeaks_nan": #check and pass on any
                results without values
                pass
            elif z == "NA":
                pass
            elif z == "frequencytoohigh_nan":
                pass
            else:
                RESULTS = RESULT.split("-") #results are formatted
                value_error; splitting into value and error

```

```

Value = RESULTS[0]
Error = RESULTS[1]
if Error == "0.0":    #eliminate any values with
    problematic errors
    pass
elif float(Value) > 28:    #eliminate any values with
    impossible period lengths
    pass
else:
    FRes = sigfig.round(Value, Error)
    FR = f"TIC{TICID}- {FRes} days. Result from 1 Light
        curve."
    FinalerResults = np.append(FinalerResults, FR)

else:
    NSP = 0    #these are noting the false positive sources
    NHP = 0
    FTH = 0
    values = []
    for l in RESUL:
        j = l.replace(" ", "").replace("\n", "")
        k = str(j)
        if k == "nosignificantpeaks_nan":
            NSP += 1
        elif k == "NA":
            NHP += 1
        elif k == "frequencytoohigh_nan":
            FTH += 1
        else:
            values = np.append(values, k)

    if len(values) == 0:
        pass    #ignore objects with no value from routine
    else:
        Close_Val = []
        Close_Err = []
        Close_Val_Half = []
        Close_Err_Half = []
        for v in values:
            w = v.split("_")
            Value = float(w[0])
            Error = float(w[1])
            if Value > 28:
                pass
            else:
                FRes = sigfig.round(Value, Error)
                Close_Val = np.append(Close_Val, Value)
                Close_Err = np.append(Close_Err, Error)
                Close_Val_Half = np.append(Close_Val_Half, Value/2)
                Close_Err_Half = np.append(Close_Err_Half, Error/2)

```

```

if len(Close_Val) == 1:
    pass
elif len(Close_Val) == 0:
    pass
else:
    #following code evaluates closeness of each value to
    #one another, round robin style
    truth = 0 - len(Close_Val)
    lies = 0
    for n in range(0, len(Close_Val)):
        for m in range(0, len(Close_Val)):
            if Close_Err[n] > Close_Err[m]:
                Err = Close_Err[n]*5
            else:
                Err = Close_Err[m]*5

            closeness = np.isclose(Close_Val[n], Close_Val[
                m], atol=Err, equal_nan=False)
            if closeness == False:
                closeness = np.isclose(Close_Val[n]/2,
                    Close_Val[m], atol=Err, equal_nan=False)
                if closeness == False:
                    closeness = np.isclose(Close_Val[n],
                        Close_Val[m]/2, atol=Err, equal_nan=
                            False)
                    if closeness == False:
                        pass
                    else:
                        Close_Val[m] = Close_Val[m]/2
                else:
                    Close_Val[n] = Close_Val[n]/2
            if closeness == True:
                truth += 1
            else:
                lies += 1
    if lies == 0: #automatically pass through any result
        with no conflicting values
        final_val = np.average(Close_Val)
        uncertainty = np.std(Close_Val)
        uncertainty = float(uncertainty)
        fina_val = float(final_val)
        FResu = sigfig.round(fina_val, uncertainty)
        numby = len(Close_Val)
        FR = f"TIC{TICID}- {FResu} days. Result from {numby
            } Light curves, all in agreement."
        FinalerResults2 = np.append(FinalerResults2, FR)
    elif truth == 0: #automatically ignore any result
        with no non-conflicting

```

```
        pass
    else:    #note down any with some conflicting values ,
            for manual inspection
                vallie = (truth , lies , FTH, NHP, NSP)
                f = open('Manually_Evaluated_TICID_AGAIN.txt', 'a')
                f.write(f'TIC{TICID}\n')
                f.write(f'{ vallie}\n')
                f.write(f'{ values}\n')
                f.close()
                numb += 1

#write final results to a text document to later analyse
for y in FinalerResults:
    print(y)
    f = open('OtherResults.txt', 'a')
    f.write(f'{y}\n')
    f.close()

for y in FinalerResults2:
    print(y)
    f = open('OtherResults2.txt', 'a')
    f.write(f'{y}\n')
    f.close()
```